International Journal of High Speed Electronics and Systems
Vol. 13, No. 2 (2003) 601–676

World Scientific
www.worldscientific.com

T-RAY SENSING AND IMAGING

S. P. MICKAN* and X.-C. ZHANG†
Department of Physics, Applied Physics & Astronomy, and
Department of Electrical, Computer & System Engineering,
Rensselaer Polytechnic Institute, Troy NY 12180, USA.
† *Corresponding author. Email: zhangxc@rpi.edu*

Terahertz (THz) radiation occupies part of the electromagnetic spectrum between the infrared and microwave bands. Until recently, technology at THz frequencies was underdeveloped compared to the rest of the electromagnetic spectrum, leaving a gap between millimeter waves and the far-infrared (FIR). In the past decade, interest in the THz gap has been increased by the development of ultrafast laser-based T-ray systems and their demonstration of diffraction-limited spatial resolution, picosecond temporal resolution, DC-THz spectral bandwidth and signal-to-noise ratios above 10^4.

This chapter reviews the development, the state of the art and the applications of T-ray spectrometers. Continuous-wave (CW) THz-frequency sources and detectors are briefly introduced in comparison to ultrafast pulsed THz systems. An emphasis is placed on experimental applications of T-rays to sensing and imaging, with a view to the continuing advance of technologies and applications in the THz band.

Keywords: Ultrafast; Terahertz, THz; T-rays; sensing; imaging.

1. Introduction

Terahertz (THz) radiation can be generated and detected by various systems, each with different output powers, sensitivities, bandwidths and technological implementations. Recently the terahertz band has become more accessible due to ultrasensitive pulsed sources and detectors based on pulsed laser excitation, which generate and detect picosecond (ps) pulses of free-space THz radiation, dubbed *T-rays*.[1]

T-ray spectrometers are wide-spread in the optics community and are being used in an increasing number of research and industrial applications. T-rays are complemented by a number of other techniques for generating and detecting THz radiation, specifically CW systems, which use electronic or optical methods, as

*Permanent address: Centre for Biomedical Engineering (CBME), and Department of Electrical and Electronic Engineering, The University of Adelaide 5005 Australia. Email: spmickan@eleceng.adelaide.edu.au.

discussed in 2. In this chapter we will generally refer to ultrafast pulsed THz as T-rays.

As shown in Fig. 1, THz radiation lies at the boundary between electronics and photonics. The THz bandwidth centers on the frequencies 0.3 to 3 THz, overlapping with high-frequency mm-waves and the long wavelengths of the far-infrared. At this boundary, THz has improved far-field spatial resolution, $\approx 300\ \mu$m, over mm-waves, and reduced Rayleigh scattering, $\propto \lambda^{-4}$, compared to infrared light.

THz radiation has a spatial resolution limited by wavelength, λ, to approximately 0.3 mm at 1 THz, which is better than millimeter (mm)-waves, and THz Rayleigh scattering is less than for IR light due to its λ^{-4} dependence.

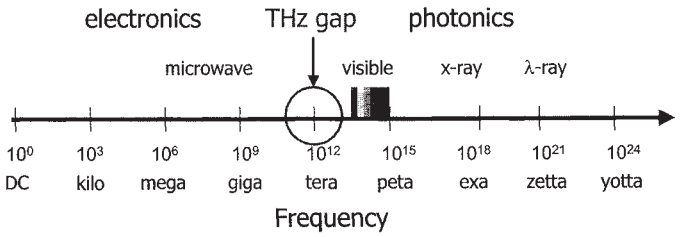

Fig 1. A representation of the electromagnetic spectrum, showing the THz gap between the well-developed fields of mm-waves and the infrared.

Research interest in T-rays stems from the broadband pulsed nature of the radiation and the THz-frequency response of materials, ranging from semiconductors to human tissue. The wavelength of the radiation corresponds to a photon energy, and thus to certain energy transitions in materials. The THz regime is populated by the rotational and vibrational energy states of polar molecules, either in liquid or gas form. Larger molecules show many collective vibrational and librational (bending) modes at THz frequencies. Polar molecules interact strongly with T-rays; water molecules absorb THz very strongly, on the one hand limiting penetration of the radiation into moist substances, and on the other making it readily detectable even in very low concentrations.

T-ray photons have energy quanta corresponding to many discrete energy levels in matter. In molecules, vibrational states are typically separated by energy transitions of approximately 0.1 eV and rotational states are separated by approximately 0.001 eV. Multi-atomic molecules have many vibrational and rotational modes, resulting in a very large number of T-ray transitions for large molecules.[2] In larger systems, the relative vibration of sub-domains in a molecule and the vibration of hydrogen bonds between molecules interact with T-ray photons. In condensed matter systems, typical T-ray energies can excite polaritons, phonons and plasmons in semiconductors, and energy gaps in superconductors.[3,4]

Most molecules have dense and distinctive absorption spectra in the far-infrared, which has led to much interest in THz spectroscopy.[5-8] Using T-ray transmission or reflection spectroscopy, samples from gas to the solid-state can be completely characterized at THz frequencies. The density of ro-vibrational modes in the THz

bandwidth provides a wealth of information about the composition and state of samples.

In terms of applications, THz radiation will penetrate non-polar substances such as fats, cardboard, cloth and plastic with little attenuation, and can be used for detecting low concentrations of polar gases, conceivably for pollution control. Apart from detection, materials can also be differentiated spectroscopically using T-rays. The identification of a group of rotational or vibrational lines in the molecular spectrum leads to unique classification of the molecular substance itself.

Table 1. Comparison of different notations used to describe where the T-ray frequencies, from 0.3 to 3 THz, lie on the electromagnetic spectrum.

Wavenumber	Wavelength	Frequency	Photon Energy	Blackbody Temp.
1 cm^{-1}	10 mm	30 GHz	120 μeV	1.4 K
10 cm^{-1}	1 mm	300 GHz	1.2 meV	14 K
33 cm^{-1}	300 μm	1 THz	4.1 meV	48 K
100 cm^{-1}	100 μm	3 THz	12 meV	140 K
200 cm^{-1}	50 μm	6 THz	25 meV	290 K
670 cm^{-1}	15 μm	20 THz	83 meV	960 K

T-ray science has expanded rapidly during the past decade, exploring the THz gap in the electromagnetic spectrum. Two broad THz classes of T-ray generation and detection, both relying on ultrafast laser pulses, have developed over the past fifteen years. The first, using photoconductive antennas, was developed at Bell Labs and the IBM Watson Research Center and is now available in a commercial product from Picometrix Inc, MI.[9] The second, using the nonlinear effects of optical rectification and electro-optic sampling, is marketed by Zomega Technology Corp, NY.[10] Large-scale stand-alone imaging systems became available in 2002 from TeraView[11] and Nikon.[12] THz radiation is being used for an increasing range of sensing and imaging applications, discussed in Secs. 2 and 5.

T-ray spectrometers are well suited to complement existing chemical sensing and analysis tools, such as Fourier transform infrared (FTIR) and nuclear magnetic resonance spectroscopy. Pulsed THz radiation consists of ultrashort pulses, each with a bandwidth spanning the range from approximately 0.1 to 10 THz. The electric field of a typical T-ray pulse is shown in Fig. 2. The vertical axis shows the magnitude of the pulse, which is proportional to the THz electric field, and the horizontal axis shows the time-delay between the optical generation and detection pulses. The operation of a T-ray spectrometer is explained in Sec. 3. The important characteristic of a T-ray is its short pulse length. This picosecond pulse of electromagnetic radiation, that is 10^{-12} seconds, has a short time resolution and a broad spectral bandwidth, and time-gated detection is sensitive to its high peak power. Pulsed T-ray systems have demonstrated signal-to-noise ratios (SNRs) of over 10,000:1 using lock-in detection,[13] with only small pulse energies. Having very low average power, T-rays are particularly attractive for medical applications, where they are currently

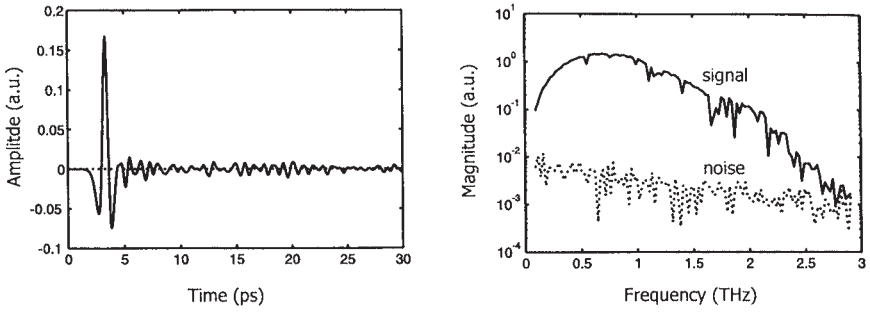

(a) Time-domain T-ray electric field pulse

(b) Spectral components of the T-ray pulse

Fig 2. The electric field of a typical broadband T-ray pulse, showing the ps duration and THz bandwidth. This pulse was generated from surface currents in unbiased GaAs, generated by 100-fs laser pulses with a pulse repetition frequency of 82 MHz. The T-rays propagated through 50 cm of air, and were detected by electro-optic sampling in ZnTe. The spectrometer was at room temperature and humidity; the oscillations in the tail of the time-domain pulse, and the frequency dips visible in the spectrum at 0.56, 0.75 and 1.1 THz are due to absorption of water molecules in the air.[5] The noise level depends on averaging time in the lock-in amplifier; these measurements were averaged with a 100-ms time constant.

considered harmless (see Sec. 4.3.4). Looking to future applications, T-ray imaging faces the hurdles of spatial resolution, size, cost, output power, SNR, bandwidth, depth penetration, water sensitivity and speed of data acquisition.

2. Continuous-wave Terahertz Systems

2.1. *Introduction*

In the THz region of the electromagnetic spectrum, there are five primary classes of CW sources and three classes of detectors. The simplest THz sources and detectors are thermal in nature; hot emitters, such as globars, and cooled detectors are used in THz FTIR spectroscopy systems. The third and fourth most common THz sources have arisen from opposite sides of the THz spectral band; electronic sources are based on microwave-style resonators and circuits, whereas nonlinear optical sources rely on optical laser technology. Three classes of THz laser have been introduced in the last thirty years, and remain in various stages of development: free-electron lasers (FELs), gas-vapor lasers and semiconductor lasers, including quantum cascade lasers.

THz radiation has historically been difficult to generate and detect.[14] Thermal sources have weak emission at long wavelengths and gas vapor lasers are cumbersome.[15] Bolometric detectors only operate under vacuum conditions at liquid-helium temperatures,[16] and although FTIR spectroscopy offers spectroscopic information down to approximately 1 THz, lower frequencies are difficult to access.[17,18] This section reviews current research on THz sources and detectors that do not rely

on ultrafast generation and detection.

2.2. *Thermal sources*

FTIR spectroscopy is a powerful and well-developed technique for studying resonances from the visible to the mid-infrared. FTIR relies on incoherent thermal sources and detectors for THz-frequency measurements. Despite the low power and poor sensitivity of thermal sources and detectors in the THz band, FTIR is used widely and extensively in material and biological studies.[19]

THz FTIR spectroscopy relies on THz radiation generated by a mercury arc lamp, or SiC rod (globar), which is directed into two arms of an optical interferometer. The sample to be studied is placed in one arm of the interferometer, and a characteristic interference pattern, influenced by the THz properties of the sample, is measured by scanning the length of one arm of the interferometer. The actual spectral response of the sample can be calculated from the interferogram using Fourier theory and the numerical Fast Fourier Transform (FFT), with consideration of zero-padding, apodization and aliasing.[17]

With regard to speed, frequency resolution and reliance on the FFT, FTIR is comparable to T-ray spectroscopy, introduced in Sec. 3. The main advantage of FTIR spectroscopy is its sensitivity spanning many frequencies, from the far-infrared up to the visible, whereas T-ray spectrometers are more sensitive below 3 THz.[18]

Table 2. CW methods for thin film characterization.

Technique	**Freq. range**	**Comments**
Ellipsometry	20 THz–800 THz	optical technique[20]
FTIR	5 THz–80 THz	for bulk and sheets[18]
Resonator	35 GHz–144 GHz	for sheets
Vector Network Analyzer	50 MHz–100 GHz	requires electrode patterning
RF Impedance Analyzer	1 MHz–1 GHz	for circuits
LCR Meter	10 Hz–1 MHz	for circuits
C-V technique	DC & low freq.	requires Hg probe contacts[21]

2.3. *Photonic sources*

The primary difficulty in developing a THz laser is finding a cheap and convenient gain medium that can be pumped efficiently, with high gain and high output power.

2.3.1. *Free-electron lasers*

The gain medium of the free-electron laser (FEL) is an oscillating beam of electron bunches, which is modulated by a spatially periodic magnetic 'wiggler' field. The emitted radiation can be tuned by changing the frequency of the wiggler and can in principle reach from mm to X-ray wavelengths. The FEL is the most powerful

source of THz radiation available, producing a CW or pulsed beam of coherent, diffraction-limited THz radiation with an efficiency potentially close to unity.[22]

Despite requiring large dedicated installations, FELs are important tools for studying THz radiation and its interaction with, for example, condensed matter and biological materials.[23] Current research aims to produce more compact FEL systems[24] and up to 50 W of average THz power has been generated at a 75 MHz pulse rate.[25]

2.3.2. *Gas-vapor lasers*

As mentioned in the introduction, simple molecules such as water have many rotational and vibrational resonances within the THz region. These molecules can be used as a laser gain medium if efficiently pumped into a long-lived excited state. The first obstacle in creating a THz source is finding a suitable radiative transition, since rotational and vibrational energy levels of large molecules are difficult to use in a laser.[15] A number of solutions have been found, including methanol and HCN vapor, pumped either optically or electronically. Methanol lasers, for example, are designed around optically exciting the rocking and asymmetric deformation modes of methanol with a CO_2 laser.[26] HCN lasers are the most popular gas-vapor lasers, with CW or pulsed lasing possible on many modes in the FIR. HCN lasers require large cavities (2 m or more), large voltages and currents (kV with up to 100s of amps), and active temperature stabilization.[27]

Gas-vapor lasers are not continuously tunable, but have been shown to operate at over 2000 wavelengths from 26 to 254 μm, with power levels ranging from μW to 10 mW.[28] Gas-vapor lasers have been used to characterize many materials in the FIR, including liquids, bulk semiconductors, thin-film semiconductors and thin film superconductors.[29] Gas-vapor laser have been reviewed by Blake *et al.*[30] and current developments continue to reduce the size and increase the tunability of gas-vapor lasers.

2.3.3. *Semiconductor lasers*

The offer of small, cheap and tunable solid-state THz sources has led to two main approaches in developing a THz semiconductor laser: p-germanium (Ge) lasers and semiconductor heterostructure (quantum cascade) lasers. Other solid-state THz lasers are proposed using narrow bandgap lead salts, intersubband quantum fountain oscillations[31] and impurity centers in silicon.[32,33]

The Ge laser operates through the electrical excitation of hot holes in p-doped Ge. The laser cavity is created by polishing the surfaces of the Ge crystal since Ge has a high THz refractive index, n=4.0.[34] Ge lasers doped with beryllium have exhibited up to 5% duty cycles, with up to 1 W of output power, continuously-tunable from 1 to 4 THz. With advances in slab design and cooling, Bründemann *et al.* expect to achieve CW lasing in the near future.[35–37] Current devices operate at 20–30 K, with 10–20 W of refrigeration. A commercial p-Ge laser was first available in 2002.[38]

THz radiation emission from quantum heterostructures in semiconductors is based around intersubband transitions.[39] The first quantum THz laser was reported by Kohler *et al* in 2002,[40] using a quantum cascade gain medium,[41] after

many groups had demonstrated THz emission from quantum structures. These devices are pumped with low voltages and mA currents, and generate narrow bandwidth radiation between 1 and 5 THz from intersubband transitions and resonant tunneling processes.[42-44] Quantum gain media are currently operational only at low temperatures (≈4.2 K) and suffer from fast depopulation of the excited states,[45] although room-temperature emission is predicted from 4-level asymmetric quantum well structures.[46,47] Quantum cascade structures have been used to generate THz in a nonlinear mixer configuration.[48] THz-frequency quantum cascade laser research has been reviewed by Tredicucci *et al.*[49]

2.4. *Nonlinear optical processes*

Nonlinear optical materials with an appreciable $\chi^{(2)}$ nonlinear optical coefficient provide a medium for generation of radiation at the beat frequency between two pump sources.[50,51] For pump sources with wavelengths offset by THz frequencies, the $\chi^{(2)}$ material can act as a source of THz.[52] Difference frequency generation (DFG), or three-wave mixing, was an early source of THz, but was hampered by low conversion efficiencies and phase matching requirements.[53-57] DFG has been revisited as a THz source using the patented organic crystal DAST (4-dimethylamino-*N*-methyl-4-stilbazolium-tosylate), designed to have a very high nonlinear electro-optic (EO) coefficient and low dielectric constant in the FIR.[58] DAST has been used to mix quasi-CW pulses from a tunable dual-wavelength Ti:sapphire laser to generate 32-ns THz pulses with over 2 μW of THz power.[59] A more compact and lower power source has been demonstrated using a Nd:YAG pump and dual wavelengths generated in a periodically-poled lithium niobate (PPLN) optical parametric oscillator;[60] the THz output wavelength is tuned from 120 to 160 μm using temperature control of the PPLN crystal. THz beat frequencies are now available from dual-frequency laser diodes[61] and injection-locked semiconductor lasers.[62] DFG is closely related to optical rectification, described in Sec. 3.3.2, where THz is generated as the difference frequency between Fourier components of the pulse.[52]

A nonlinear optical crystal can also be used to generate THz radiation via a parametric effect. In optical parametric generation (OPG), a near-infrared (NIR) pump beam generates a second NIR *idler* beam in a nonlinear crystal, and THz radiation is generated from the beating of the pump and the idler.[52] If the nonlinear crystal is placed in a cavity for the idler beam, feedback amplifies the idler beam, creating an optical parametric oscillator (OPO). OPG was used to generate THz radiation in the early 1970s, using a Nd:YAG pump beam, polariton scattering in $LiNbO_3$ to generate the Stokes (down-shifted) idler, and angular rotation of the parametric oscillator cavity to tune the THz output wavelength.[63-65] Since the mid-1990's, Kawase *et al.* have made a number of improvements to what they call the THz parametric oscillator (TPO), thereby decreasing system size, enhancing wavelength selectivity and increasing the output power by several orders of magnitude. A grating coupler on the $LiTaO_3$ crystal was used to improve the coupling of the THz radiation into free space,[66] and a prism coupler was used to remove the dependence of the THz output direction on the angle of the parametric cavity (and thus the output wavelength).[66] Rapid wavelength tuning was achieved by scanning the angle of the pump beam with a fast mirror.[67] The TPO has also been implemented in

a ring cavity configuration[68] and in cryogenically-cooled crystals, which improves the THz output power by over 100 times and reduces the gain threshold.[69] In 2001, THz parametric generation (TPG), with an injection seeded idler beam, was experimentally shown to be superior to TPO.[70] TPG shows a reduced line width ($\Delta\nu/\nu \approx 10^{-4}$) and a peak THz power of over 100 mW for 3.4-ns pulses. TPG has also been demonstrated in a compact form, admittedly with limited tunability (1.2–2.4 THz) and power (30 μW).[71]

Nonlinear optical methods of generating CW THz radiation are attractive for their simplicity, availability of solid-state pump sources, linewidth and tunability. Although more cumbersome than proposed electrically-pumped solid state sources, discussed in Sec. 2.3.3 above, DFG and OPG systems are significantly smaller than free-electron and gas-vapor lasers.

2.5. *Photomixing in biased semiconductors*

In a manner similar to DFG, biased semiconductors with very short carrier lifetimes and high carrier mobility can be used to convert a THz beat frequency between two optical beams into THz radiation.

Brown *et al.* initially developed GHz and THz photomixers, or optical-heterodyne converters, using electrodes and antennas deposited on low-temperature-grown (LT)-GaAs. LT-GaAs is characterized by sub-picosecond electron-hole recombination rates, a high carrier mobility ($\mu \approx 200$ cm^2/V-s) and a high breakdown field ($>4\times10^5$ V/cm).[72] The photomixer was an array of interdigitated electrodes with micron spacing, connected either to a strip line, for GHz generation, or a spiral antenna for free-space radiation of THz-frequency radiation.[73–75] Initially limited to 200 GHz, the bandwidth was increased to above 5 THz of coherent, tunable THz radiation,[76] and demonstrated for use in a spectrometer.[77,78] The biased photomixer is very similar to a photo-conductive antenna (Sec. 3.3.1), which is used with pulsed optical excitation.[79] Photomixing of fiber-coupled beams has been demonstrated with dipole,[80] log-spiral and slot antennas at different temperatures,[81] and analyzed with theoretical modeling.[82]

A number of optical sources have been used to generate the two pump beams for mixing, including two fiber-coupled Ti:sapphire lasers,[72] two distributed-Bragg-reflector (DBR) laser diodes,[83] two longitudinal modes in laser diodes,[84] microchip lasers (for mm-waves)[85] and iodine lasers (up to 14 GHz).[86] The advantage of using two modes in a single laser diode is the compact nature of the source, and a very narrow linewidth.[87] Other dual-mode lasers have been used to generate THz-frequency amplitude beats, for example a Ti:sapphire ring cavity, a Ti:sapphire α-cavity[88] and a laser diode array with a bandwidth reaching 7 THz.[89] A novel method of tuning the THz beat frequency is to use two linearly chirped pulses, and control the phase difference between them at the photomixer with, for example, a Michelson interferometer.[90] Biased photoconductors are also very important in generating THz pulses from ultrashort optical pump pulses, as discussed in Sec. 3.3.1 below.

CW photomixing systems have been used for scanning imaging, analogous to T-ray imaging systems, as detailed in Sec. 5 below.[91] With CW THz power output levels of approximately 1 mW,[75] photomixing systems are useful in applications

requiring excellent tunability, small system size and narrow linewidth.

2.6. *Electronic sources*

The frequency of electronic sources has increased steadily for many years, from MHz to the GHz frequencies. State-of-the-art electronic sources remain limited to frequencies in the hundreds of GHz and sub-mW powers.[92] High-speed electronic devices are suited to low-power CW operation, although a non-contact system based on complex impedance bridges[93] has been used to accurately characterize the dielectric constant of thin films between 30 GHz and 1 THz.[94] Nonlinear transmission lines (NLTLs) have also been used to generate electronically-tunable sub-ps transients,[95] which can drive antennas[96] to generate THz radiation.[97] NLTL THz sources have demonstrated very narrow linewidths in room-temperature spectroscopy applications.[98,99]

Backward wave oscillators (BWOs) are electrically-driven microwave generators that can generate CW radiation from mm-waves up to 2 THz.[100] BWOs are large table-top devices, requiring powerful magnetic fields and water cooling, but provide up to 300 mW of polarized, narrowband ($\Delta\nu/\nu \approx 10^{-5}$), tunable THz radiation.[101] Each BWO is tunable within approximately $\pm 30\%$ of its central value, therefore a number of devices are required for full frequency coverage. BWOs have been used in THz spectroscopy of gases,[102–104] thin film superconductors,[105] and biomolecules.[106]

Electronic CW generation techniques are primarily of interest for their simplicity and integratability with other electronic systems. The BWO provides a high quality source of CW THz at power levels between electronic and large laser systems.

2.7. *Detection*

As with sources, THz radiation can be detected using thermal, optical or electronic effects. Detecting THz signals is difficult because blackbody radiation at room temperature is strong in the FIR, as shown in Table 1. The most common THz detectors are thermal detectors, for example the helium-cooled bolometer, which is desensitized to ambient temperature and registers only the heating effect of the THz radiation.[16] The bolometer is an incoherent detector, registering only incident power, which is appropriate for CW detection, but limits the information available in broadband systems. FTIR, for example, uses an interferometric technique to resolve the different frequency components of the broadband source.[17,18]

In an analogous manner to nonlinear optical mixing and photomixing in biased semiconductors, CW THz radiation can be coherently detected using homodyne mixing in nonlinear crystals[107] and photoconductive switches.[78,90] For CW detection with THz local oscillators, electronic detectors have been developed based on cooled photodetectors,[108] electron plasmas in semiconductors,[109,110] semiconductor superlattices,[111] mesoscopic quantum devices,[112] resonant quantum well infrared photodetectors (QWIPS)[113] and high-electron-mobility transistors (HEMTs).[114] Purely electronic systems incorporate symmetrical sources and detectors.[94,97]

THz imaging with CW systems is widely relevant in FIR astronomy, as reviewed by Siegel.[115] CW imaging has been demonstrated with QWIP arrays[116] and in laboratory conditions using photomixing.[117]

3. Pulsed T-ray Spectrometers

3.1. *Introduction*

Pulsed THz, or T-ray, spectrometers are based on ultrafast pulsed generation and detection using mode-locked lasers. Mode-locked Ti:sapphire ultrafast lasers became commonly available in the 1980s, triggering increased research into ultrafast sources and detectors of THz radiation.[118] The cost and size of T-ray spectrometers is dominated by the cost and size of the ultrafast laser, a technology that is continuously becoming more convenient, compact and economical.

T-ray spectrometers have come out of the lab in recent years and are now commercially available as entire systems. The designs of T-ray systems continue to increase in variety as they are improved and applied to many fields in science, medicine and industry.

3.2. *Pulsed systems*

The development of pulsed THz radiation (T-rays) generated using ultrafast optical lasers has provided a new method for accessing the THz frequency regime. Pulsed THz techniques were initially developed for waveguide and circuit characterization.[119–122] Free-space THz time-domain spectroscopy grew from the development of both photoconductive dipole antennas and EO crystals as sources and detectors.[123–130] The first complete T-ray spectrometers were used for spectroscopy of bulk dielectrics at THz frequencies.[131–133] Many varieties of T-ray spectrometers now exist, detailed in the following sections. The most common is the commercially available spectrometer using an PCA emitter and detector.

T-ray spectrometers are inherently broadband systems, a result of using ultrafast optical pulses to generate pulses of THz radiation. The broadband nature of T-rays means they are able to probe a wide region of the FIR, depending on the actual system, from DC to the mid-infrared (>30 THz).

3.3. *Generation*

Many methods have been exploited to develop sources of pulsed THz. Apart from the most common techniques of photoconductive switching, optical rectification and semiconductor surface current generation, T-rays have been generated using the inverse Franz-Keldysh effect,[134] coherent control concepts[135] and plasma oscillations.[136] These are methods of producing an ultrafast current or polarization transient, which acts as a broadband source as predicted in Hertz's equations.[127] The radiation is then directly emitted into free space or coupled out with an antenna.

T-ray generation has been reviewed in many publications, for example by Gornik and Kersting.[39] The state-of-the-art in 1988 is well covered by Auston and Nuss[119,137] and nonlinear generation is developed in a text by Shen.[52]

3.3.1. *Photoconductive antennas*

A photoconductive antenna (PCA) has two important features: an antenna structure and a photoconductive substrate. The antenna structure is designed to radiate sub-mm-wavelength electromagnetic waves into free space. The antenna is driven

by an ultrafast current transient in the switch consisting of photocarriers swept by an applied DC bias field. The photocarriers are generated in the photoconductive substrate, which acts as a switch, by an ultrafast laser pulse. A PCA can be designed with different substrates and different actual antenna designs, which in turn influence the possible T-ray bandwidth and output power. When an ultrafast optical pulse is absorbed by an appropriate substrate, carriers are generated and swept apart by the DC bias field, which creates the current transient to drive the antenna. The substrate must be able to have sufficiently fast carrier recombination time and high carrier mobility to support an ultrafast transient. A sub-picosecond transient will generate a free-space pulse with a duration of a few picoseconds, which corresponds to a THz bandwidth.

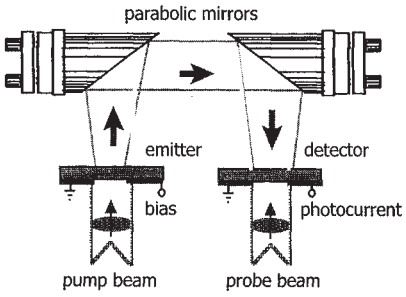

(a) Elementary T-ray beam system with PCA emitter and detector

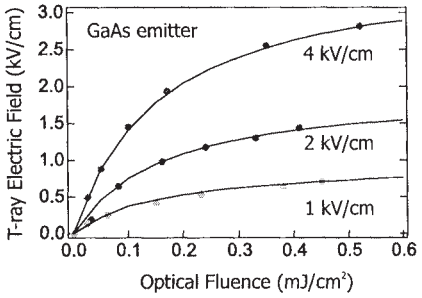

(b) PCA output power dependence on optical pump power, with DC bias field as a parameter

Fig 3. A T-ray beam is generated and detected using two PCAs.[128] The ultrafast probe beam pulse shorts the biased electrodes and the resulting current transient is coupled into free space. Gold or Al-coated parabolic mirrors collimate and focus the T-rays onto a second PCA. The PCA detector, described in Sec. 3.4.1, is gated by the probe pulse; when the PCA is conducting, a current can be measured across the electrodes that is directly proportional to the amplitude of the T-ray electric field. Fig. 3(a) shows how the emitted T-ray electric field depends both on the power in the optical pump pulse and the DC bias field applied to the PCA electrodes. The T-ray output saturates for high levels of optical fluence. The DC bias is limited by breakdown in the photoconductive switch.

The first PCA was demonstrated by Mourou *et al.* at microwave frequencies in 1981.[138] PCA sources used in T-ray spectrometers, or THz time-domain spectroscopy (THz-TDS) systems, were developed primarily by Lucent Technologies and IBM in 1988 and 1989,[5,128,131,139] although other groups were actively developing sources and detectors, as reviewed by Auston *et al.*[127] A schematic of the first T-ray spectrometer, based on PCAs, is shown in Fig. 3(a). The basic elements of a PCA, the antenna geometry, the photoconductive switch, the electric bias and the optical pulse have been subsequently varied in many ways to study and improve the generated T-ray power, bandwidth, radiation pattern and pulse characteristics.

The high SNR of T-ray spectrometers is due to high emitter power and sensitive

detection (Sec. 3.4). The average T-ray power in a focused beam has developed from nW to μW levels,[140,141] with current systems achieving 30–40 μW of average THz power.[142,143] The availability of high power, high repetition rate femtosecond laser sources has enabled PCAs to be driven into saturation,[144,145] and photoconductive substrates with high breakdown voltages permit large bias fields.[146]

The maximum power emitted from a PCA depends on the photoconductive substrate and the coupling efficiency of the antenna. THz power scales with both the optical pulse power and the DC bias field, as indicated in Fig. 3(b). A photoconductive switch material should have a high breakdown voltage, a low optical refractive index, low bandgap, low carrier lifetime, high optical absorption and high carrier mobility.[147–149] The polarization of the normally-incident optical pulse is perpendicular to the bias electrodes.[150] High power PCAs were demonstrated initially on implanted silicon-on-sapphire and low-temperature-grown (LT) GaAs,[151] and since with semi-insulating GaAs,[143,144] ion-implanted GaAs and InGaAs.[142] Antenna design and coupling influences the efficiency, bandwidth and radiation pattern of T-ray emission.[141,152] Many antenna geometries have been explored,[141,153–160] however high power T-rays are still generated with coplanar strip lines and large aperture emitters.[142,143]

A broad bandwidth is the second most desirable characteristic of a T-ray source, which relies on a short THz pulse duration. PCAs in GaAs typically have a useful bandwidth extending from less than 100 GHz to 2 THz,[133] which can be extended to 4 THz by injecting carriers close to the band edge.[158,161] Bandwidths up to 6 THz[143] have been reported for PCAs, but pulse duration continues to be limited by carrier mobility, leading to interest in optical rectification emitters (Sec. 3.3.2). T-ray bandwidth can be controlled by shaping the optical pulse, to either tune the output frequency or increase the overall output power.[90,162–164]

The radiation pattern of a PCA is important for designing beam-steering optics and imaging systems. Generally, THz radiation is coupled out from the antenna and collimated into a beam with a hemispherical lens.[5,139,165–167] The radiation pattern for the common dipole antenna is essentially dipolar, with a weak quadrupole component perpendicular to the bias field,[168] weak elliptical polarization[169] and propagates as a Gaussian into the far-field[170] with high frequency components concentrated in the center of the beam.[171,172] Near-field effects are important for understanding screening of the bias field, pulse propagation and applications in near-field imaging, and are detailed in Sec. 5.6.

PCA emitters have been integrated into commercial optical fiber-coupled T-ray systems, for their convenience and high power.[9] Miniature PCAs have been demonstrated on optical fibers for potential endoscopic applications.[173] T-ray emission has been observed from air as the photoconductive switch[174] and PCAs have been incorporated directly into ultrafast laser cavities to produce up to 7 μW of pulsed THz power.[175]

3.3.2. *Optical rectification*

Optical rectification (OR) is a nonlinear optical effect that can generate T-ray pulses with very large bandwidth from ultrafast optical pulses.[178] OR is a second-order effect that occurs in materials with a non-zero $\chi^{(2)}$, or EO, coefficient, and is referred

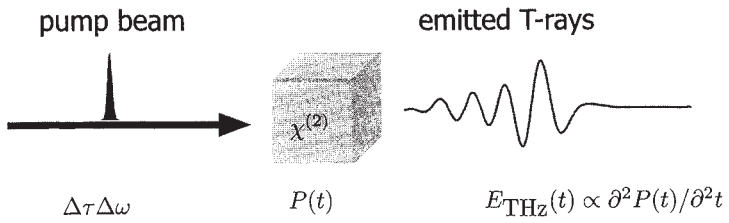

Fig 4. OR is a second-order nonlinear effect, whereby an ultrafast electric field pulse is rectified in a $\chi^{(2)}$ medium. The ultrafast pump pulses induce an transient polarization, $P(t)$, which in turn emits a THz-bandwidth pulse. The time evolution of the THz pulse is given by the second time derivative of the polarization transient.[176,177]

to as the inverse EO, or Pockel's effect.[52,179,180] OR was first observed in 1962, with a high intensity 100-ns laser pulse causing a DC polarization in certain crystals.[181] With the development of ps and fs laser systems, faster polarization transients were induced, with bandwidths reaching to THz frequencies.[182–186] The ultrafast 'shock wave' propagating through a nonlinear medium was observed to generate Čerenkov THz radiation, but was confined to the medium due to total internal reflection.[187–189]

After the development of the PCA for free-space THz generation, the Čerenkov radiation was coupled out of $LiTaO_3$ into THz beams.[129] The power and bandwidth of T-rays generated by OR are determined by the driving optical pulse, the nonlinear $\chi^{(2)}$ coefficient of the crystal, the crystal damage threshold, the output coupling constraints and the visible-to-THz phase matching.[177,190]

Unlike a PCA, the THz power generated by OR is due only to the incident laser power.[191] The maximum optical power is limited by available ultrafast laser sources and by damage to the medium.[192] With the development of high-power solid-state mode-locked lasers, sub-100-fs pulse trains can be generated at 10s of MHz repetition rates and up to 2 W of average power. The generation efficiency depends on the magnitude of the $\chi^{(2)}$ coefficient, THz absorption in the material and phase matching between the optical and THz pulses.[193,194] The magnitude of the $\chi^{(2)}$ coefficient varies with the crystal cut and orientation.[176,195–197] Although DAST has a very large EO coefficient,[198,199] it is hygroscopic. The most popular EO material is ZnTe, because of its physical durability and excellent phase matching.[177] With a broadly focused optical pump beam, to avoid damaging the medium, and a ZnTe crystal, nW T-ray average power can be generated by OR. OR saturation due to second harmonic generation of the pump beam at high optical fluence has been studied in ZnTe.[192] OR saturation has also been studied in $LiTaO_3$, $LiNbO_3$ and DAST.[191]

OR owes its intrinsically broad bandwidth to Pockel's effect, which operates on a fs time scale.[179] The actual bandwidth depends on the duration of the optical pump pulse. With ultrashort optical pulses, down to 15 fs in duration, THz pulses have been generated with spectra extending to the mid-infrared.[200,201]

OR effects have been observed in air,[202] in biased quantum wells (QWs),[203]

periodically-poled $LiNbO_3$ (PPLN), in poled polymers,[204] in polymer thin films,[205] in super-conducting thin films,[206] and from beating in coupled quantum wells.[207] T-rays generated from OR in PPLN can be tuned by the poling period, the temperature or the crystal orientation.[208–211] Typically, OR is driven by ultrafast pulses from a solid state Ti:sapphire mode-locked laser, although 1.55-μm light has been used in optical fiber-based systems.[212]

3.3.3. *Pulsed photomixing*

Pulsed photomixing in biased semiconductors is related to THz generation in PCAs (Sec. 3.3.1), CW photomixing (Sec. 2.5) and CW nonlinear DFG (Sec. 2.4). Photomixing in a PCA uses two pulses from an ultrafast laser, split in an interferometer with consequent phase control, which provides control over the output T-ray pulse shape.[140,213,214] Shaping of the optical near-infrared pump pulse enables T-ray pulse shaping generated from nonlinear optical mixing effects.[59,215,216] Mixing pulses with an equal frequency chirp creates a difference frequency that depends on the phase delay of the two pulses in the arms of the interferometer. Chirped pulse mixing therefore generates relatively narrowband, frequency-tunable T-rays.[217,218] Photomixing has been observed in quantum well structures using resonant excitation of plasmons.[219]

3.3.4. *Photoexcited semiconductors and superconductors*

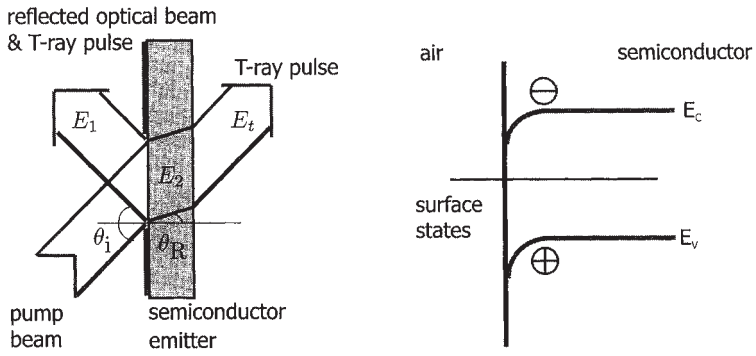

(a) THz surface current generation

(b) Surface bias field in a bare semiconductor

Fig 5. T-ray generation from surface fields in unbiased semiconductors.[220,221] The intrinsic bias at a semiconductor surface is shown in Fig. 5(b). This bias field sweeps ultrafast photo-generated carriers, and for high-mobility semiconductors, the resulting current transient acts as a source of THz. Fig. 5(a) shows THz generation from a semiconductor surface either in transmission or reflection. θ_i is set at Brewster's angle to improve coupling of the optical and THz beams at the air-semiconductor interface.

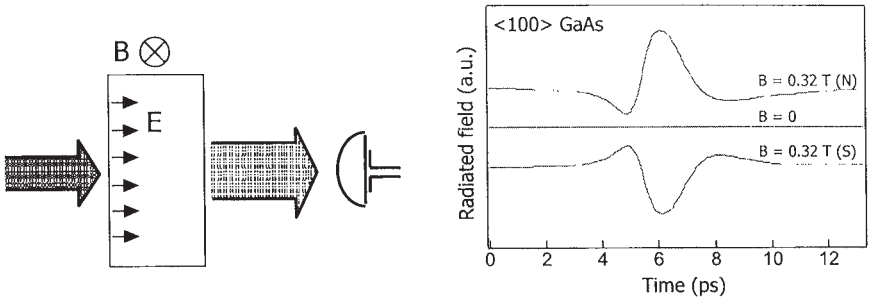

(a) Emission schematic

(b) Dependence on applied magnetic field

Fig 6. T-ray generation from an unbiased semiconductor in a magnetic field. The intrinsic bias field, E, is shown normal to the semiconductor surface. The THz generated from an unbiased semiconductor is enhanced by the application of a DC magnetic field, as seen in Fig. 6(b). This effect is discussed in Sec. 3.3.4.

T-ray emission has been observed from unbiased semiconductors, and attributed to a number of effects. Notably among these are OR, photocarriers accelerated in the semiconductor surface field, coherent polarization oscillations,[222] coherent phonons,[223-226] coherent plasmon oscillations,[227,228] coherently controlled photocurrents,[135] transitions in coupled quantum wells,[229] intersubband transitions in quantum wells,[230] coherent charge oscillations in quantum wells,[231] Rabi oscillations,[232] Stark wave packets,[233] coherent Bloch oscillations in superlattices,[234-238] photo-Dember fields[239,240] and superluminal ionization fronts.[136]

T-ray emission has been observed in high-T superconductors due to ultrafast modulation of the superconductuvity.[241]

T-ray emission from unbiased semiconductor surfaces excited with ultrafast optical pulses was first observed in 1990 by Zhang *et al.*[220,221] Fig. 5 shows a schematic of THz generation from an unbiased semiconductor surface and the intrinsic bias field at the surface. The radiated THz field is proportional to the optical pump power and is due to a combination of OR,[176,242] bulk DFG[243] and photocarrier acceleration in the surface field of the semiconductor.[244,245] T-ray emission from semiconductor surfaces is influenced by the magnetic field surrounding the emitter,[246,247] which can be used to switch or enhance the generation efficiency.[248-252] T-ray emission from an unbiased GaAs wafer in a switchable magnetic field is shown in Fig. 6, indicating enhancement and phase reversal of the generated THz pulse. This enhancement has been explained by considering the alignment of the induced radiating dipoles and total internal reflection at the semiconductor-air interface.[253,254]

Optical pulse shaping and magnetic field control enables both enhancements and spectral control of the emitted T-rays.[255,256] T-ray emission from semiconductor heterostructures has been coherently controlled by shaping the optical pump pulse [257]

3.4. *Detection*

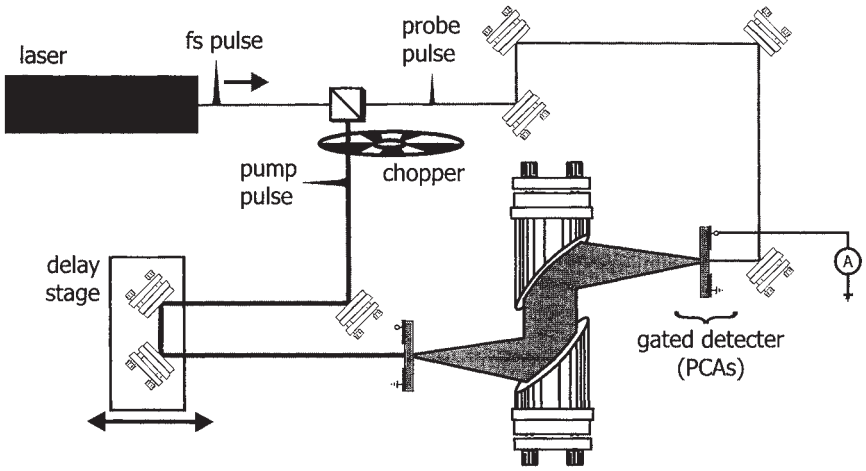

Fig 7. This T-ray generation and detection schematic is an example of a pump–probe experiment. The pump pulse initiates an effect, which is detected by a gated detector. The time delay is varied between the commencement of the effect and when the detector operates. Thus the time evolution of the effect, in this case a T-ray pulse, can be sequentially sampled. The chopper AC modulates the THz beam at an audio to RF frequency f, and the signal current is demodulated in a lock-in amplifier. The gated detector is a PCA, described in Sec. 3.4.1.

Although CW detection techniques can be used for T-ray detection, the high SNR of T-ray spectrometers is due to time-gated detection (pump-probe) techniques. Gated detection relies on an optically switched detector, and part of the pulse split from a mode-locked laser, as illustrated in Fig. 7.

A feature of PCA and EO detection is the large DC background in the probe compared to the modulation due to the THz field. A common method to observe a T-ray signal is to AC modulate the free-space THz beam at a certain frequency, indicated by the chopper in Fig. 7, then electronically filter out any signals not at this modulation frequency. This modulation frequency is pushed as high as possible because laser noise is greater at low frequencies (it has a $1/f$ characteristic[258]), up to around 3.5 MHz, where the noise floor is set by instrumentation and photon noise.[259]

Gated detection systems acquire a time-domain response by scanning the time delay of the detector across the generated waveform. For T-ray generation, the detector operates on a fs time scale, which is orders of magnitude faster than the ps duration of the THz pulse that is being sampled. This delay is achieved with a variable path length, represented by the delay stage in Fig. 7. The total length of the delay stage movement determines the duration of the sampled pulse. The speed at which the waveform is acquired is limited by the desired SNR. A faster scan leaves less time for the signal at each point to be averaged with, for example, a lock-in amplifier, thus increasing the noise level.

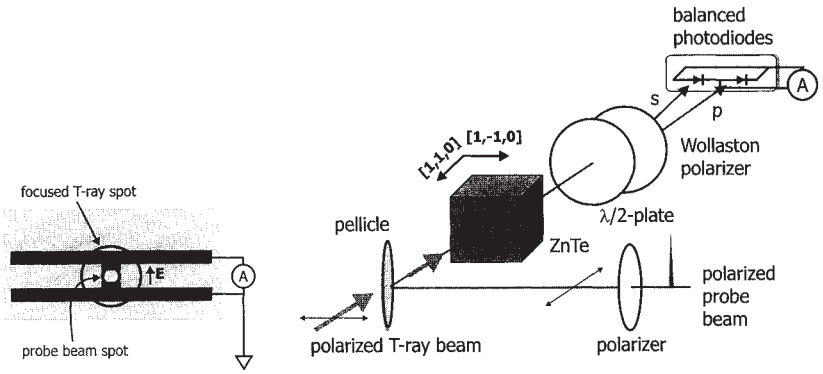

(a) PCA detection (b) EO sampling

Fig 8. PCA and EO sampling. Fig. 8(a) shows a photoconductive dipole antenna. The large T-ray spot biases the electrodes with a free-space electric field of ps duration. The fs probe switches the electrodes with transient photocarriers, allowing a current to flow, which is detected by an ammeter. The current flow is proportional to the applied THz field. Fig. 8(b) shows the EOS scheme, which is more complex than PCA detection, but has better sensitivity and a broader bandwidth. The polarized T-ray electric field induces a birefringence in the detector, depending on the $\chi^{(2)}$ coefficient of the specific crystallographic orientation of the crystal.[197] A pellicle beam-splitter directs the pump and probe beam collinearly through the EO detector. The polarization of the probe beam is rotated by the birefringent medium, which is converted to an intensity modulation using an analyzer. The analyzer is a polarizing beam splitter or second polarizer rotated 90° from the first polarizer. This is a typical crossed polarizer detection method.[179,180] The analyzer, in this diagram a Wollaston beam splitter, directs the two polarizations to balanced photodiodes. A half-wave plate is rotated to balance the difference current to zero for zero THz field, accounting for residue birefringence in the EO crystal.

The two major methods of T-ray detection, as with generation, use PCAs or EO crystals.

3.4.1. *Photoconductive sampling*

Photoconductive sampling was developed in conjunction with PCA emitters. For T-ray detection, an unbiased PCA is placed in the T-ray beam path and gated with an optical probe pulse. A PCA in detection configuration is shown in Fig. 8(a). The gating pulse allows current to flow in the PCA, which is connected to an ammeter. The THz electric field biases the PCA, and the current is therefore proportional to the T-ray field. The optical probe pulse has a far shorter duration than the T-ray pulse, so the T-ray waveform is sampled in time by changing the time delay of the two optical pulses.[121,260] The detected T-ray signal is a convolution of the incident T-ray waveform and the response of the PCA.[261,262] In spectroscopy experiments, the detector and emitter responses are accounted for by deconvolution, or signal normalization with a reference pulse, as discussed in Sec. 4.2.

Initially fabricated on LT-GaAs, PCA detectors achieved a maximum bandwidth

of ≈2 THz.[127,139] Recent experiments with ultrafast gating pulses of 15-fs duration have extended the detection bandwidth to 40 THz.[263,264] LT-GaAs PCAs can be gated with 1.55-μm wavelength light through a two-photon absorption process.[265]

3.4.2. *Electro-optic sampling*

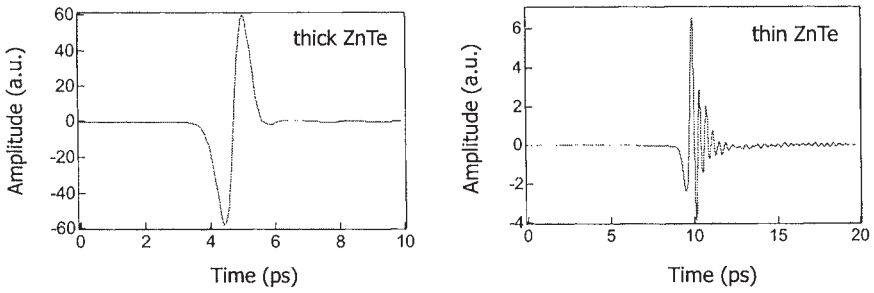

(a) Broadband T-ray pulse

(b) Ultra-broadband T-ray pulse

Fig 9. Crystal thickness determines signal sensitivity and bandwidth in EOS. The two figures above show a T-ray pulse sampled with two ZnTe detectors. Typically a 2-mm-thick ZnTe crystal provides a high signal, but a bandwidth limited to under 10 THz. ZnTe is a good EO sensor because of phase matching between the THz and optical pulses. Ultra-broadband phase matching is, however, not possible, so a thinner crystal detects higher frequencies. Using a 10-μm-thick crystal, frequencies up to 70 THz have been measured.[266]

Electro-optic sampling (EOS) is a broadband T-ray sampling technique. Like photoconductive sampling, the detector is gated by a time-delayed probe pulse. The detector is an EO crystal, placed between crossed polarizers, and the optical and THz beams propagate collinearly through it, shown in Fig. 8(b). The incident T-ray pulse modulates the birefringence of the crystal, through Pockel's effect.[52,179,195] The induced birefringence in the crystal is proportional to the electric field strength of the T-ray pulse, and causes a rotation of the polarization of the optical pulse. The crossed polarizers effect an amplitude modulation of the optical pulse, which is proportional to the polarization modulation and thus the THz field strength.

Initially used in the characterization of high-speed electronic circuits,[120,121,269–271] EOS was first used for free-space THz detection in 1995 by Wu and Zhang.[130] Although more difficult to align experimentally than PCA detectors,[164,197,272–275] EOS soon demonstrated a wide bandwidth and high sensitivity.[193,194,276–279] The sensitivity of EOS depends on the EO $\chi^{(2)}$ nonlinear coefficient of the detection crystal, which must be transparent to the probe beam, and the quality of phase matching between the T-ray and optical pulses.[164]

The central trade-off for EOS is the thickness of the crystal. A thicker crystal provides a longer interaction length for the coupled pulses, hence a larger signal. However, since perfect phase matching between the optical and THz pulses is not possible, a thinner crystal with less dispersion and provides a broader detection

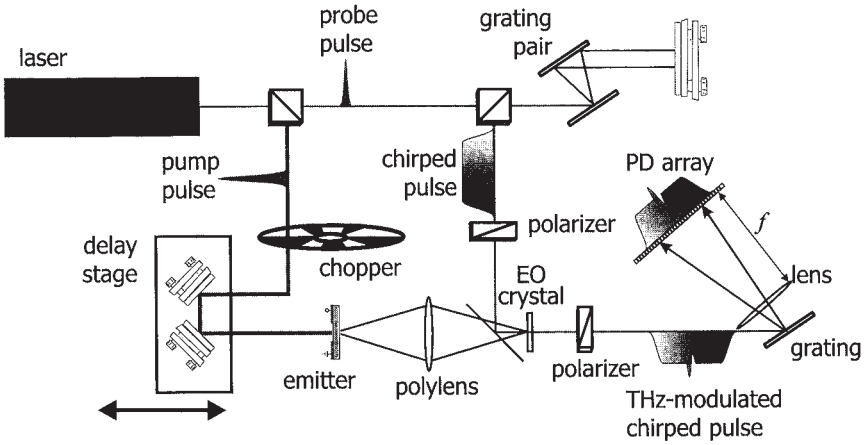

Fig 10. The chirped pulse single-shot T-ray pulse detection technique. This is similar a typical T-ray detection system, using OR and EOS, except the probe pulse is stretched to a ps duration with a grating pair. When the T-ray and probe pulses propagate collinearly through the EO detector, they both have approximately the same duration, thus different parts of the probe pulse experience different intensity modulation in the EOS. As the pulse is chirped, these different parts are separated with a spectral grating, and detected with a linear photodiode (PD) array. Apart from a background measurement of the unmodulated chirped pulse required to extract the T-ray waveform, the technique can measure the entire T-ray waveform in a single shot. The T-rays are focused from emitter to detector in this scheme with a polyethylene lens, which had a very low dielectric constant for THz.[267] For single-shot imaging, discussed in Sec. 5.4, the T-ray beam is spatially expanded in 1D and the PD array is replaced with a CCD.

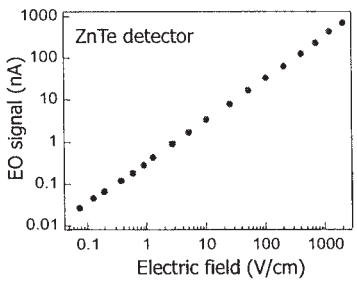

(a) To electric field

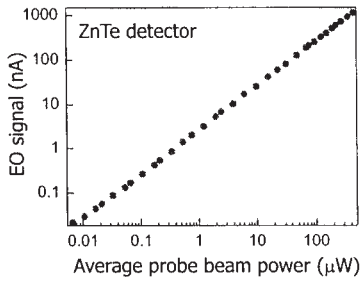

(b) To probe beam power

Fig 11. These results demonstrate the linearity of ZnTe as a T-ray sensor, to both the probe beam power and the T-ray electric field. The linearity is (<2%) for over more than 5 orders of magnitude.[268]

bandwidth.[280] Fig. 9 shows T-ray waveforms detected with an EO crystal, indicating the increased bandwidth but reduced signal amplitude for a thinner detector. Using sub-100-μm-thick crystals, mid-infrared pulses are detectable.[266,281,282] The most popular crystal used for THz EOS is ZnTe due to its high EO coefficient, low group velocity mismatch between THz pulses and optical probe pulses, and good mechanical properties.[283] GaP,[284] GaAs,[285] multilayered EO polymer films,[205] poled polymers[286] and DAST are among alternative materials used for EOS.[287–289]

A primary advantage of EOS is its extension to 2D imaging. With a larger EO crystal and an expanded optical beam, the intensity modulation across the transverse T-ray beam can be imaged with a CCD.[268,290] Rapid 2D, 3D and single-shot T-ray imaging is discussed in Sec. 5.4.[172,267,291–294]

Single-shot detection is fundamentally different to normal gated detection in that the entire T-ray waveform is measured by each probe beam pulse, and then detected spatially. The ps time duration of the T-ray pulse is transferred to the spatial domain using non-collinear propagation of the T-ray and probe beams in an EO crystal[292] or collinear propagation of a chirped probe beam. In chirped probe detection, the spatial distribution of the T-ray pulse along the propagation axis in the EO crystal is mapped onto the different wavelengths of a chirped probe pulse, and then separated with an optical grating[267] or streak camera.[295] A schematic of chirped pulse detection is shown in Fig. 10. Chirped pulse detection can be designed with automatic background cancelling with dual photodetector arrays,[291] or extended to 1D imaging with a CCD. Single-shot detection is used for electron bunch measurements in FELs[296] and rapid imaging applications (Sec. 5.4).

3.4.3. *Magneto-optic detection*

Magneto-optic detection is analogous to EOS in that the transient magnetic component of a propagating free-space THz pulse can be detected using crossed polarizers and a magneto-optic crystal.[297] The THz magnetic field is detected using the Faraday effect in an optical medium.[179]

3.5. *T-ray propagation*

3.5.1. *Propagation & filters*

With the development of free-space T-ray emitters and detectors, interest increased in the propagation of THz-bandwidth pulses in a vacuum and through quasi-optical elements. T-ray systems use quasi-optical collimation and focusing elements, including gold-coated off-axis parabolic mirrors,[131] silicon hyperhemispherical lenses,[167,298] anti-reflection coatings,[299] variable phase polarization compensators,[300] reflective gratings, teflon prisms,[301] and transmissive optics fabricated from silicon or polyethylene.[302] T-rays have been used to study single cycle pulse propagation,[303] the Gouy phase shift at a focus[304] and THz whispering-gallery modes in cylinders.[305] Spatial filters are fabricated using metal, which has a very high absorption at THz frequencies,[306] including high-pass filters with metal slits,[307,308] apertures,[309,310] band-pass filters,[311] low pass filters of glass beads in polyethylene,[312] filter cascades[313] and dichoric filters.[314,315] Fresnel lenses have been modeled and constructed from silicon to allow frequency-dependant focusing of the broadband T-ray beams.[316] A silicon binary lens for THz wavelengths is pictured in Fig. 12(a) and the sharp THz

focus is shown in Fig. 12(b). T-ray beam propagation has been studied in scattering media[317] and simulated with finite-difference time-domain techniques.[318]

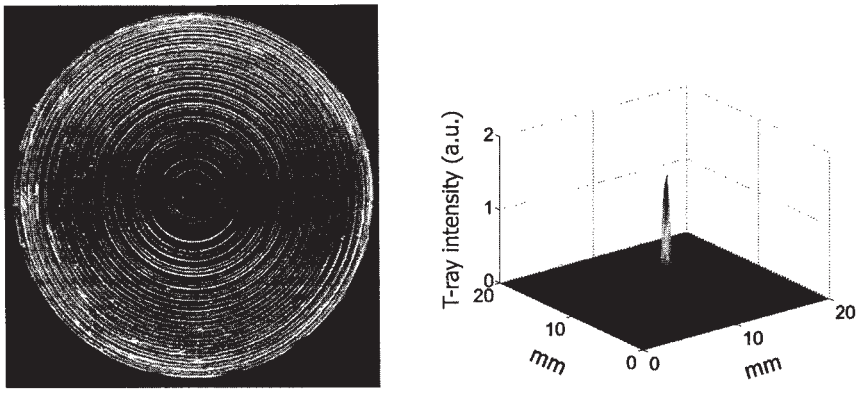

(a) 8-level silicon Fresnel lens

(b) Focused T-ray electric field

Fig 12. A Fresnel lens constructed from high-resistivity silicon demonstrates sharp focusing of the terahertz beam. This is comparable to a conventional refractive THz lens.[316]

The study of T-rays propagating through air and optical elements has been greatly enhanced by techniques for imaging the T-ray emission patterns and beam profiles using either scanned PCAs (Sec. 5.2) or EO detection (Sec. 5.6).

Dynamic T-ray filters have been demonstrated using free carrier generation in a semiconductor to block, or reflect, the THz pulse. This transient mirror can be used to slice up very short duration sections of a T-ray pulse,[319] or reflect a sub-wavelength diameter cross-section of the beam for near-field studies, as discussed in Sec. 5.6.

3.5.2. *Transmission and reflection*

T-ray spectrometers can be used either in transmission or in reflection.[320] The T-ray pulses are detected after transmission through a sample, or reflection from its surface. The mode used depends on the type of sample being studied. For samples with very high absorption, no transmitted signal is detectable. However, normalizing the system response is more difficult with a reflective system, because a reference pulse must be taken without the sample present, and it is difficult to maintain exactly the same free-space path length between the emitter and detector. Alternative geometries used for T-ray spectroscopy and analysis techniques are discussed in Sec. 4.2

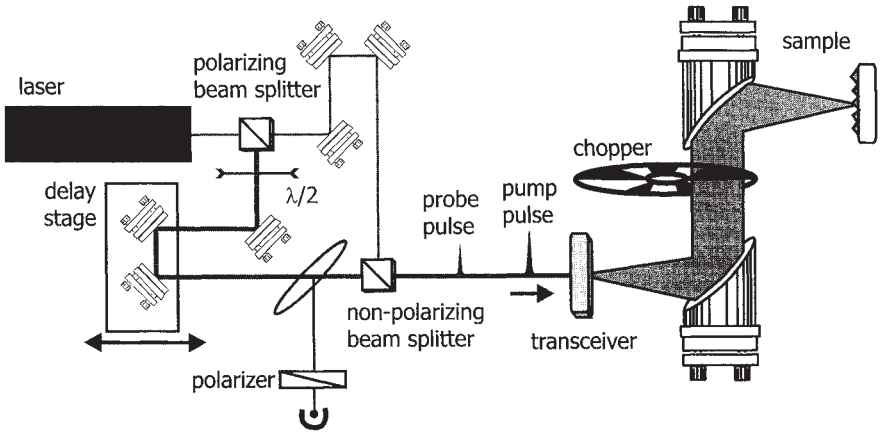

Fig 13. free-space EOS transceiver schematic. An EO transceiver combines optical rectification and EOS in the same EO crystal. The pump and probe beams, with variable path lengths, are combined collinearly with a non-polarizing beam splitter and directed into a EO crystal. The pump beam generates T-rays, which are focused onto a sample and reflected back into the transceiver. The delayed probe beam, with orthogonal polarization to the pump, detects the reflected T-ray pulse by EOS and is then passed though an analyzing polarizer into a photodetector. The half-wave plate, $\lambda/2$, is used to rotate the polarization of the pump beam to the optimal polarization for the orientation of the EO crystal and the probe polarization.[197] A PCA transceiver has a similar geometry, except the reflected T-ray pulse is detected as a gated current in the PCA.[321]

3.5.3. *Transceivers*

In an extension of the standard T-ray reflection system, the roles of emitter and detector can be combined into one device, either a PCA or an EO crystal.[197,321–323] In a T-ray transceiver, the pump and probe pulses travel collinearly with opposite polarization and an adjustable time-delay to reflect off a sample, as shown in the schematic in Fig. 13. The EO transceiver extends into free space the concepts of early spectroscopy with THz confined to a single crystal by total internal reflection.[124,324]

3.5.4. *Waveguides*

THz propagation in waveguides is related to microwave technology in the same way that focusing and filtering in free space are related to optical techniques.[325] Waveguide propagation is important in studying near-field T-ray devices,[326–330] THz interconnects,[331–333] THz cavities[334] and ultra-sensitive T-ray spectroscopy.[335]

4. Sensing

4.1. *Introduction*

T-ray sensing involves applying T-ray techniques to the study of materials by monitoring transmitted or reflected radiation. The THz spectrum is populated by energy transitions of less than 0.1 eV, which correspond to different rotational and torsional states of a whole molecule.[336] For larger molecules, the FIR has fewer transitions

than the near-infrared, which can be very densely populated. The THz bandwidth corresponds to energy transitions in superconductors, plasma states, lattice vibrations and other resonances in crystals.[337]

Pulsed THz spectroscopy is a coherent technique, where both the amplitude and phase of the THz pulse are measured. Coherent detection enables direct calculation of absorption and refraction profiles without using the Kramers-Kronig relations. T-ray spectrometers provide very high SNRs and a broad bandwidth, making them attractive to sensitive spectroscopic studies on the THz regime. T-ray spectroscopy builds upon a rich history of sub-mm and FIR spectroscopy.[338]

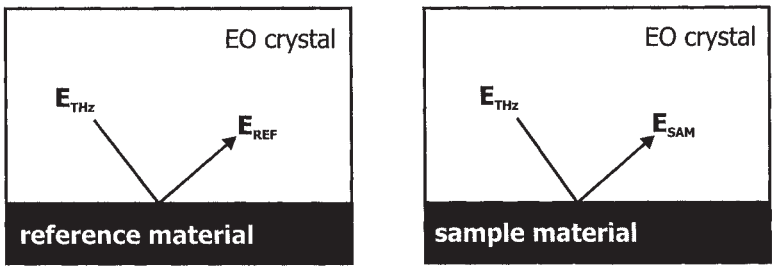

(a) TIR reference (b) TIR sample

Fig 14. Geometry for TIR THz-TDS. T-rays are generated in the EO material and detected by a probe pulse after interacting with a reference or sample by frustrated TIR.[124]

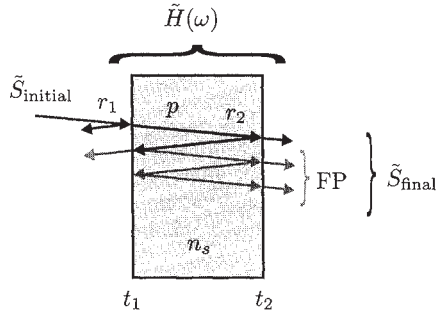

Fig 15. Transmission through a dielectric slab.

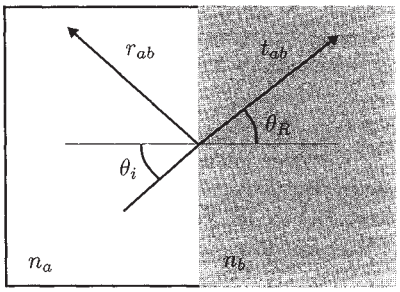

Fig 16. Notation for the reflection and transmission coefficients at a dielectric interface.[179,339]

4.2. *T-ray time-domain spectroscopy*

The first pulsed THz spectroscopy measurements were performed in reflection, with the THz confined by total internal reflection to an EO crystal that acted as both

emitter and detector. THz spectroscopy could only be performed on the EO crystal itself,[324] or on materials placed in direct contact with the EO crystal, into which the radiated pulses were coupled by frustrated total internal reflection.[124] Fig. 14 is a sketch of TIR THz time-domain spectroscopy (TDS). The basic elements of THz-TDS are present: a pump pulse to generate the THz radiation and a time-delayed probe pulse to sample the THz pulses, both with a sample and without.

Time-domain spectroscopy is a long-established method in the study of electronic circuits, but THz-TDS was its first application to the quasi-optical study of dielectrics. THz-TDS is markedly different from optical spectroscopic techniques that rely primarily on incoherent detectors. Any sample can be characterized by a complex dielectric constant $\tilde{\epsilon}(\omega)$, which describes the attenuation and delay of transmitted radiation at a given frequency ω. A coherent detector is able to determine the delay, or phase relationship, between incident radiation with and without a sample present, and thus directly measure both the real and imaginary parts of $\tilde{\epsilon}$. With an incoherent detector, however, additional processing is required to estimate the phase delay caused by a material, using the Kramers-Kronig relationships, integrals that relate the real and imaginary parts of the complex dielectric constant.[339]

In THz-TDS, we are interested in measuring $\tilde{\epsilon}(\omega) = \epsilon'(\omega) - j \cdot \epsilon''(\omega)$, or equivalently $\tilde{n}(\omega) = n(\omega) - j \cdot \kappa(\omega)$, which is the complex index of refraction of the material, where $(\tilde{n})^2 = \tilde{\epsilon}$. The dielectric constant is typically referred to in the field of high-speed electronics and the refractive index in THz optics. Estimating these material properties from THz-TDS measurements requires calculations that depend on the system configuration. Essentially, an expression is derived for the expected delay and attenuation of the pulse due to passing through or reflecting from the material of interest. This expression is in terms of the complex material properties and the thickness of the sample(s), and can be written as a product of factors in the frequency domain. The interaction between a sample and the spectral components $\tilde{S}(\omega)$ of the T-ray radiation can be expressed as a transfer function $\tilde{H}(\omega)$, which is a product of reflection r, propagation p and transmission t coefficients, depending on the geometry of the system, as sketched in Fig. 15,

$$\tilde{S}_{\text{final}}(\omega) = \tilde{H}(\omega) \cdot \tilde{S}_{\text{initial}}(\omega). \tag{1}$$

The reflection and transmission at each material interface depend on $\tilde{\epsilon}$ (or equivalently $\tilde{n}$) of the adjacent dielectrics, and the polarization of the incident light, as shown in Fig. 16. For TE polarization, the complex frequency-dependent coefficients of transmission $t(\omega)$ and reflection $r(\omega)$ are

$$r^s_{ab}(\omega) = \frac{\tilde{n}_a \cos\theta_i - \tilde{n}_b \cos\theta_R}{\tilde{n}_a \cos\theta_i + \tilde{n}_b \cos\theta_R}, \tag{2}$$

$$t^s_{ab}(\omega) = 1 + r^s_{ab}, \tag{3}$$

and for TM polarization,

$$r^p_{ab}(\omega) = \frac{\tilde{n}_b \cos\theta_i - \tilde{n}_a \cos\theta_R}{\tilde{n}_b \cos\theta_i + \tilde{n}_a \cos\theta_R}, \tag{4}$$

$$t^p_{ab}(\omega) = \frac{\tilde{n}_a}{\tilde{n}_b}(1 + r^p_{ab}), \tag{5}$$

where $\tilde{n}_a$ and $\tilde{n}_b$ are the complex refractive indicies of the homogeneous materials before and after the interface, θ_i is the incident angle and θ_R is the refracted angle. With knowledge of the refractive indicies $\tilde{n}_a$ and $\tilde{n}_b$, θ_R can be determined from θ_i and Snell's Law, $\tilde{n}_a \sin\theta_i = \tilde{n}_b \sin\theta_R$. For a sample oriented normal to the radiation path, $\theta_i = 90°$, the propagation equations simplify to[6]

$$t_{ab}(\omega) = \frac{2\tilde{n}_a}{(\tilde{n}_a + \tilde{n}_b)}, \tag{6}$$

$$r_{ab}(\omega) = \frac{\tilde{n}_a - \tilde{n}_b}{\tilde{n}_a + \tilde{n}_b}. \tag{7}$$

Radiation propagating a distance d through a linear medium, $\tilde{n}_a$, is delayed and attenuated according to the factor

$$p(\omega) = e^{-j\tilde{n}_a \omega d/c_0}, \tag{8}$$

where c_0 is the speed of light in a vacuum.

A final linear propagation effect occurs due to multiply-reflected radiation between two plane parallel interfaces, shown in Fig. 15. These are Fabry-Pérot reflections, or *etalon* effects, and are described by a sum of reflections,

$$\mathrm{FP}(\omega) = \sum_{k=0}^{\infty} \left\{ r_{23} \cdot p_2^2 \cdot r_{21} \right\}^k, \tag{9}$$

where k is the number of reflections, and depends on the time duration of the measured waveform and the delay caused by propagation between the interfaces. For a very large number of multi-reflections, $k \to \infty$, the Fabry-Pérot factor can be approximated by

$$\mathrm{FP}(\omega) = \frac{1}{1 - \left(\frac{\tilde{n}_2 - \tilde{n}_1}{\tilde{n}_2 + \tilde{n}_1}\right)\left(\frac{\tilde{n}_2 - \tilde{n}_3}{\tilde{n}_2 + \tilde{n}_3}\right) \cdot e^{-j2\tilde{n}_2 \omega d_2/c_0}}. \tag{10}$$

The Fabry-Pérot factor introduces frequency-domain interference fringes into transmitted or reflected radiation from thin samples, and is unavoidable in very thin samples.

Typically in THz-TDS experiments, it is simplest to measure two time-domain pulses, a reference y_r and a sample pulse y_s. The characteristic response of the entire system, which depends on many factors including the emitter and detector, is canceled out by normalizing the sample pulse with the reference pulse in the frequency domain. This is *deconvolution*. The complex frequency spectra $\tilde{S}_r$ and $\tilde{S}_s$ are calculated using numerical Fourier transforms from the time-domain waveforms sampled in the the experiment,

$$\tilde{S}_r = \mathcal{FT}(y_r), \tag{11}$$

$$\tilde{S}_s = \mathcal{FT}(y_s). \tag{12}$$

The effect of the sample on the propagating pulses can be modeled using Eqs. (6)–(10), which provide a theoretical expression relating $\tilde{S}_r$ and $\tilde{S}_s$ to the material properties $\tilde{\epsilon}$. The material properties are then estimated by comparing the model to the

measured spectra. Depending on the complexity of the model expression, it may be possible to solve it analytically, otherwise an iterative curve-fitting procedure is used. The method described in this section is used for most THz-TDS measurements, with the model expressions for $\tilde{S}_r$ and $\tilde{S}_s$ varying with sample geometry. The expression of interest is the ratio of the complex sample spectrum to the complex reference spectrum, which enables the responses (transfer functions) of all invariant system components (for example, the emitter, detector, free-space propagation and mirror surfaces) to be canceled out. This ratio will be referred to as the deconvolved sample spectrum.

4.2.1. *Transmission*

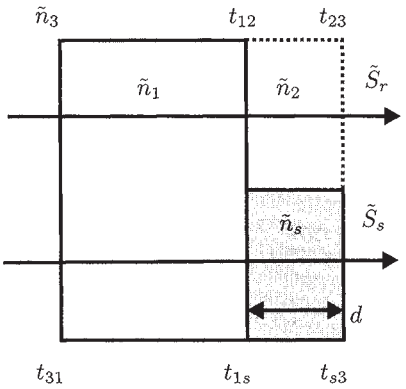

Fig 17. Notation for transmission geometry.

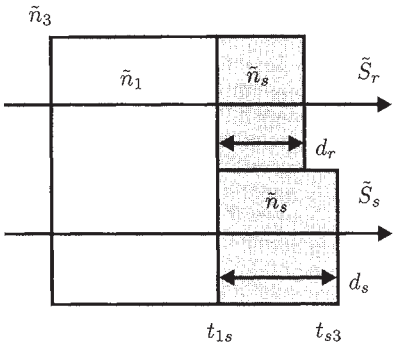

Fig 18. Notation for a dual-thickness geometry.

The simplest and most common geometry for free-space THz-TDS is transmission through an orthogonally-positioned slab of homogeneous material, characterized by $\tilde{n}_s$ (Fig. 15). This slab may be free-standing in air, or either deposited on or implanted into a substrate or holder. The model for the normalized sample spectrum depends on each individual experiment, but three main classes can be discerned: 1) thick samples, 2) thin samples and 3) dual-thickness samples.

A thick sample is a sample that causes sufficient delay so that the transmitted pulse can be measured without any overlap with the first Fabry-Pérot (FP) reflection. The exact requirements for the delay will depend on the desired total scan length (see Sec. 4.2.8). A diagram of a thick sample and the reference and sample paths is shown in Fig. 17. Note that the substrate material both before and after the sample must also be sufficiently thick to avoid any FP reflections in the measured pulses. Thin substrates are discussed below with thin samples.

In the thick sample geometry, the experimentally-measured spectral components of the reference and sample pulses can be modeled by

$$\tilde{S}_r(\omega) = A(\omega) \cdot t_{12} \cdot p_2 \cdot t_{23}, \tag{13}$$

$$\tilde{S}_s(\omega) = A(\omega) \cdot t_{1s} \cdot p_s \cdot t_{s3}, \tag{14}$$

where $A(\omega)$ is the product of all other system responses that remain constant between the sample and reference measurements. Using Eqs. (6) to (8), the ratio of transmission spectra can be entirely determined in terms of refractive indicies and the sample thickness,

$$\frac{\tilde{S}_s}{\tilde{S}_r} = \frac{\tilde{n}_s(\tilde{n}_1+\tilde{n}_2)(\tilde{n}_2+\tilde{n}_3)}{\tilde{n}_2(\tilde{n}_1+\tilde{n}_s)(\tilde{n}_s+\tilde{n}_3)} \cdot e^{-j(\tilde{n}_s-\tilde{n}_2)\omega d/c_0}. \tag{15}$$

This set of equations can be solved for the real and imaginary parts of $\tilde{n}_s$ using iterative techniques.[6] For the common case where the sample $\tilde{n}_s$ is placed in a vacuum, $\tilde{n}_1 = \tilde{n}_2 = \tilde{n}_3 = 1.0$, a simplified expression can be determined for the transmitted pulse (and any time-separated FP pulses).[340] For a sample with very low THz absorption, that is $\kappa_s \ll n_s$, analytic expressions for n_s and κ_s can be written in terms of the magnitude ρ and phase ϕ of the deconvolved sample spectrum,

$$\frac{\tilde{S}_s(\omega)}{\tilde{S}_r(\omega)} = \rho(\omega) \cdot e^{-j\phi(\omega)}, \tag{16}$$

$$n_s(\omega) = \phi(\omega) \cdot \frac{c_0}{\omega d} + 1, \tag{17}$$

$$\kappa_s(\omega) = \ln\left(\frac{4n_s(\omega)}{\rho(\omega)\cdot(n_s(\omega)+1)^2}\right) \cdot \frac{c_0}{\omega d}. \tag{18}$$

A thin sample is one where a number of Fabry-Pérot reflections overlap in the measured pulse train. Theoretically, this geometry can be modeled by multiplying Eq. (15) by an FP factor from Eq. (9) or (10), and then solving iteratively. In practice, however, this method amplifies errors from the measurement of d and from alignment; it is difficult, for example, to maintain collinearity between the multi-reflections in sample positioning.[340]

Thin substrates introduce a further level of complexity, as FP reflections from the substrate are overlaid on the detected pulse. The FP reflections depend on n_s and so cannot be deconvolved without approximations. An expression in the form of Eq. (15) can be written and solved iteratively, although not aligning all the FP reflections collinearly can introduce errors.

A dual-thickness measurement greatly simplifies modeling, and involves the reference pulse passing through the sample material, where the thickness is different from the sample pulse measurement, as shown in Fig. 18. The advantage of dual-thickness measurements is that both reference and sample pulses pass through the same interfaces, so for a thick sample, the normalized transmission is

$$\frac{\tilde{S}_s}{\tilde{S}_r} = \frac{p_s}{p_r}. \tag{19}$$

This results in two simple expressions for n_s and κ_s in terms of the difference between the two thicknesses. For the case where the sample thickness d_s is greater than the reference thickness d_r,[341]

$$n_s(\omega) = \phi(\omega) \cdot \frac{c_0}{\omega(d_s-d_r)} + 1, \tag{20}$$

$$\kappa_s(\omega) = \ln\left(\frac{1}{\rho(\omega)}\right) \cdot \frac{c_0}{\omega(d_s-d_r)}. \tag{21}$$

For thin dual-thickness samples, where multiple FP reflections are present, the expression for the normalized transmission is more complex and must be solved iteratively. The accuracy of these estimates can be calculated from the partial derivatives of Eqs. 20 and 21, using multiple measurements to obtain the experimental fluctuation of the normalized transmission.[342]

One of the major sources of error in material constant estimation is the measurement of the thickness d.[340] To increase the accuracy of measuring d and integrate it with T-ray spectroscopy, a number of schemes have been proposed to use a train of time-separated FP pulses from a sufficiently thick sample to simultaneously estimate $\tilde{n}_s$ and d.[340,343]

4.2.2. *Reflection*

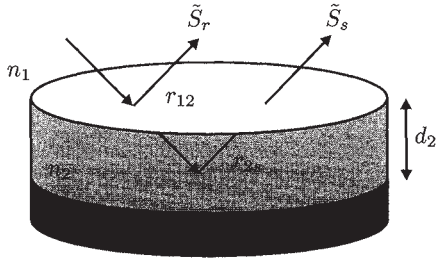

Fig 19. TIR spectroscopy using a first surface reflection as the reference pulse (Sec. 4.2.2).

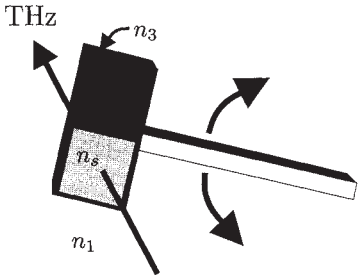

Fig 20. The dithered sample used in DTDS (Sec. 4.2.5).

Reflection spectroscopy is used for large or highly-absorbing samples. As with transmission spectroscopy, the structure of the sample plays a role in the analysis and accuracy of the parameter estimations.

The geometry of first surface THz spectroscopy is the same as the TIR geometry in Fig. 14, except the initial medium is typically air or vacuum. The measured spectral components of the reference and sample pulses are given by

$$\tilde{S}_r(\omega) = A(\omega) \cdot r_{12}, \tag{22}$$

$$\tilde{S}_s(\omega) = A(\omega) \cdot r_{1s}, \tag{23}$$

where r, the reflection coefficient, is found from the Fresnel equations above, and $A(\omega)$ represents the common factors between reference and sample. The reference interface is created with a material of known $\tilde{n}$. It is critical that the reference and sample path lengths are identical, which means the sample interface must be placed at the same position as the reference interface. This geometry allows the deconvolved spectrum $\tilde{S}_s/\tilde{S}_r$, which is calculated from the measured data, to be modeled in terms of the reflectivity of the reference r_{12},

$$\frac{\tilde{S}_s(\omega)}{\tilde{S}_r(\omega)} = \frac{r_{1s}(\omega)}{r_{12}(\omega)}. \tag{24}$$

r_{12} can be calculated from Eq. (4), or (2), depending on the T-ray polarization, since $\tilde{n}_1$, $\tilde{n}_2$ and the incident angle θ_i are known. Once r_{12} is known, Eq. (24) can be rearranged to estimate r_{1s}. The dielectric constant of the sample, $\tilde{\epsilon}_s = \tilde{n}_s^2$, is estimated by re-arranging Eq. (4) (or (2)),[124]

$$\tilde{\epsilon}_s(\omega) = \left[\sin^2\theta_i + \cos^2\theta_i \left(\frac{1 - r(\omega)}{1 + r(\omega)}\right)^2\right] \tilde{\epsilon}_1(\omega). \tag{25}$$

For reflection spectroscopy at or near normal incidence, which includes T-ray transceiver applications (Sec. 3.5.3), the above expressions simplify by setting $\theta_i \approx 90°$.

For measurements using total internal reflection (TIR), the position of the interface is set by the edge of the TIR prism. The difficulty is knowing accurately the refractive indicies of the prism and the reference material.[124] One method to avoid making a separate reference measurement is to use the pulse reflected from the top of a TIR prism, as shown in Fig. 19.[344] The reference pulse is detected from the air-silicon window interface, and the sample pulse comes from the silicon window-sample interface. The spectral reflection ratio of sample to reference can be written

$$\frac{\tilde{S}_s(\omega)}{\tilde{S}_r(\omega)} = \rho e^{-j\phi} \tag{26}$$

$$= \frac{t_{12} \cdot r_{2s} \cdot t_{21}}{r_{12}} \cdot e^{-j2\tilde{n}_2 d_2 \omega / c_0}, \tag{27}$$

for a deconvolved sample spectrum $\rho \cdot e^{-j\phi}$. The equations can then be solved iteratively.

If $n_1 \gg \kappa_1$ and $n_2 \gg \kappa_2$, for a Si TIR prism in air, the sample properties can be estimated by

$$n_s(\omega) = \frac{n_2(1 - \rho^2)}{1 + \rho^2 + 2\rho\cos\phi}, \tag{28}$$

$$\kappa_s(\omega) = \frac{2n_2\rho\sin\phi}{1 + \rho^2 + 2\rho\cos\phi}. \tag{29}$$

For samples with internal surface reflections, for example multiple quantum wells, the expression for reflection is complicated by FP factors.[324]

An integrated method for determining the thickness d of a thin surface layer, analyzed in reflection, is to observe frequencies where destructive interference occurs. This technique relies on the broadband nature of the T-ray pulse, requiring a bandwidth of 12 THz to measure films of 1-μm thickness.[345]

4.2.3. *Goniometric*

Measuring reflectance as a function of incident angle, specifically near Brewster's angle, involves a reflection geometry where the angle of incidence is variable.[8,346] These measurements require rotation of the sample by an angle θ and the detector by 2θ in a goniometer. With a series of measurements, the amplitude and phase

shift of the T-ray pulse can be observed around Brewster's angle, specifically the 180° phase shift for p-polarized radiation.

The refractive index of the thin film, $\tilde{n}_s$, can be estimated by measuring the reflectance at different angles and comparing it to a model based on the Drude and Fresnel equations. The Drude equation predicts the complex reflectance $\tilde{r}_D$ from a thin film,

$$\tilde{r}_D = \frac{r_{1s} + r_{s2}p_s}{1 + r_{1s}r_{s2}p_s}, \tag{30}$$

where r and p are given by Eqs. (7) and (8). The angles θ_s and θ_2 can be expressed in terms of θ_1, $\tilde{n}_1$, $\tilde{n}_s$ and $\tilde{n}_2$ with Snell's law. The values of d, $\tilde{n}_2$, $\tilde{n}_1$, λ and θ_1 are known for each measurement, so the reflectance can be modeled using estimates for $\tilde{n}_s$, and compared to experimental measurements. For two angles of θ_1, θ_{1A} and θ_{1B}, the T-ray spectra are $\tilde{S}_A(\omega) = A(\omega)\,\tilde{r}_{DA}$ and $\tilde{S}_B(\omega) = A(\omega)\,\tilde{r}_{DB}$, where $A(\omega)$ is a product of the transfer functions of the system which remain constant as the angle is varied. Thus the ratio of reflectances

$$\frac{\tilde{r}_{DB}}{\tilde{r}_{DA}} = \frac{\tilde{S}_B(\omega)}{\tilde{S}_A(\omega)}. \tag{31}$$

The value of $\tilde{n}_s$ that fits the model can be estimated by iteratively fitting the experimental reflectance ratio to the modeled reflectance ratio, using Eq. (30). Specifically, when measurements are made close to Brewster's angle, the large variation in phase enables more reliable estimates of $\tilde{n}_s$ than normal reflection or transmission measurements.[346]

4.2.4. *Ellipsometry*

THz ellipsometry is a technique to estimate a sample's dielectric constant by measuring two reflected pulses with s and p polarized T-rays.[347] The advantages of this technique over simple reflection spectroscopy is that there is no need to position a reference mirror. The equipment is simpler than for goniometric measurements.

4.2.5. *Differential*

THz thin film characterization requires very high sensitivity. Even with an SNR of 10^7, it is difficult to see phase shifts that are less than the coherence length of the radiation.[350] Picosecond T-ray pulses with a bandwidth of approximately 2 THz and a center frequency of 0.8 THz have a coherence length of approximately 150 μm. The phase shift caused by a dielectric sample in the T-ray radiation path is proportional to $(\tilde{n}-1)d/\lambda$, where $\tilde{n}$ is the complex refractive index of the medium, d is the sample thickness and λ is the T-ray wavelength. For small $\tilde{n}$ and d, this phase change is very difficult to detect in background noise. A differential technique may be used to reduce background noise.

Differential THz-TDS (DTDS) involves modulating the T-ray signal using only the thin film, and detecting the magnitude of this modulation using a lock-in amplifier (LIA).[351,352] The sample is a substrate half-covered with the film and half bare, as shown in Fig. 20. The thin film, characterized by the complex refractive index $\tilde{n}_s$, is supported by a substrate, $\tilde{n}_1$.

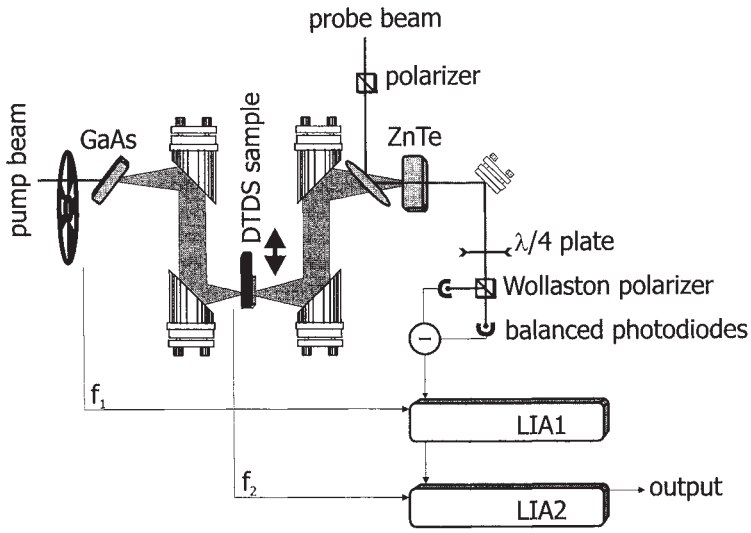

Fig 21. Double-modulated DTDS schematic. The pump and probe beams are split from a femtosecond laser and act to generate and detect the T-rays. The T-rays, shaded in grey, are collimated and focused with gold-plated parabolic mirrors. The T-ray electric field is converted to an electronic signal with the EO crystal, a quarter wave plate ($\lambda/4$) and balanced photodiodes. Two lock-in amplifiers (LIAs), with the shaker and an optical modulator, implement the double modulation scheme. The DTDS output signal depends on the differences between the films on opposite ends of the slide.[348,349]

For a typical T-ray spectrometer, the major source of noise is the pump laser, which is very sensitive to slow fluctuations in temperature. These fluctuations can cause larger changes in the detected T-ray signal than the thin film sample itself. The advantage of differential spectroscopy is that the signal transmitted through the film is compared to the signal through the substrate at each point of the delay stage, thus normalizing the laser-based fluctuations. A more complete discussion of the noise present in DTDS and how it can be further reduced by double modulation is found in Mickan *et al.*[353–355] The differential waveform is equivalent to the difference between the reference and sample waveforms, $y_d = y_r - y_s$. The material parameters can be simply estimated by measuring y_r and y_d, calculating y_s, and using the transmission equations above for thin samples. For a thin film with thickness d and $n_s \gg \kappa_s$, deposited (so $n_2 = n_1$) on a substrate n_3, where $n_1 \gg \kappa_1$, $n_2 \gg \kappa_2$ and $n_3 \gg \kappa_3$, an analytic expression for the refractive index can be derived:[351]

$$n_s(\omega) = \sqrt{(1 + \frac{c_0}{\omega d}\left|\frac{S_d}{S_r}\right|)(n_1 + n_3) - n_1 n_3}, \tag{32}$$

where $S_d = \mathcal{FT}(y_d)$.

4.2.6. *Interferometry*

Another method to increase the sensitivity of T-ray spectrometers to thin films is interferometry. T-ray interferometric techniques typically induce a 180° phase shift between two arms of an interferometer, then detect phase changes introduced by a thin sample into one arm. Enhanced depth and spatial resolution have been achieved with T-rays focused to a point on a reflective sample in one arm of an interferometer, where the Gouy shift occurs at the focal point on the sample.[356] The peak amplitude showed a 20% change for a 12.5-μm-thick air gap in Teflon. Other interferometers have been constructed using silicon prisms as reflectors, where the 180° phase shift was induced by a fixed end reflection from one of the faces ,[357] and using counter-propagating OR to generate T-ray pulses with an opposing sign.[358]

The signal at the detector in a T-ray interferometer is the sum of the pulses in the two arms, $y = y_1 + y_2$. For a system with identical pulses in both arms, differing only by a (small) phase difference $\phi(\omega)$,

$$\tilde{S}_1(\omega) = A(\omega), \tag{33}$$

$$\tilde{S}_r(\omega) = A(\omega)(1 - e^{j\phi(\omega)}), \tag{34}$$

$$\tilde{S}_s(\omega) = A(\omega)(1 - t_{1s}p_s t_{s2}e^{j\phi}), \tag{35}$$

where $\tilde{S}_1(\omega)$ is the spectral response of arm 1 of the interferometer when arm 2 is blocked, and t and p are the transmission and propagation coefficients for the sample placed in arm 2 of the interferometer. The phase difference $\phi(\omega)$ can be calculated by normalizing the reference spectrum to the spectrum in arm 1 alone

$$\frac{\tilde{S}_r(\omega)}{\tilde{S}_1(\omega)} = 1 - e^{j\phi(\omega)}. \tag{36}$$

Typically, interferometric precision is required for samples with very low refractive index, so the transmission coefficients can be approximated $t \approx 1$. For very thin samples, where $k_0(n_s - 1)d \ll 1$, the sample spectrum can be normalized to the spectrum measured by arm 1 alone, giving an approximate expression for the sample's properties[357]

$$\frac{\tilde{S}_s(\omega)}{\tilde{S}_1(\omega)} = \rho e^{-j\phi} \tag{37}$$

$$\approx k_0\kappa(\omega)d + jk_0(n(\omega) - 1)d + j\phi(\omega). \tag{38}$$

4.2.7. *Waveguide resonators*

An important new demonstration of T-ray spectroscopy is in micro-stripline resonators.[335] In this geometry, T-rays propagate along a micro-stripline rather than through free space, returning to the original experiments with THz radiation in circuits.[271] The presence of a different dielectric in the resonator cavity causes a frequency and amplitude shift in the transmitted THz.

Currently, this geometry has only demonstrated qualitative estimates of the sample dielectric, although it is potentially a method for measuring $\tilde{n}_s$ of extremely small sample sizes ($\approx 250 \times 50$ μm^2).[335,359]

4.2.8. *Numerical Fourier spectra*

The FFT algorithm is used for all analysis in time-domain spectroscopy. A number of points need to be made regarding the relationship between the sampled time-domain waveform data and the FFT spectra. These issues are typical of systems using numerical Fourier transforms, including well-established Fourier Transform spectroscopy.[360]

Of primary concern in spectroscopy are the frequency range and resolution of measurements. From basic Fourier considerations, the time between data points, Δt, determines the maximum frequency observable in a spectrum $f_{\max} = 1/(2\Delta t)$, and the total duration of the data T determines the frequency resolution, and thus minimum frequency, $\Delta f = 1/T$. However, when a time-domain signal is represented as discrete data points, high-frequency signals above $f_{\max}$ can be aliased to frequencies below $f_{\max}$, thus it is important to ensure that there are no signals present above the $f_{\max}$ set by Δt. For T-rays, this upper signal cut-off is typically determined by the emission or detection bandwidth of between 5 and 10 THz.

The sample duration T is often limited in T-ray spectroscopy by physical considerations or by FP reflections. Spectral resolution can be improved by artificially adding zeros to the time-domain data. This provides smoother spectra, but if the time duration is more than doubled, no new information is actually present. The extra points in the spectra are just sinusoidal interpolations. FP reflections can arise in the sample, the emitter and the detector. When an EO crystal is used, FP reflections can be removed by bonding a refractive index-matched material to the crystal itself, thereby increasing its thickness. For example, the $\langle 110 \rangle$ ZnTe emitter or sensor can be bonded to a $\langle 100 \rangle$ ZnTe crystal, which has a null transverse EO coefficient.[193]

One of the advantages of T-ray spectroscopy over other THz optical techniques is the acquisition of phase information. Unfortunately, the phase spectrum from the FFT output needs to be *unwrapped* before it is useful. Common unwrapping algorithms can distort the unwrapped phase due to noise at low frequencies. One method to overcome this is to take phase information only at frequencies where the SNR is high, then artificially extrapolate back to DC.[6]

4.3. *Materials studied with T-rays*

Many materials, molecules and mixtures have been studied with T-rays, as outlined in the sections below. T-ray experiments have provided information on the THz response of samples, enhancing theoretical models and previous studies, including CW methods reviewed in Sec. 2.

4.3.1. *Gases and vapors*

T-rays were first used for accurate spectroscopy of water vapor in the air, measuring the frequencies and strengths of absorption due to rotational water molecule transitions.[5] Gas and vapor transmission (absorption) experiments typically use PCA emitters and detectors with an enclosed metal gas sample cell with thick (> 10-mm) high resistivity ($\approx$ 10-kΩ/cm) silicon windows, which are designed to minimize T-ray attenuation and avoid multiple Fabry-Pérot reflections inside the windows. The length of the sample cell is chosen depending on the strength of the absorption

for the pressures of interest. The entire T-ray path must be dried or evacuated to remove absorption from residue polar molecules, such as water, in the beam path.

T-ray gas spectrometers can accurately measure absorption lines and collision broadening for molecules that have a permanent dipole moment, as demonstrated with H_2O,[5] SO_2,[77] methyl halides,[361] ammonia[362,363] and CH.[364] T-ray measurements allow absorption, dispersion and line shape data to support theoretical models of these molecules.[77,361,362] Although demonstrating low average power, the ps time scale of the T-ray pulses results in very high peak powers, therefore T-rays can be used for spectroscopy of samples with large average background THz radiation, such as flames. Gases with no permanent dipole moments, such as N_2, O_2 and CO_2, show no T-ray absorption, whereas the concentrations of H_2O, CH and NH_3 in flames can be estimated from the T-ray spectra.[364] T-ray spectra of flames can be used to estimate flame temperature and study the higher rotational absorption states of hot water molecules.[365]

Detecting gases in a mixture is an important task for gas spectrometers. Gas identification, and classification using a linear predictive coding algorithm, has been demonstrated from the T-ray power spectra of NH_3 and H_2O.[363,366] An accurate gas filter correlation (GFC) system for detecting specific gas species has been demonstrated for H_2S.[367] The GFC system uses a calibrated sample cell in one arm of an interferometer and the unidentified gas mixture in the other, and was implemented using a pulsed photomixer emitter. A detection sensitivity of 30 ppm was achieved using GFC.

An important characteristic of polar gases and vapors at room temperatures and atmospheric pressures is line broadening. The broadened absorption lines from most gases severely overlap, making identification difficult.[5,363,367] To avoid line broadening, the sample cell (or the calibration cell in GFC) must be held at a reduced pressure. A review of collision-broadened rotational lines in gases studied with T-rays was prepared by Harde, Cheville and Grischkowsky.[368]

Vapors have been shown to re-emit THz pulses after excitation with a primary THz pulse, for example, N_2O[369] and methyl chloride.[370] These experiments have been used to characterize rotational and vibrational constants, and to study line shape broadening, which shows excellent agreement with linear dispersion theory.

4.3.2. *Liquids*

Liquid studies at THz frequencies are concerned with characteristic relaxation times of permanent or induced molecular dipole moments. Keiding *et al.* have studied THz spectra of liquid water as a function of temperature, modeled using a Debye relaxation model and numerical simulation.[344,371] These experiments are performed using a reflective TIR method, described in Sec. 4.2.2 above. The temperature dependence of liquid water has also been compared to D_2O.[372] An alternative model of the THz response of liquid water, describing molecular plasma oscillations in an ice-like crystalline lattice, has been proposed from transmission data.[373]

Liquid water shows a very high THz absorption, greater than 200 cm^{-1} at 1 THz, whereas non-polar liquids have coefficients around 100× smaller (for example, benzene, carbon tetra-chloride and cyclohexane).[374] Keiding *et al.* have studied the temperature dependence of the solvents benzene and toluene, observing rotational

and librational bands.[375] Schmuttenmaer *et al.* have studied numerous liquids of varying polarity with a dual-thickness sample cell, based on a polyethylene bag held between two movable silicon or polyethylene windows, including water, methanol, 1-propanol and liquid ammonia.[376] All results have been matched to Debye relaxation dielectric models with good accuracy. A number of optical-pump and T-ray-probe studies have explored the response of solvents and dyes to photoexcitation,[377] and linked these results to finite difference time-domain models.[318] The solvation dynamics of polar and non-polar liquids, including acetonitrile and water,[378] acetone, acetonitrile and methanol[379] and water,[380] have been related to molecular dynamics simulations to explore the relationship of decreasing THz absorption with increasing liquid structure.[381] The solvation dynamics of lithium salts in water, methanol and propylene carbonate have been explained with Debye relaxation models.[382]

Mittleman *et al.* have measured and modeled the THz response of inverse surfactant micelles of water in heptane compared to bulk water.[383] The reduced dielectric constant of the micelles is attributed to confinement effects on the water molecules.

4.3.3. *Solids*

The earliest studies using pulsed THz spectroscopy were on $LiTaO_3$, generating and detecting the THz radiation inside the same crystal.[324] The importance of EO materials in OR and EOS has led to further studies, characterizing the complex dielectric of ZnTe,[283] GaAs,[384] $LiTaO_3$ and organic crystals,[385] and the temperature-dependent power absorption spectrum of two-phonon processes in ZnTe and CdTe.[386]

Table 3. Dielectric constants of select solids at 1 THz, as measured using THz-TDS. n_o refers to the *ordinary* refractive index and n_e refers to the *extraordinary* refractive index for birefringent materials. High-resistivity (10-kΩ-cm) silicon demonstrates the lowest dispersion, with n almost constant across the spectrum from 0.2 to 2 THz. The accuracy of the first 6 measurements is better than 0.0004.

Solid	Refractive index	Power absorption	Ref.
sapphire	$n_o = 3.070$, $n_e = 3.415$	$\alpha \approx 1$ cm^{-1}	133
crystalline quartz	$n_o = 2.108$, $n_e = 2.156$	$\alpha = 0.1$ cm^{-1}	
fused silica	$n = 1.952$	$\alpha = 1.5$ cm^{-1}	
intrinsic Ge	$n = 4.002$	$\alpha = 0.5$ cm^{-1}	
high-$\mathcal{R}$ GaAs	$n = 3.595$	$\alpha = 0.5$ cm^{-1}	
high-$\mathcal{R}$ Si	$n = 3.418$	$\alpha < 0.05$ cm^{-1}	
ice	n = 1.793	$\alpha = 8.6$ cm^{-1}	387
0.19-Ω-cm N-GaAs	n ≈ 2.97	α= 320 cm^{-1}	388
0.36-Ω-cm P-GaAs	n ≈ 3.44	α= 270 cm^{-1}	

Early free-space T-ray systems were used for spectroscopy of common homogeneous solids. Arjavalingham *et al.* measured the complex dielectric constants, and their polarization and angular dependence, of fused silica, sapphire and plexiglass slabs up to 130 GHz with ps optical pump pulses.[132,341,389–391] Wire grid polarizers were used to control the THz polarization. Grischkowsky *et al.* extended these measurements to 2 THz, studying common solids, as summarized in Table 3, and modeled the conductivity of doped Si with an extension of the Drude dielectric model to include energy-dependent carrier relaxations.[392]

T-ray spectroscopy is an attractive non-contact, non-destructive and rapid technique that has been applied to semiconductor wafer characterization in a variety of geometries. Transmission measurements, detailed above, are limited to samples with low absorption. Doped n-GaAs, doped n-Si and bulk GaAs wafers have been characterized in reflection, with an Al mirror providing the reference pulse, and modeled using Drude theory to determine carrier density and mobility.[384,393] The dielectric properties of 600 to 15-μm films of highly doped semiconductors have been measured in reflection, where the thickness is measured by observing frequency of destructive interference in the THz spectrum.[345] THz ellipsometry has been demonstrated on doped Si wafers to estimate $\tilde{\epsilon}$,[347] and the Hall effect has been used to estimate the full conductivity tensor of n-GaAs, implemented with a 1.3-T magnetic field and dual detectors for the two emitted polarizations.[298,383]

The optical pulse driven nature of T-rays lends itself to the study of photoexcited carrier dynamics in semiconductors; optical-pump and THz-probe experiments have the advantage of ultrafast resolution coupled with THz bandwidth.[394] The THz reflectivity of photoexcited GaAs can be measured by T-ray reflection.[395] The time-dependent conductivity of GaAs-AlGaAs quantum wells,[396] bulk GaAs and epitaxial LT-GaAs have been studied under 800-nm and 400-nm light, and modeled using a modified Drude model.[397,398] Two-color EOS, with time-delayed collinear pulses transmitted through a GaAs sample, has been used to study T-ray generation from surface field dynamics.[245] Using ultrafast optical excitation pulses, T-rays have been used to observe photocarrier generation and the subsequent screening processes in semiconductors.[282,399,400] Optical-pump and THz-probe experiments have also enabled a form of near-field imaging with a dynamic aperture, as detailed in Sec. 5, and the creation of transient mirrors for T-ray pulse slicing.[319]

Characterization of insulating and conducting materials in the GHz-THz range is invaluable for the future development of high speed circuits. As potential substrates for superconducting circuits, MgO has been measured with a low THz transmission loss, unlike YSZ (yttrium stabilized zirconia) and $LaAlO_3$.[401] T-rays can be used to observe static and dynamic characteristics of superconducting films themselves.[402,403] Goniometric measurements have been made of FLARE, TiO_x and PZT thin films[346] and parylene-N films have been characterized with differential spectroscopy.[404] Non-contact characterization, and modeling with localization-modified Drude theory, is particularly valuable for conducting polymers, such as polypyrrole and poly-3-methylthiophene,[405,406] and single-walled carbon nanotube films.[407] Organic thin polymer films were first characterized by T-rays in 1992.[408] Microwave ceramics for telecommunications have been analyzed in transmission[409] and corrosion layers beneath opaque paints analyzed in reflection.[410]

4.3.4. *Biological materials*

With the development of T-ray spectroscopy, increasingly complex materials are being characterized, specifically biological and medical samples. Many of these materials are particularly sensitive to sample preparation and environmental conditions.

THz-TDS has been previously used to monitor broadband THz optical properties of biomolecules in binding, denaturation, temperature and humidity studies.[411,412] Biomolecules, such as proteins and nucleic acids, have broad THz features arising from a multitude of dense rotational, vibrational, inter-domain and hydrogen bond energy transitions.[413,414] Molecular dynamics simulations of simple biomolecules can be used to understand the measured THz spectra.[415,416]

Using planar waveguides and a THz resonator, Bolívar *et al.* have demonstrated a highly sensitive device for probing the binding state of DNA.[335,359] This thin film micro-stripline approach could be extended to two-dimensional gene chips for high speed DNA analysis. The THz waveguide and resonator structure is sensitive to single-base defects in an 1.1 femtomol volume of 0.52 g/L DNA-in-water.

Biomolecular films are extremely sensitive to conditions of humidity, temperature, pH and preparation.[417] At room temperature, the THz spectra of protein structures is heavily populated, resulting in a continuous spectral response with few signature resonances. The THz spectrum is difficult to measure because dried biomolecular films have very small THz responses. These problems can be overcome by careful sample preparation and the highly sensitive technique of DTDS, detailed in Sec. 4.2.5. Another solution to environmental control of biomolecules is to study them as suspensions in a non-polar organic solvent, where activity and hydration studies can be carried out with high accuracy.[418,419]

An important consideration in inhomogeneous structures is scattering. Scattering of single-cycle T-rays has been studied with samples constructed from teflon balls, with expressions derived for the mean free THz path length in the model medium.[317]

Larger, more complex structures have been studied phenomenologically, with an emphasis on contrast rather than full spectroscopic information. This is typically the case for sensor applications, or in imaging of tissues (see Sec. 5). One example is the image of a desiccating leaf,[420] which has been studied spectroscopically with CW techniques in the 100 to 500-GHz range.[421] THz biosensing, using contrast derived from a combination of sample properties, including thickness, absorption, scattering and phase delay, has been used to detect the binding of lipids to proteins with a sensitivity of 1 ng/mm^2.[348] The push to clinical applications of T-rays (see Sec. 5) has led to studies of potential damage caused by THz.[422,423] Two reviews of T-ray studies in biomedicine have been written by Chamberlain *et al.*[424,425]

4.4. *Radar and ranging sensing*

T-rays can be used for purposes other than spectroscopy. As free-space pulses of radiation, T-rays have been used for scaled-down versions of radar applications, such as distance and thickness measurements. T-rays can be used to study the radar profiles of scaled-down objects, such as 1/200th-sized model planes and tanks,[427,428] or to characterize micromachined components.[429] Ranging measurements occur in

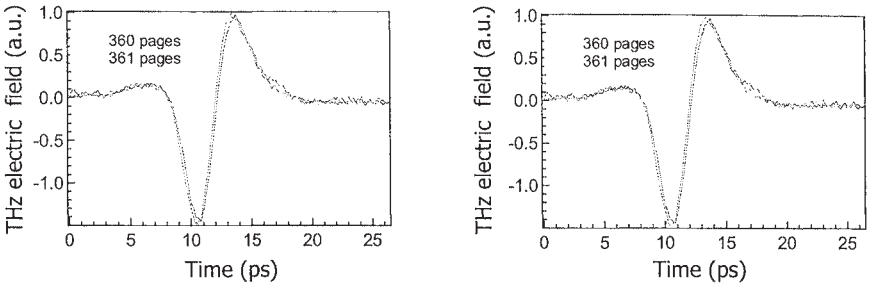

(a) Time-domain waveforms (b) Magnified portion of the pulse

Fig 22. The number of pages in a book can be counted be measuring the phase delay of T-ray pulses in transmission. The resolution shown here is better than 1 in 400.

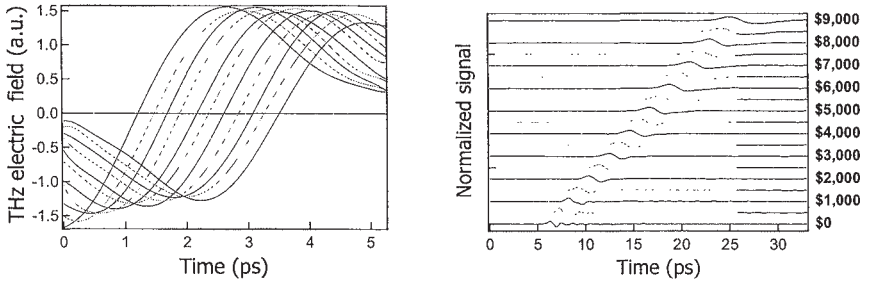

(a) Time waveforms (b) Normalized waveforms

Fig 23. In a similar application to Fig. 22, the time delay of T-ray pulses in transmission have been used to count stacks of paper currency. Fig. 23(a) shows an expanded part of the time-domain waveform. Fig. 23(b) shows both the time delay and pulse spreading as T-ray pulses are transmitted through thicker stacks of paper currency.[426]

reflection, either using a small incidence angle or a transceiver.[197,323]

The interpretation of reflected pulses necessitates the modeling of single-cycle electro-magnetic pulse interactions with dielectric objects.[430,431] Measuring T-ray pulse delay though a sample enables the THz refractive index profile of a flame to be estimated[298] and the number of pages in a book to be counted, as demonstrated in Fig. 22. This work has been applied to studying the THz time delay caused by dollar bills, whereby cash can be counted by its thickness, seen in Fig. 23.

T-ray scattering from objects has been extended to imaging research, including quasi-optical imaging,[432] synthetic aperture imaging[433] and T-ray propagation around a cylinder.[434,435] These topics are further discussed in Sec. 5.

4.5. *Terahertz-induced activity*

T-rays, despite their low average power, can be used for coherent manipulation of states in atoms, for spectroscopy and for quantum information processing. Rydberg wave packets have been created, probed and ionized using ultrashort THz pulses.[436-439] T-ray pulses have similarly been used to excite Rabi oscillations in donor impurities in GaAs.[319] Theoretical modeling suggests that narrowband THz could be used for tuning the resonance of semiconductor microcavities, and pulsed THz may be used to control coherent mode oscillations.[440]

5. Imaging

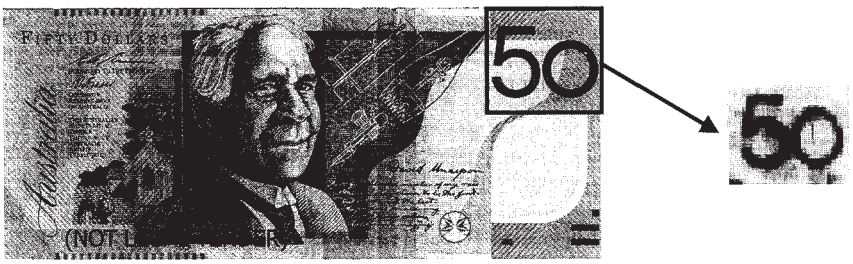

Fig 24. T-ray transmission through ink on currency. This figure indicates how a T-ray image can detect contrast in dry, non-polar samples. This image was taken with a raster-scanned imaging system. Most interestingly, the T-ray image remains unchanged when the plastic Australian $50 note is placed inside a paper envelope.[441]

5.1. *Introduction*

T-rays have been extended to two-dimensional imaging using a variety of scanning and CCD techniques, which provide parallel processing for speed and image processing for visualization. The first T-ray imaging systems involved raster scanning a sample to build up a 2D image, as discussed in Sec. 5.2. Using EO detection, this has been extended capturing the THz image of the whole sample with a CCD. Using a 2D array of data speeds up the acquisition of information at the expense of losing signal power at each pixel. Simple contrast images in the THz domain can be developed using absorption information, delay information or a combination of the two. A T-ray image is shown in Fig. 24 of two digits on a plastic $50 note, showing the different THz transmission of the inks. Dry substances, such as paper and plastic, transmit T-rays with less than 1% attenuation. More interesting than a simple contrast image is a two-dimensional array of waveforms. Spectral analysis at each pixel can then provide molecular information about the whole sample. With a metric of FIR molecular classification, it would be possible to map samples in terms of their specific molecular composition, potentially valuable in chemistry, biology and medicine.

5.2. *Scanning and synthetic aperture imaging*

The first T-ray images were obtained by simply scanning a sample across the T-ray beam, and presenting neighboring data points as pixels. The images were constructed of transmitted T-ray waveforms, with a number of contrast mechanisms available: total transmitted amplitude, peak delay at each pixel, and transmitted amplitude or delay of a given Fourier component. The technical advances that led to T-ray imaging were primarily methods of increasing the T-ray signal strength, coupled with faster acquisition speeds. The first demonstration of T-ray imaging had a 10–20 pixel-per-second waveform acquisition rate with an SNR of 100:1. This system relied on a 50-μm-gap SI-GaAs PCA emitter, a 5-μm-gap PCA detector, a 7.5-mm, 20-Hz scanning delay line for the gated detector, and a dedicated DSP chip to sample, process and display the data.[420]

T-ray imaging based on detector scanning has been simplified by the availability of fiber-coupled PCA detectors, where the probe time delay and alignment remain fixed by the fiber.[9] A scanned PCA detector has been used to characterize the emission patterns from PCAs,[167–169] and image the spatial reshaping of T-rays as they tunnel through a narrow air gap.[442]

Reflection imaging requires reconstruction algorithms to estimate the shape and structure of the reflecting object. The reflected data can be acquired along a straight line, perpendicular to the emitter-sample normal, and the object shape can be reconstructed using Kirchhoff migration,[443] or for data acquired over a hemisphere, the object profile can be calculated by numerical back-propagation.[444] Enhanced depth resolution is achieved by scanning the sample in an interferometer, as described in Sec. 4.2.6.[356,445]

Synthetic aperture processing is used to reconstruct 3D T-ray images[433] and images with enhanced resolution.[446]

5.3. *PCA array imaging*

It is preferable in an imaging system to have a 2D array of detectors, so the sample and detector remain stationary. Imaging array detectors are available for CW terahertz detection, from applications in mm and sub-mm astronomy .[447] Arrays of gated PCAs have been proposed but not yet developed.[441,448]

5.4. *EOS CCD imaging*

An effective method of 2D T-ray detection is to use an expanded probe beam in EOS, and detect the probe beam's polarization rotation with a polarizer and a CCD, as shown in Fig. 25. The advantage of using EOS is the increased bandwidth over PCAs and the simplicity of array imaging. The central trade-off remains between speed and SNR; for 2D imaging, the T-ray beam is expanded to encompass the entire object, which spreads out the available T-ray power over the number of pixels. The main advantage is that neither sample nor detector need be moved to acquire the entire image.

An advance of EOS imaging is the ability to use chirped optical probe pulses, as described above in Sec. 3.4.2. The advantage of chirped probe measurements is that the entire T-ray waveform can be sampled with only one pulse, as schematically described in Fig. 10. Full waveforms can be acquired from 1D images with a CCD.[291]

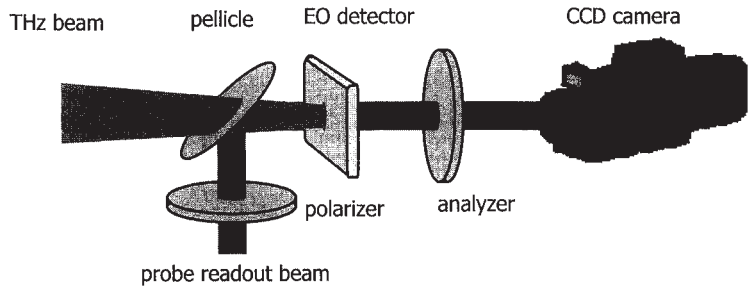

Fig 25. 2D EOS differs from point EOS in that both the probe beam and the T-ray beam are expanded onto the EO detector, and the transverse intensity modulation of the probe is detected by a CCD camera. The data is loaded directly to a computer for presenting a visual image. 3D data sets can be built up and analyzed in XY slices, or with time on one axis (YT, XT).[268,290]

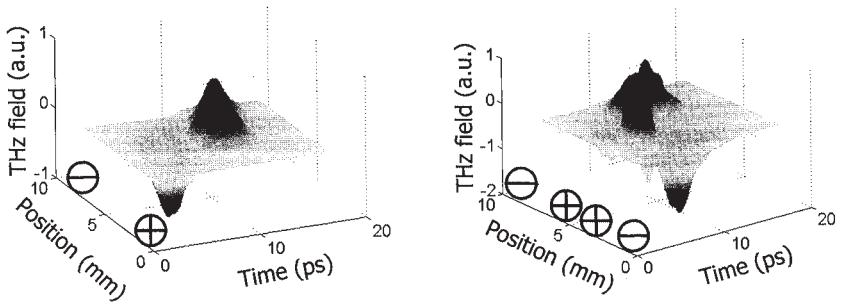

(a) Dipole field

(b) Quadrupole field

Fig 26. Examples of single-shot 1D imaging of dipole and quadrupole T-ray fields. In this data, the emitted field of dipole and quadrupole PCA emitters have been imaged using EOS. The time evolution of the T-ray pulse is shown simultaneously across the X-dimension of the emitter.[449,450]

Two example waveforms are shown in Fig. 26, where a cross-sectional array of time-domain waveforms have been imaged simultaneously. This technique is close to the theoretical speed limit of T-ray imaging, although a reference measurement needs to be made to interpret the chirped waveform.[450]

5.5. *Tomography*

When detected in reflection, the pulsed nature of T-rays enables analysis of a sample's internal structure, using tomographic reconstruction.[298] Tomography is an extension of T-ray ranging studies to more complex internal structures and 1D or 2D imaging. Tomography enables the visualization of internal structure as different

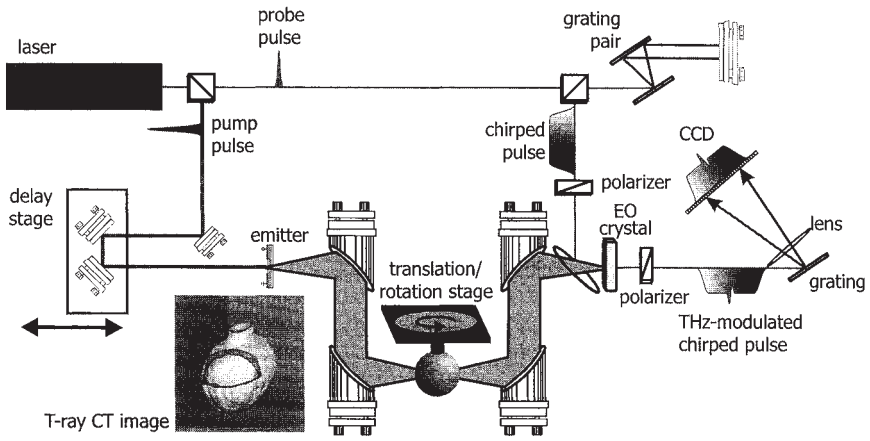

Fig 27. Schematic layout of a T-ray CT experiment. Data is acquired with a single-shot imaging system using chirped probe pulses. The sample, in this case a hollow plastic ball, is scanned X–Y and rotated about its axis. It takes approximately 1 hour to scan 100x100 images at 18 projection angles, which is sufficient to reconstruct a 3D sectionable profile of the object using computed tomography algorithms. A T-ray CT profile is shown in the bottom left, with a quarter cut away to reveal the internal structure. The spatial resolution of THz CT is given by the angular rotation multiplied by the radius of rotation at the edge of target. For the plastic ball, the radius is approximately 2 cm, therefore the spatial resolution on the surface of the ball is 3.5 mm.[451]

interfaces reflect pulses with varying delay and intensity. For example, a slice of a floppy disc reveals layers of air, plastic and metal.[452] Information on the complex dielectric profile of a multilayered object can be estimated using Fresnel equations (Sec. 4.2) and an iterative algorithm.[428] Using the frequency-dependent focal length of a Fresnel lens (Fig. 12(a)) enables images at different depths in a sample to be obtained using the different Fourier components of the broadband T-ray pulse.[316]

T-ray computed tomography (CT) and diffraction tomography are techniques for reconstructing an estimate of the internal structure of an object based on numerous transmission measurements.[453-455] Fig. 27 shows a schematic T-ray CT spectroscopy system for imaging a small, in this case a ping-pong ball.

5.6. *Near-field imaging*

The lateral resolution of far-field T-ray images is limited by the wavelength of the radiation, λ, to approximately $0.61\lambda/(n\sin\theta)$, where the refractive index of the focusing medium n is typically unity for air and θ is the half angle of the focal point.[179] T-ray pulses have wavelengths spanning from 3 mm to 100 μm (0.1–3 THz), limiting the average resolution at the T-ray peak to approximately 500 μm. By selecting only high-frequency components after numerical Fourier analysis, the resolution can be improved to approximately 100 μm.[428] To study broadband T-ray pulses interacting with sub-wavelength areas, however, near-field techniques are required. Near-field techniques rely on an aperture, diameter a, placed in the optical near-field of the sample to be studied, with separation distance $L < a$, so the size

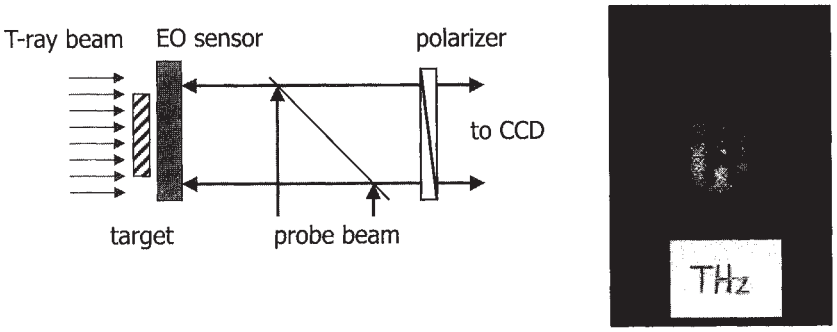

Fig 28. Collection mode near-field EO imaging is performed by holding an EO sensor in the THz near-field of a sample, and measuring the T-ray electric field with a probe pulse reflected from the sample side of the crystal. This technique has a reduced signal because the internal reflection is small, but it provides resolution sufficient for the image of the letters 'THz'; the line width of the word is 0.5 mm and the image was taken in less than 1 s.

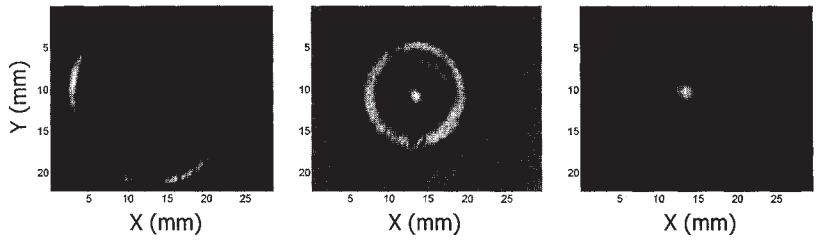

Fig 29. These images of the T-ray beam wavefront were taken with collection mode near-field EOS.[171] The measurements were made in real-time and time evolution of the wavefront can be directly observed. The circular waves are due to the curved nature of the wavefront.

of the interaction spot is defined by a and not the wavelength of the radiation.[459] A review of the development of FIR nearfield microscopy was prepared in 2002 by Rosner and van der Weide.[460]

An early evaluation of using tapered waveguides as apertures for THz light was carried out using CW THz from a gas-vapor laser,[461] and the first reports of near-field T-ray imaging used an elliptical aperture in the end of a tapered metal tip, $a \approx 50$ μm by 80 μm.[462] T-rays were focused to a diffraction-limited spot with a parabolic mirror, the tapered tip was placed at the focal point and a sample was placed in the near-field of the aperture, that is, within a length less than a.[463] A resolution of approximately 50 μm was achieved. Two typical aperturing effects were observed: the transmitted THz electric field dropped by approximately 130 times, and THz frequencies below 0.5 THz were strongly attenuated. A similar

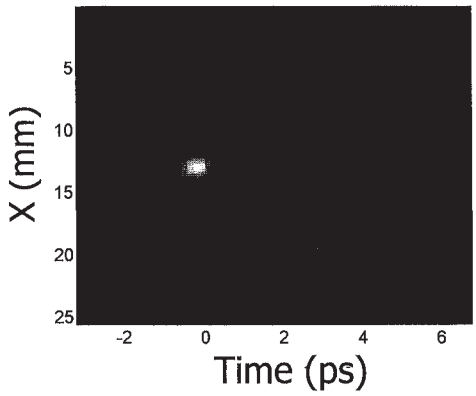

Fig 30. 1D image of T-ray propagation through a focus. This image shows an image of a T-ray pulse passing through the focus of a lens. The focal point and Gouy phase shift are clearly visible. This image was sampled using 2D EOS and a 2-f imaging configuration with a polyethylene lens.[171]

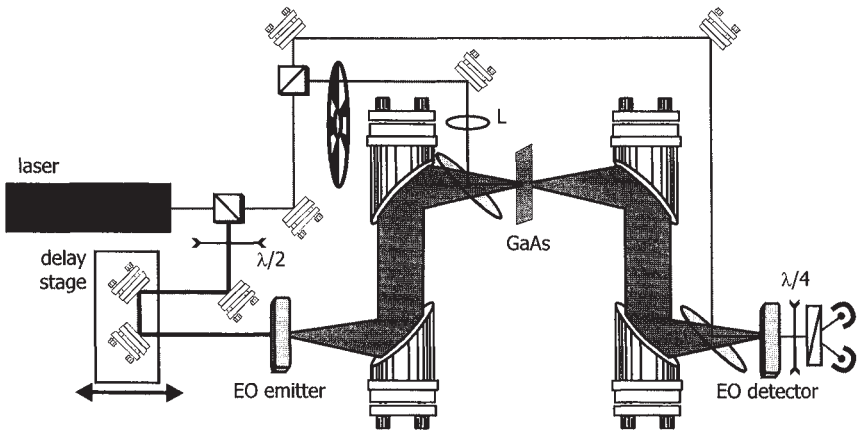

Fig 31. Near-field dynamic aperture schematic. As described in Sec. 5.6, a sub-wavelength-sized spot of THz can be blocked by the gated generation of photocarriers in a semiconductor. GaAs is normally transparent to T-rays, but the photocarriers act as a mirror screen.[456] The schematic is the same as a typical T-ray spectrometer based on OR and EOS, except a gated beam for the sample is incorporated. Such a layout allows other optical-pump THz-probe experiments on ultrafast processes.[400] The $\lambda/2$ and $\lambda/4$ waveplates are used to optimize the pump polarization and balance the photodiodes. The lens, L, is used to focus the optical beam to a sub-100 μm spot on the GaAs wafer.

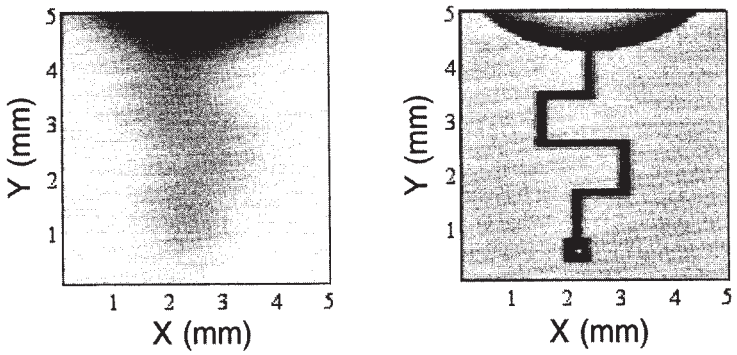

(a) Standard far-field T-ray image

(b) Dynamic aperture near-field T-ray image

Fig 32. This figure demonstrates the improved spatial resolution achieved by near-field imaging with a dynamic aperture. The sample is a metal circuit deposited on a GaAs wafer. This technique has demonstrated resolution of better than 50 μm.[457]

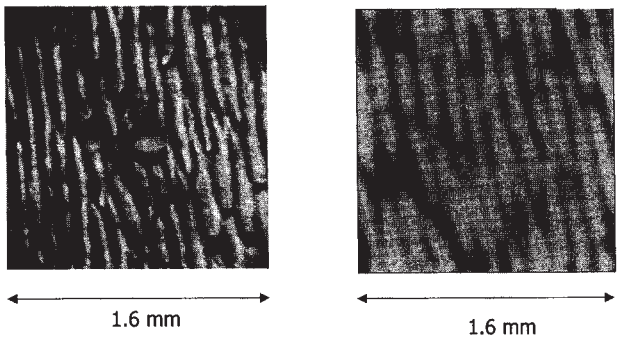

(a) Microscope image

(b) T-ray image image

Fig 33. T-ray contrast in biological tissue, showing diffraction-limited resolution and cell structure visible in the THz band.[458]

resolution was achieved without an aperture, by holding the sample in the near-field of a PCA – in this case a virtual aperture existed due to the sub-wavelength dimensions of the spot where T-rays are generated.[464]

Images can easily be acquired with the detector placed in the near-field of the sample, or in collection mode, using a large area EO detector.[171] A schematic of near-field collection mode EO imaging is shown in Fig. 28. This provides a method to directly measure the 3D T-ray beam profile by moving the detector crystal along the beam path, and generates images of T-ray wavefronts or passing through a focus, shown in Figs. 29 and 30.

A resolution of 7 μm was achieved in 2001 using a collection-mode PCA detector.[465,466] The detector had a 10-μm diameter aperture fabricated directly onto a 4-μm-thick PCA, so T-rays passed through the aperture and were detected by the PCA all in the near-field. The operation of the aperture is enhanced by having a high-refractive-index GaAs tip, $n_{\mathrm{GaAs}} = 3.6$, protruding through it. The tip refracts the T-rays, decreasing the wavelength of the radiation as it passes through the aperture by a factor n_{GaAs}.[467] Two important considerations in T-ray near-field imaging are temporal reshaping of the pulse and the finite thickness of the aperture itself.[310,330,468] Sub-wavelength T-ray spatial resolution can also be achieved using near-field metal tips,[469] based on work in the infrared.[470,471]

As mentioned in Sec. 4.3.3 above, dynamic T-ray experiments can be performed by generating transient mirrors in semiconductors, using photocarriers generated by an optical pulse. If the optical pulse is tightly focused, a dynamic inverse aperture can be created to block a sub-μm cross-section of the T-ray beam.[457] A schematic of the dynamic aperture system is shown in Fig. 31. For a semiconductor placed at the focal point of a T-ray beam, and samples placed in the near-field of the aperture ($L < a$), a 40-μm resolution has been achieved with the dynamic aperture.[456]

Wynne *et al.* mounted a sample directly onto a EO crystal, so T-rays were generated in the near-field of the sample.[472] A resolution of 200 μm was demonstrated, limited by two-photon absorption due to high intensity at the focal point.[192] THz generation via OR in sub-THz-wavelength volumes is optimal when the optical spot size is comparable with the wavelength of the generated T-rays.[473,474]

5.7. *Speed*

The trade-off of speed versus SNR is central to all T-ray spectrometers, particularly in imaging where large data sets have to be acquired in a realistic time, for example, while a person waits in proposed clinical applications. The speed of image acquisition can be estimated from the time taken to acquire a sufficiently-long T-ray waveform at each pixel at a certain SNR. For example, the first scanning PCA imaging system demonstrated 25-ps-long scans acquired in 5 ms with an SNR of 100:1.[420] In 2001, high-power PCA T-ray systems reported 35-ps-long scans acquired in 20 ms with an SNR $\approx$ 3000:1.[143] The SNR increases proportional to $\sqrt{t}$, where t is the time spent averaging data samples. For an SNR of 100:1, 2D EO imaging can be used to sample 200-pt-long 20-ps T-ray waveforms over a 288×384-pixel array in approximately 200 ms. Signal processing can be used to improve the SNR of T-ray images[298] including wavelets.[475,476]

5.8. *Dielectric imaging*

Samples that have been studied in the search for applications of T-ray imaging include those where spectroscopic information is of interest, such as gas flames, and more complex samples, where contrast cannot be clearly linked to a single dielectric constant. Dielectric studies have been performed to image the carrier concentration and mobility in silicon wafers,[477] the Hall effect (Sec. 4.3.3), biological tissues,[458,478] currency watermarks[479] and thin ceramic oxide with tomography.[480] An example of T-ray contrast in biological tissue is shown in Fig. 33.

5.9. *Classification algorithms*

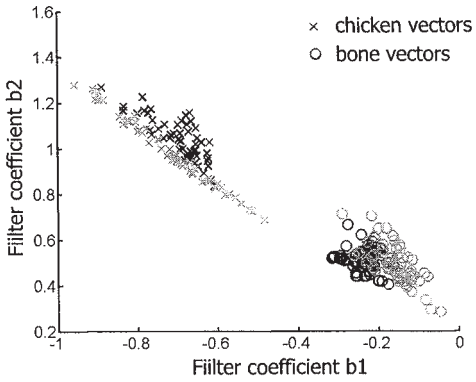

Fig 34. Finite impulse response filter classification. This plot shows the effective classification of T-ray waveforms using coefficients $b1$ and $b2$ derived by fitting the data to one of two finite impulse response filters. The filters were developed with known training data. The fast algorithm clearly differentiates between bone and meat in this chart, depending only on the two coefficients.[294] The use of classification in imaging is shown in Fig. 35.

One of the advantages of T-ray imaging over incoherent imaging techniques, such as those using X-rays or visible light, is the coherent nature of the measurements. A full T-ray waveform can be acquired for each pixel and used to interpret the image spectroscopically. For 2D images, the intensity of each pixel can be linked to a number of spectroscopic parameters, including absorption or phase delay of a specific spectral component, peak absorption or peak delay. Images of flames have been false color coded to indicate the magnitude of T-ray pulse delay in transmission.[298] The magnitude of the pulse peak has been used to code images of currency.[441,481] More complex metrics can be developed to represent a combination of factors, specifically chosen to emphasize differences in spectra of different materials. This becomes a classification task, and the metrics can be algorithms trained from known data to be either one sample or another. The results of the application of a simple classification algorithm are shown in Fig. 34. Classification is a digital signal processing task, often using linear filters to generate the parameters of importance. T-ray images colored by classification metrics have been used for imaging the Hall effect in

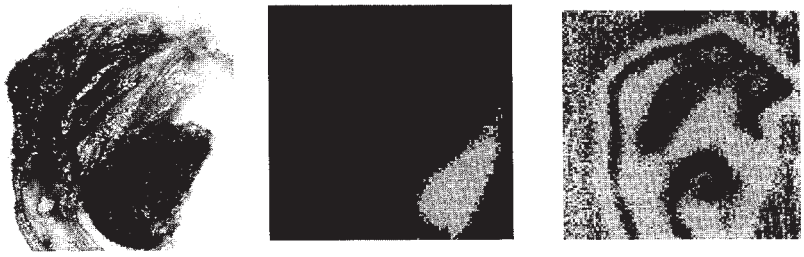

(a) Normal photograph (b) Classified image (c) T-ray amplitude image

Fig 35. These three images demonstrate the utility of a simple classification algorithm.[294] The visible image on the left shows the sample biological imaged with T-rays: meat and bone. Using the classifier algorithm, the background, meat and bone can be automatically and clearly differentiated, as shown in the center image. Using the classifier provides far clearer data than just using transmission amplitude information. The image on the right is a plot of transmitted THz amplitude, and shows poor discrimination between the sample meat and bone. Classification is a method of utilizing the entire sample waveform to differentiate between just two classes.

semiconductors,[298] and biological tissues.[294,478]

6. Conclusion

T-ray sensing and imaging has developed and spread widely since the early 1990s. Initially present primarily in physics and electrical and electronic engineering research groups, T-rays are now used by physicists, engineers, chemists and biologists. The THz bandwidth can play a role in industry, homeland security and medicine.

There are currently over a hundred groups world-wide using T-rays and commercial systems are on the market. There are, however, still numerous hurdles to be overcome before T-ray spectrometers compete with other techniques in spectroscopy, biosensing, medical diagnostics and industrial imaging. These challenges include size, cost, output power, SNR, bandwidth, depth penetration, water sensitivity, spatial resolution, speed of data acquisition and the lack of a THz-frequency knowledge base. As indicated in this chapter, these challenges are being addressed and future development will probably find T-rays implanted in vital applications.

Acknowledgements

This work was funded in part by the US National Science Foundation, the US Army Research Office and the Australian Research Council. S. P. Mickan would like to acknowledge the support of the Fulbright Commission and Clough Engineering, Australia, and his supervisors Prof. Derek Abbott (the Centre for Biomedical Engineering, and the Department of Electrical and Electronic Engineering) and Prof. Jesper Munch (the Department of Physics, Applied Physics and Astronomy) of The University of Adelaide, Australia.

References

1. M. C. Nuss, *Chemistry is right for T-rays*, *IEEE Circuits and Devices* **12**(2) (1996) 25–30.
2. S. Svanberg, *Atomic and molecular spectroscopy: Basic aspects and practical applications*, vol. 6 of *Springer series on atoms and plasmas*, Springer-Verlag, Berlin (1991).
3. K. D. Möller and W. G. Roschild, *Far-Infrared Spectroscopy*, Wiley series in pure and applied optics. Wiley-Interscience, New York (1971).
4. P. M. A. Sherwood, *Vibrational Spectroscopy Of Solids*, vol. 1 of *Cambridge monographs in physical chemistry*, Cambridge University Press, London (1972).
5. M. van Exter, C. Fattinger and D. Grischkowsky, *Terahertz time-domain spectroscopy of water vapor*, *Optics Letters* **14**(20) (1989) 1128–1130.
6. L. Duvillaret, F. Garet and J.-L. Coutaz, *A reliable method for extraction of material parameters in terahertz time-domain spectroscopy*, *IEEE Journal of Selected Topics in Quantum Electronics* **2**(3) (1996) 739–746.
7. G. Gallot and D. Grischkowsky, *THz time-domain spectroscopy (THz-TDS) with electro-optic sampling*, *Conference on Lasers and Electro-Optics '99*, 492–493, Optical Society of America, Baltimore, MD, U.S.A. (1999).
8. M. Li, G. C. Cho, T.-M. Lu, X.-C. Zhang, S.-Q. Wang and J. T. Kennedy, *Time-domain dielectric constant measurement of thin film in GHz-THz frequency range near Brewster angle*, *Applied Physics Letters* **74**(15) (1999) 2113–2115.
9. J. V. Rudd, D. Zimdars and M. Warmuth, *Compact fiber-pigtailed terahertz imaging system*, J. Neev and M. K. Reed eds., *Commercial and Biomedical Applications of Ultrafast Lasers II*, vol. 3934, 27–35, SPIE, Washington, DC, U.S.A., San Jose, CA, U.S.A. (2000).
10. M. Li, X.-C. Zhang, G. D. Sucha and D. J. Harter, *Portable terahertz system and its applications*, J. Neev and M. K. Reed eds., *Commercial and Biomedical Applications of Ultrafast Lasers*, vol. 3616, 126–135, SPIE, Washington, DC, U.S.A., San Jose, CA, U.S.A. (1999).
11. TeraView Limited, *cambridge, uk*, Www.teraview.co.uk.
12. Tochigi Nikon Corporation, *tochigi, japan*, Www.tochigi-nikon.co.jp/ technologies/ terahertz/.
13. M. van Exter and D. Grischkowsky, *Characterization of an optoelectronic terahertz beam system*, *IEEE Transactions on Microwave Theory and Techniques* **38**(11) (1990) 1684–1691.
14. P. D. Coleman, *Reminiscences on selected millennium highlights in the quest for tunable terahertz-submillimeter wave oscillators*, *IEEE Journal of Selected Topics in Quantum Electronics* **6**(6) (2000) 1000–1007.
15. B. Lax, *Applications of far infrared lasers*, A. Mooradian, T. Jaeger and P. Stokseth eds., *Tunable Lasers and Applications*, vol. 3 of *Springer Series in Optical Sciences*, 340–347, Springer-Verlag, Berlin (1976).
16. E. L. Dereniak and G. D. Boreman, *Infrared Detectors and Systems*, Wiley series in pure and applied optics. John Wiley & Sons, Inc., New York, NY, U.S.A. (1996).
17. L. Genzel, L. Santo and S. C. Shen, *Far-infrared Fourier transform spectroscopy*, G. Grüner ed., *Millimeter and submillimeter wave spectroscopy of solids*, vol. 74 of *Topics in Applied Physics*, 169–220, Springer Verlag, Berlin, Germany (1998).

18. P. Y. Han, M. Tani, M. Usami, S. Kono, R. Kersting and X.-C. Zhang, *A direct comparison between terahertz time-domain spectroscopy and far-infrared Fourier transform spectroscopy*, *Journal of Applied Physics* **89**(4) (2001) 2357–2359.
19. T. R. Globus, D. L. Woolard, A. C. Samuels, B. L. Gelmont, J. Hesler, T. W. Crowe and M. Bykhovskaia, *Submillimeter-wave fourier transform spectroscopy of biological macromolecules*, *Applied Physics Letters* **91**(9) (2002) 6105–6113.
20. A. Ulman, ed., *Characterization of organic thin films*, Materials characterization. Butterworth-Heinemann, Stoneham, MA USA (1995).
21. D. K. Schroder, *Semiconductor material and device characterization*, John Wiley & Sons, Inc., New York (1990).
22. E. L. Saldin, E. A. Schneidmiller and M. V. Yurkov, *The Physics of Free Electron Lasers*, Advanced Texts in Physics. Springer-Verlag, Berlin (2000).
23. H. A. Schwettman, ed., *Free-electron laser spectroscopy in biology, medicine, and materials science*, vol. 1854. SPIE, SPIE, Washington, DC, U.S.A., Los Angeles, CA (1993).
24. G. P. Gallerano, A. Doria, E. Giovenale and A. Renieri, *Compact free electron lasers: from Cerenkov to waveguide free electron lasers*, *Infrared Physics and Technology* **40**(3) (1999) 161–174.
25. G. P. Williams, *Far-IR/THz radiation from the Jefferson Laboratory, energy recovered linac, free electron laser*, *Review of Scientific Instruments* **73**(3) (2002) 1461–1463.
26. E. M. Telles, R. C. Viscovini, A. Scalabrin and D. Pereira, *Far-infrared laser lines from CH_3-rocking of $^{13}CD_3OD$*, M. N. Afsar ed., *Millimeter and Submillimeter Waves IV*, vol. 3465, 60–63, SPIE, Washington, DC, U.S.A., San Diego, CA, U.S.A. (1998).
27. M. Ghoranneviss, M. A. M. Kashani, A. Hogabri, A. Kohiyan and A. Anvari, *Design and modification of the FIR HCN laser*, M. N. Afsar ed., *Millimeter and Submillimeter Waves IV*, vol. 3465, 85–87, SPIE, Washington, DC, U.S.A., San Diego, CA, U.S.A. (1998).
28. M. Jackson, E. M. Telles, M. D. Allen and K. M. Evenson, *Short-wavelength far-infrared laser cavity yielding new laser emissions in CD_3OH*, *Applied Physics B: Lasers and Optics* **72**(7) (2001) 815–818.
29. B. L. Bean and S. Perkowitz, *Far infrared submillimeter spectroscopy with an optically pumped laser*, *Infrared and Millimeter Waves*, vol. 2 of *Infrared and Millimeter Waves*, 273–298, Academic Press, New York (1979).
30. G. A. Blake, K. B. Laughlin, R. C. Cohen, K. L. Busarow, D.-H. Gwo, C. A. Schmuttenmaer, D. W. Steyert and R. J. Saykally, *Tunable far infrared laser spectrometers*, *Review of Scientific Instruments* **62**(7) (1991) 1693–1700.
31. O. Gauthier-Lafaye, F. H. Julien, S. Cabaret, J.-M. Lourtioz, G. Strasser, E. Gornik, M. Helm and P. Bois, *High-power GaAs/AlGaAs quantum fountain unipolar laser emitting at 14.5 μm with 2.5% tunability*, *Applied Physics Letters* **74**(11) (1999) 1537–1539.
32. V. N. Shastin, R. K. Zhukavin, E. E. Orlova, S. G. Pavlov, M. H. Rümmeli, H.-W. Hübers, J. N. Hovenier, T. O. Klaassen, H. Riemann, I. V. Bradley and A. F. G. van der Meer, *Stimulated terahertz emission from group-V donors in silicon under intracenter photoexcitation*, *Applied Physics Letters* **80**(19) (2002) 3512–3514.
33. S. G. Pavlov, H.-W. Hübers, M. H. Rümmeli, R. K. Zhukavin, E. E. Orlova, V. N. Shastin and H. Riemann, *Far-infrared stimulated emission from optically excited bismuth donors in silicon*, *Applied Physics Letters* **80**(25) (2002) 4717–4719.

34. E. Gornik, K. Unterrainer and C. Kremser, *Tunable far-infrared solid-state lasers based on hot holes in germanium*, *Optical and Quantum Electronics* **23**(2) (1991) 267–286.
35. E. Bründermann, D. R. Chamberlin and E. E. Haller, *Thermal effects in widely tunable germanium terahertz lasers*, *Applied Physics Letters* **73**(19) (1998) 2757–2759.
36. E. Bründermann, D. R. Chamberlin and E. E. Haller, *Novel design concepts of widely tunable germanium terahertz lasers*, *Infrared Physics and Technology* **40**(3) (1999) 141–151.
37. E. Bründermann, D. R. Chamberlin and E. E. Haller, *High duty cycle and continuous terahertz emission from germanium*, *Applied Physics Letters* **76**(21) (2000) 2991–2993.
38. R. E. Peale, A. V. Muravjov, E. W. Nelson, C. Fredricksen, S. G. Pavlov and V. N. Shastin, *The far-infrared p-Ge laser: cavity and modulation advances*, *Conference on Lasers and Electro-Optics '02*, 181–182, Long Beach, CA, U.S.A. (2002).
39. E. Gornik and R. Kersting, *Coherent THz emission in semiconductors*, K. T. Tsen ed., *Ultrafast Physical Processes in Semiconductors*, vol. 67 of *Semiconductors and Semimetals*, 389–440, Academic Press, New York (2001).
40. R. Köhler, A. Tredicucci, F. Beltram, H. E. Beere, E. H. Linfield, A. G. Davies, D. A. Ritchie, R. C. Iotti and F. Rossi, *Terahertz semiconductor-heterostructure laser*, *Nature* **417**(6885) (2002) 156–159.
41. J. Faist, F. Capasso, D. L. Sivco, C. Sirtori, A. L. Hutchinson and A. Y. Cho, *Quantum cascade laser*, *Science* **264** (1994) 553–556.
42. M. Rochat, J. Faist, M. Beck, U. Oesterle and M. Ilegems, *Far-infrared (λ = 88 μm) electroluminescence in a quantum cascade structure*, *Applied Physics Letters* **73**(25) (1998) 3724–3726.
43. S. Blaser, M. Rochat, M. Beck, J. Faist and U. Oesterle, *Far-infrared emission and Stark-cyclotron resonances in a quantum-cascade structure based on photon-assisted tunneling transition*, *Physical Review B* **61**(12) (2000) 8369–8374.
44. S. S. Dhillon, A. G. Davies, R. Harrell, E. H. Linfield, D. A. Ritchie, M. Pepper and D. D. Arnone, *Terahertz (THz) electro-luminescence from AlGaAs-GaAs quantum cascade heterostructures*, *Conference on Lasers and Electro-Optics '01*, 483–484, Optical Society of America, Baltimore, MD, U.S.A. (2001).
45. B. Xu, Q. Hu and M. R. Melloch, *Electrically pumped tunable terahertz emitter based on intersubband transition*, *Applied Physics Letters* **71**(4) (1997) 440–442.
46. P. Harrison and R. W. Kelsall, *Population inversion in optically pumped asymmetric quantum well terahertz lasers*, *Journal of Applied Physics* **81**(11) (1997) 7135–7140.
47. P. Kinsler, P. Harrison and R. W. Kelsall, *Intersubband terahertz lasers using four-level asymmetric quantum wells*, *Journal of Applied Physics* **85**(1) (1999) 23–28.
48. G. Gagliardi, S. Viciani, M. Inguscio, P. De Natale, C. Gmachl, F. Capasso, D. L. Sivco, J. N. Baillargeon, A. L. Hutchinson and A. Y. Cho, *Generation of tunable far-infrared radiation with a quantum cascade laser*, *Optics Letters* **27**(7) (2002) 521–523.
49. A. Tredicucci, C. Gmachl, F. Capasso, M. C. Wanke, A. L. Hutchinson, D. L. Sivco, S.-N. G. Chu and A. Y. Cho, *Novel quantum cascade devices for long wavelength IR emission*, *Optics Materials* **17**(1–2) (2001) 211–217.
50. P. A. Franken, A. E. Hill, C. W. Peters and G. Weinreich, *Generation of optical harmonics*, *Physical Review Letters* **7**(4) (1961) 118–119.

51. J. E. Bjorkholm, *Optical second-harmonic generation using a focused Gaussian laser beam*, *Physical Review* **142**(1) (1966) 126–136.
52. Y. R. Shen, *The Principles of Nonlinear Optics*, Wiley, New York (1984).
53. F. Zernike, Jr. and P. R. Berman, *Generation of far infrared as a difference frequency*, *Physical Review Letters* **15**(26) (1965) 999–1001.
54. F. Zernike, *Temperature-dependent phase matching for far-infrared difference-frequency generation in InSb*, *Physical Review Letters* **22**(18) (1969) 931–933.
55. R. L. Aggarwal, B. Lax, H. R. Fetterman, P. E. Tannenwald and B. J. Clifton, *cw generation of tunable narrow-band far-infrared radiation*, *Journal of Applied Physics* **45**(9) (1974) 3972–3974.
56. Y.-R. Shen, *Far-infrared generation by optical mixing*, *Progress in Quantum Electronics* **4**(3) (1976) 207–232.
57. J. R. Morris and Y. R. Shen, *Theory of far-infrared generation by optical mixing*, *Physical Review A* **15**(3) (1977) 1143–1156.
58. H. Nakanishi, *Organic material for nonlinear optics*, *Japanese Patent* **1,716,929** (1990).
59. K. Kawase, M. Mizuno, S. Sohma, H. Takahashi, T. Taniuchi, Y. Urata, S. Wada, H. Tashiro and H. Ito, *Difference-frequency terahertz-wave generation from 4-dimethylamino-n-methyl-4-stilbazoliu-tosylate by use of an electrically tuned Ti:sapphire laser*, *Optics Letters* **24**(15) (1999) 1065–1067.
60. K. Kawase, T. Hatanaka, H. Takahashi, K. Nakamura, T. Taniuchi and H. Ito, *Tunable terahertz-wave generation from DAST crystal by dual signal-wave parametric oscillation of periodically poled lithium niobate*, *Optics Letters* **25**(23) (2000) 1714–1716.
61. L. P. Barry, J. M. Dudley, B. C. Thomsen and J. D. Harvey, *Measurement of 1.4 THz beat frequencies from a dual wavelength gain-switched laser diode using frequency-resolved optical gating*, T. Elsaesser, J. G. Fujumoto, D. A. Wiersma and W. Zinth eds., *Ultrafast Phenomena XI*, vol. 63 of *Springer Series in Chemical Physics*, 185–187, Springer-Verlag, Berlin (1998).
62. T. Chattopadhyay and M. Bhattacharya, *Submillimeter wave generation through optical four-wave mixing using injection-locked semiconductor lasers*, *Journal of Lightwave Technology* **20**(3) (2002) 502–506.
63. M. Yarborough, S. S. Sussman, H. E. Puthoff, R. H. Pantell and B. C. Johnson, *Efficient, tunable emission from $LiNbO_3$ without a resonator*, *Applied Physics Letters* **15**(3) (1969) 102–105.
64. B. C. Johnson, H. E. Puthoff, J. SooHoo and S. S. Sussman, *Power and linewidth of tunable stimulated far-infrared emission in $LiNbO_3$*, *Applied Physics Letters* **18**(5) (1971) 181–183.
65. M. A. Piestrup, R. N. Fleming and R. H. Pantell, *Continuously tunable submillimeter wave source*, *Applied Physics Letters* **26**(8) (1975) 418–421.
66. K. Kawase, M. Sato, K. Nakamura, T. Taniuchi and H. Ito, *Uni-directional radiation of widely tunable THz-wave using a prism coupler under noncollinear phase matching condition*, *Applied Physics Letters* **71**(6) (1997) 753–755.
67. K. Imai and K. Kawase, *A frequency-agile terahertz-wave parametric oscillator*, *Optics Express* **8**(13) (2001) 699–704.
68. H. Minamide, K. Kawase, K. Imai, A. Sato and H. Ito, *A continuously tunable ring-cavity THz-wave parametric oscillator*, *Review of Laser Engineering* **29**(11) (2001) 744–748.

69. J. Shikata, K. Kawase, M. Sato, T. Taniuchi and H. Ito, *Enhancement of THz-wave output from $LiNbO_3$ optical parametric oscillators by cryogenic cooling*, *Optics Letters* **24**(4) (1999) 202–204.

70. K. Kawase, J. Shikata, K. Imai and H. Ito, *Transform-limited, narrow-linewidth, terahertz-wave parametric generator*, *Applied Physics Letters* **78**(19) (2001) 2819–2821.

71. A. Sato, K. Kawase, H. Minamide, Wada and H. Ito, *Tabletop terahertz-wave parametric generator using a compact, diode-pumped Nd:YAG laser*, *Review of Scientific Instruments* **72**(9) (2001) 3501–3504.

72. E. R. Brown, K. A. McIntosh, F. W. Smith, M. J. Manfra and C. L. Dennis, *Measurements of optical-heterodyne conversion in low-temperature-grown GaAs*, *Applied Physics Letters* **62**(11) (1993) 1206–1208.

73. E. R. Brown, F. W. Smith and K. A. McIntosh, *Coherent millimeter-wave generation by heterodyne conversion in low-temperature-grown GaAs photoconductors*, *Journal of Applied Physics* **73**(3) (1993) 1480–1484.

74. E. R. Brown, K. A. McIntosh, F. W. Smith, K. B. Nichols, M. J. Manfra, C. L. Dennis and J. P. Mattia, *Milliwatt output levels and superquadratic bias dependence in a low-temperature-grown GaAs photomixer*, *Applied Physics Letters* **64**(24) (1994) 3311–3313.

75. E. R. Brown, K. A. McIntosh, K. B. Nichols and C. L. Dennis, *Photomixing up to 3.8 THz in low-temperature-grown GaAs*, *Applied Physics Letters* **66**(3) (1995) 285–287.

76. K. A. McIntosh, E. R. Brown, K. B. Nichols, O. B. McMahon, W. F. DiNatale and T. M. Lyszczarz, *Terahertz photomixing with diode lasers in low-temperature-grown GaAs*, *Applied Physics Letters* **67**(26) (1995) 3844–3846.

77. A. S. Pine, R. D. Suenram, E. R. Brown and K. A. McIntosh, *A terahertz photomixing spectrometer: application to SO_2 self broadening*, *Journal of Molecular Spectroscopy* **175**(1) (1996) 37–47.

78. S. Verghese, K. A. McIntosh, S. Calawa, W. F. Dinatale, E. K. Duerr and K. A. Molvar, *Generation and detection of coherent terahertz waves using two photomixers*, *Applied Physics Letters* **73**(26) (1998) 3824–3826.

79. T. M. Goyette, W. Guo, F. C. D. Lucia, J. C. Swartz, H. O. Everitt, B. D. Guenther and E. R. Brown, *Femtosecond demodulation source for high-resolution submillimeter spectroscopy*, *Applied Physics Letters* **67**(25) (1995) 3810–3812.

80. S. Matsuura, M. Tani and K. Sakai, *Generation of coherent terahertz radiation by photomixing in dipole photoconductive antennas*, *Applied Physics Letters* **70**(5) (1997) 559–561.

81. S. Verghese, K. A. McIntosh and E. R. Brown, *Highly tunable fiber-coupled photomixers with coherent terahertz output power*, *IEEE Transactions on Microwave Theory and Techniques* **45**(8) (1997) 1301–1309.

82. S. M. Duffy, S. Verghese, A. McIntosh, A. Jackson, A. C. Gossard and S. Matsuura, *Accurate modeling of dual dipole and slot elements used with photomixers for coherent terahertz output power*, *IEEE Transactions on Microwave Theory and Techniques* **49**(6) (2001) 1032–1038.

83. P. Chen, G. A. Blake, M. C. Gaidis, E. R. Brown, K. A. McIntosh, S. Y. Chou, M. I. Nathan and F. Williamson, *Spectroscopic applications and frequency locking of THz photomixing with distributed-Bragg-reflector diode lasers in low-temperature-grown GaAs*, *Applied Physics Letters* **71**(12) (1997) 1601–1603.

84. T. Hidaka, S. Matsuura, M. Tani and K. Sakai, *CW terahertz wave generation by photomixing using a two-longitudinal-mode laser diode*, *Electronics Letters* **33**(24) (1997) 2039–2040.
85. M. Hyodo, M. Tani, S. Matsuura, N. Onodera and K. Sakai, *Generation of millimetre-wave radiation using a dual-longitudinal-mode microchip laser*, *Electronics Letters* **32**(17) (1996) 1589–1591.
86. J. W. Nicholson, W. Rudolph and G. Hager, *Generation of 14 GHz radiation using a two frequency iodine laser*, *Applied Physics Letters* **72**(26) (1998) 3402–3404.
87. P. Gu, M. Tani, M. Hyoho, K. Sakai and T. Hidaka, *Generation of cw-terahertz radiation using a two-longitudinal-mode laser diode*, *Japanese Journal of Applied Physics* **37**(8B) (1998) L976–L978.
88. F. Siebe, K. Siebert, R. Leonhardt and H. G. Roskos, *A fully tunable dual-color CW Ti:Al_2O_3 laser*, *IEEE Journal of Quantum Electronics* **35**(11) (1999) 1731–1736.
89. C.-L. Wang and C.-L. Pan, *Tunable multiterahertz beat signal generation from a two-wavelength laser-diode array*, *Optics Letters* **20**(11) (1995) 1292–1294.
90. A. S. Weling and D. H. Auston, *Novel sources and detectors for coherent tunable narrow-band terahertz radiation in free space*, *Journal of the Optical Society of America B: Optical Physics* **13**(12) (1996) 2783–2791.
91. T. Kleine-Ostmann, P. Knobloch, M. Koch, S. Hoffmann, M. Breede, M. Hofmann, G. Hein, K. Pierz, M. Sperling and K. Donhuijsen, *Continuous-wave THz imaging*, *Electronics Letters* **37**(24) (2001) 1461–1463.
92. H. Eisele, A. Rydberg and G. I. Haddad, *Recent advances in the performance of InP Gunn devices and GaAs TUNNETT diodes for the 100–300-GHz frequency range and above*, *IEEE Transactions on Microwave Theory and Techniques* **48**(4) (2000) 626–631.
93. S. Sridhar, D. Reagor and G. Gruner, *Complex conductivity measurements between 26 and 110 GHz using complex impedance bridges*, *Review of Scientific Instruments* **56**(10) (1985) 1946–1952.
94. J. A. Reedijk, H. C. F. Martens, B. J. G. Smits and H. B. Brom, *Measurement of the complex dielectric constant down to helium temperatures. II. Quasioptical technique from 0.03 to 1 THz*, *Review of Scientific Instruments* **71**(2) (2000) 478–481.
95. D. W. van der Weide, J. S. Bostak, B. A. Auld and D. M. Bloom, *All-electronic free-space picosecond pulse generation and detection*, *Electronics Letters* **27**(16) (1991) 1412–1413.
96. D. W. van der Weide, *Planar antennas for all-electronic terahertz systems*, *Journal of the Optical Society of America B: Optical Physics* **11**(12) (1994) 2553–2560.
97. D. W. van der Weide and F. Keilmann, *Coherent periodically pulsed radiation spectrometer*, *US Patent* **5,748,309** (1998), www.uspto.gov.
98. J. S. Bostak, D. W. van der Weide, D. M. Bloom and B. A. Auld, *All-electronic terahertz spectroscopy system with terahertz free-space pulses*, *Journal of the Optical Society of America B: Optical Physics* **11**(12) (1994) 2561–2565.
99. D. W. van der Weide, J. Murakowski and F. Keilmann, *Gas-absorption spectroscopy with electronic terahertz techniques*, *IEEE Transactions on Microwave Theory and Techniques* **48**(4) (2000) 740–743.
100. G. Kozlov and V. Volkov, *Coherent source submillimeter wave spectroscopy*, G. Grüner ed., *Millimeter and submillimeter wave spectroscopy of solids*, vol. 74 of *Topics in Applied Physics*, 51–109, Springer-Verlag, Berlin (1998).
101. M. Dressel, *Microspectroscopy in the millimeter and far-infrared spectral range using coherent CW radiation*, J. M. Chamberlain and M. A. Smith eds., *First International*

Conference on Biomedical Imaging & Sensing Applications of Terahertz Technology, Leeds, UK (2001).

102. T. Klaus, S. Takano and G. Winnewisser, *Laboratory measurement of the $N = 1 \leftarrow 0$ rotational transition of NH at 1 THz*, *Astronomy and Astrophysics* **322** (1997) L1–L4.
103. S. Takano, T. Klaus and G. Winnewisser, *The ND radical: Laboratory measurement of the N=2–1 rotational transition at 1 THz*, *Journal of Molecular Spectroscopy* **192**(2) (1998) 309–319.
104. J. Morino, K. M. T. Yamada, H. Klein, S. P. Belov, G. Winnewisser, R. Bocquet, G. Wlodarczak and W. L. M. Kreglewski, *Terahertz rotational spectra of NH_2OH in the ground and some low excited vibrational states*, *Journal of Molecular Structure* **517-518** (2000) 367–373.
105. A. Pimenov, A. V. Pronin, A. Loidl, A. P. Kampf, S. I. Krasnosvobodtsev and V. S. Nozdrin, *Submillimeter spectroscopy of tilted $Nd_{1.85}Ce_{0.15}CuO_{4-\delta}$ films: Observation of a mixed ac-plane excitation*, *Applied Physics Letters* **77**(3) (2000) 429–431.
106. D. Woolard, R. Kaul, R. Suenram, A. H. Walker, T. Globus and A. Samuels, *Terahertz electronics for chemical and biological warfare agent detection*, M. Matloubian and E. Ponti eds., *IEEE MTT-S International Microwave Symposium Digest*, vol. 3, 925–928, IEEE, Anaheim, CA (1999).
107. A. Nahata, J. T. Yardley and T. F. Heinz, *Free-space electro-optic detection of continuous-wave terahertz radiation*, *Applied Physics Letters* **75**(17) (1999) 2524–2526.
108. R. Katterloher, G. Jakob, E. Bauser, S. Zehender, E. E. Haller, J. Beeman, T. Henning and G. Pilbratt, *Recent results from the development of a far infra-red n-type GaAs detector array for FIRST*, M. S. Scholl and B. F. Andresen eds., *Infrared Spaceborne Remote Sensing III*, vol. 2553, 524–535, SPIE, Washington, DC, U.S.A. (1995).
109. M. I. Dyakonov and M. S. Shur, *Plasma wave electronics: Terahertz detectors and sources using two dimensional electronic fluid in high electronic mobility transistors*, *1997 Advanced Workshop on Frontiers in Electronics, WOFE*, 105–108, Piscataway, NJ, USA (1997).
110. K. S. Yngvesson, *Ultrafast two-dimensional electron gas detector and mixer for terahertz radiation*, *Applied Physics Letters* **76**(6) (2000) 777–779.
111. F. Klappenberger, A. A. Ignatov, S. Winnerl, E. Schomburg, W. Wegscheider, K. F. Renk and M. Bichler, *Broadband semiconductor superlattice detector for THz radiation*, *Applied Physics Letters* **78**(12) (2001) 1673–1675.
112. P. Orellana and F. Claro, *A mesoscopic terahertz pulse detector*, *Applied Physics Letters* **75**(11) (1999) 1643–1645.
113. M. A. Gadir, P. Harrison and R. A. Soref, *Responsivity of quantum well infrared photodetectors at terahertz detection wavelengths*, *Applied Physics Letters* **91**(9) (2002) 5820–5825.
114. M. S. Shur, J.-Q. Lü and M. I. Dyakonov, *Terahertz applications of plasma wave electronics*, M. Matloubian and E. Ponti eds., *IEEE MTT-S International Microwave Symposium Digest*, vol. 3, 937–940, IEEE, Anaheim, CA (1999).
115. P. H. Siegel, *Terahertz technology*, *IEEE Transactions on Microwave Theory and Techniques* **50**(3) (2002) 910–928.
116. E. Dupont, M. Byloos, M. Gao, M. Buchanan, C.-Y. Song, Z. R. Wasilewski and H. C. Liu, *Pixelless thermal imaging with integrated quantum-well infrared photodetector and light-emitting diode*, *IEEE Photonics Technology Letters* **14**(2) (2002) 182–184.

117. K. J. Siebert, H. Quast, R. Leonhardt, T. Löffler, M. Thomson, T. Bauer, H. G. Roskos and S. Czasch, *Continuous-wave all-optoelectronic terahertz imaging*, *Applied Physics Letters* **80**(16) (2002) 3003–3005.
118. H. A. Haus, *Mode-locking of lasers*, *IEEE Journal of Selected Topics in Quantum Electronics* **6**(6) (2000) 1173–1185.
119. D. H. Auston and M. C. Nuss, *Electrooptic generation and detection of femtosecond electrical transients*, *IEEE Journal of Quantum Electronics* **24**(2) (1988) 184–197.
120. J. A. Valdmanis, G. Mourou and C. W. Gabel, *Picosecond electro-optic sampling system*, *Applied Physics Letters* **41**(3) (1982) 211–212.
121. J. A. Valdmanis, G. A. Mourou and C. W. Gabel, *Subpicosecond electrical sampling*, *IEEE Journal of Quantum Electronics* **19**(4) (1983) 664–667.
122. M. Y. Frankel, J. F. Whitaker and G. A. Mourou, *Optoelectronic transient characterization of ultrafast devices*, *IEEE Journal of Quantum Electronics* **28**(10) (1992) 2313–2324.
123. D. H. Auston, K. P. Cheung and P. R. Smith, *Picosecond photoconducting Hertzian dipoles*, *Applied Physics Letters* **45**(3) (1984) 284–286.
124. D. H. Auston and K. P. Cheung, *Coherent time-domain far-infrared spectroscopy*, *Journal of the Optical Society of America B: Optical Physics* **2**(4) (1985) 606–612.
125. A. P. DeFonzo and C. R. Lutz, *Optoelectronic transmission and reception of ultrashort electrical pulses*, *Applied Physics Letters* **51**(4) (1987) 212–214.
126. A. P. DeFonzo, M. Jarwala and C. R. Lutz, *Transient respose of planar integrated optoelectronic antennas*, *Applied Physics Letters* **50**(17) (1987) 1155–1157.
127. P. R. Smith, D. H. Auston and M. C. Nuss, *Subpicosecond photoconducting dipole antennas*, *IEEE Journal of Quantum Electronics* **24**(2) (1988) 255–260.
128. C. Fattinger and D. Grischkowsky, *Point source terahertz optics*, *Applied Physics Letters* **53**(16) (1988) 1480–1482.
129. B. B. Hu, X.-C. Zhang and D. H. Auston, *Free-space radiation from electro-optic crystals*, *Applied Physics Letters* **56**(6) (1990) 506–508.
130. Q. Wu and X.-C. Zhang, *Free-space electro-optic sampling of terahertz beams*, *Applied Physics Letters* **67**(24) (1995) 3523–3525.
131. M. van Exter, C. Fattinger and D. Grischkowsky, *High-brightness terahertz beams characterized with an ultrafast detector*, *Applied Physics Letters* **55**(4) (1989) 337–339.
132. Y. Pastol, G. Arjavalingham, J.-M. Halbout and G. V. Kopscay, *Coherent broadband microwave spectroscopy using picosecond optoelectronic antennas*, *Applied Physics Letters* **54**(4) (1989) 307–309.
133. D. Grischkowsky, S. Keiding, M. van Exter and C. Fattinger, *Far-infrared time-domain spectroscopy with terahertz beams of dielectrics and semiconductors*, *Journal of the Optical Society of America B: Optical Physics* **7**(10) (1990) 2006–2015.
134. B. B. Hu, X.-C. Zhang and D. H. Auston, *Terahertz radiation induced by subband-gap femtosecond optical excitation of GaAs*, *Physical Review Letters* **67**(19) (1991) 2709–2712.
135. D. Côté, J. M. Fraser, M. DeCamp, P. H. Bucksbaum and H. M. van Driel, *THz emission from coherently controlled photocurrents in GaAs*, *Applied Physics Letters* **75**(25) (1999) 3959–3961.
136. D. Hashimshony, A. Zigler and K. Papadopoulos, *Conversion of electrostatic to electromagnetic waves by superluminous ionization fronts*, *Physical Review Letters* **86**(13) (2001) 2806–2809.

137. D. H. Auston, *Ultrafast optoelectronics*, W. Kaiser ed., *Ultrashort Laser Pulses and Applications*, vol. 60 of *Topics in Applied Physics*, 183–233, Springer-Verlag, Berlin, Germany (1988).
138. G. Mourou, C. V. Stancampiano and D. Blumenthal, *Picosecond microwave pulse generation*, *Applied Physics Letters* **38**(6) (1981) 470–472.
139. C. Fattinger and D. Grischkowsky, *Terahertz beams*, *Applied Physics Letters* **54**(6) (1989) 490–492.
140. S. E. Ralph and D. Grischkowsky, *THz spectroscopy and source characterization by optoelectronic interferometry*, *Applied Physics Letters* **60**(9) (1992) 1070–1072.
141. Y. Cai, I. Brener, J. Lopata, J. Wynn, L. Pfeiffer and J. Federici, *Design and performance of singular electric field terahertz photoconducting antennas*, *Applied Physics Letters* **71**(15) (1997) 2076–2078.
142. S. R. Andrews, P. G. Huggard and A. Armitage, *Optimisation of photoconducting receivers for THz spectroscopy*, J. M. Chamberlain and M. A. Smith eds., *First International Conference on Biomedical Imaging & Sensing Applications of Terahertz Technology*, Leeds, UK (2001).
143. G. Zhao, R. N. Schouten, N. van der Valk, W. T. Wenckebach and P. C. M. Planken, *Design and performance of a THz emission and detection setup based on a semi-insulating GaAs emitter*, *Review of Scientific Instruments* **73**(4) (2002) 1715–1719.
144. E. Budiarto, J. Margolies, S. Jeong, J. Son and J. Bokor, *High-intensity terahertz pulses at 1-kHz repetition rate*, *IEEE Journal of Quantum Electronics* **32**(10) (1996) 1839–1846.
145. S.-G. Park, A. M. Weiner, M. R. Melloch, C. W. Siders, J. L. W. Siders and A. J. Taylor, *High-power narrow-band terahertz generation using large-aperture photoconductors*, *IEEE Journal of Quantum Electronics* **35**(8) (1999) 1257–1268.
146. H. Yoneda, K. Tokuyama, K. Ueda, H. Yamamoto and K. Baba, *High-power terahertz radiation emitter with a diamond photoconductive switch array*, *Applied Optics* **40**(36) (2001) 6733–6736.
147. P. K. Benicewicz and A. J. Taylor, *Scaling of terahertz radiation from large-aperture biased InP photoconductors*, *Optics Letters* **18**(16) (1993) 1332–1334.
148. P. K. Benicewicz, J. P. Roberts and A. J. Taylor, *Scaling of terahertz radiation from large-aperture biased photoconductors*, *Journal of the Optical Society of America B: Optical Physics* **11**(12) (1994) 2533–2546.
149. M. Tani, S. Matsuura, K. Sakai and S. Nakashima, *Emission characteristics of photoconductive antennas based on low-temperature-grown GaAs and semi-insulating GaAs*, *Applied Optics* **36**(30) (1997) 7853–7859.
150. P. G. Huggard, C. J. Shaw, J. A. Cluff and S. R. Andrews, *Polarization-dependent efficiency of photoconducting THz transmitters and receivers*, *Applied Physics Letters* **72**(17) (1998) 2069–2071.
151. A. C. Warren, N. Katzenellenbogen, D. Grischkowsky, J. M. Woodall, M. R. Melloch and N. Otsuka, *Subpicosecond, freely propagating electromagnetic pulse generation and detection using GaAs:As epilayers*, *Applied Physics Letters* **58**(14) (1991) 1512–1514.
152. A. Nahata and T. F. Heinz, *Reshaping of freely propagating terahertz pulses by diffraction*, *IEEE Journal of Selected Topics in Quantum Electronics* **2**(3) (1996) 701–708.
153. D. R. Dykaar, B. I. Greene, J. F. Federici, A. F. Levi, L. N. Pfeiffer and R. F. Kopf, *Log-periodic antennas for pulsed terahertz radiation*, *Applied Physics Letters* **59**(3) (1991) 262–264.

154. G. Arjavalingam, Y. Pastol, J.-M. Halbout and W. M. Robertson, *Optoelectronically-pulsed antennas: characterization and applications, IEEE Antennas and Propagation Magazine* **33**(1) (1991) 7–11.

155. M. M. Gitin, F. W. Wise, G. Arjavalingam, Y. Pastol and R. C. Compton, *Broadband characterization of millimeter-wave log-periodic antennas by photoconductive sampling, IEEE Transactions on Antennas and Propagation* **42**(3) (1994) 335–339.

156. T. Pfeider, H.-M. Heiliger, E. S. von Kamienski, H. G. Roskos and H. Kurz, *Fabrication and characterization of freely positionable silicon-on-sapphire photoconductive probes, Journal of the Optical Society of America B: Optical Physics* **11**(12) (1994) 2547–2552.

157. I. Brener, D. Dykaar, A. Frommer, L. N. Pfeiffer, J. Lopata, J. Wynn, K. West and M. C. Nuss, *Terahertz emission from electric field singularities in biased semiconductors, Optics Letters* **21**(23) (1996) 1924–1926.

158. M. C. Nuss and J. Orenstein, *Terahertz time-domain spectroscopy*, G. Grüner ed., *Millimeter and submillimeter wave spectroscopy of solids*, vol. 74 of *Topics in Applied Physics*, 7–50, Springer-Verlag, Berlin, Germany (1998).

159. S. Feng and H. G. Winful, *Fields of single-cycle terahertz pulses generated by loop antenna, Conference on Lasers and Electro-Optics '98*, 59–60, Optical Society of America, San Francisco, CA, U.S.A. (1998).

160. D. Liu, D. Carette, M. Bergeron, H. Karwacki, S. Adams, B. Lanning and F. Kustas, *Structurally embedded photoconductive silicon bowtie antenna, IEEE Photonics Technology Letters* **10**(5) (1998) 716–718.

161. N. Katzenellenbogen and D. Grischkowsky, *Efficient generation of 380 fs pulses of THz radiation by ultrafast laser pulse excitation of a biased metal-semiconductor interface, Applied Physics Letters* **58**(3) (1991) 222–224.

162. Y. Liu, S.-G. Park and A. M. Weiner, *Terahertz waveform synthesis via optical pulse shaping, IEEE Journal of Selected Topics in Quantum Electronics* **2**(3) (1996) 709–719.

163. A. S. Weling and T. F. Heinz, *Enhancement in the spectral irradiance of photoconducting terahertz emitters by chirped-pulse mixing, Journal of the Optical Society of America B: Optical Physics* **16**(9) (1999) 1455–1467.

164. S.-G. Park, M. R. Melloch and A. M. Weiner, *Analysis of terahertz waveforms measured by photoconductive and electrooptic sampling, IEEE Journal of Quantum Electronics* **35**(5) (1999) 810–819.

165. P. U. Jepsen and S. R. Keiding, *Radiation patterns from lens-coupled terahertz antennas, Optics Letters* **20**(8) (1995) 807–809.

166. Y.-S. Chung, C. Cheon, J.-H. Son and S.-Y. Hahn, *FDTD analysis of propagation characteristics of terahertz electromagnetic pulses, IEEE Transactions on Magnetics* **36**(4) (2000) 951–955.

167. J. V. Rudd and D. M. Mittleman, *Influence of substrate-lens design in terahertz time-domain spectroscopy, Journal of the Optical Society of America B: Optical Physics* **19**(2) (2002) 319–329.

168. J. V. Rudd, J. L. Johnson and D. M. Mittleman, *Quadrupole radiation from terahertz dipole antennas, Optics Letters* **25**(20) (2000) 1556–1558.

169. J. V. Rudd, J. L. Johnson and D. M. Mittleman, *Cross-polarized angular emission patterns from lens-coupled terahertz antennas, Journal of the Optical Society of America B: Optical Physics* **18**(10) (2001) 1524–1533.

170. A. Gürtler, C. Winnewisser, H. Helm and P. U. Jepsen, *Terahertz pulse propagation in the near field and the far field, Journal of the Optical Society of America A: (Optics & Vision)* **17**(1) (2000) 74–83.
171. Z. Jiang and X.-C. Zhang, *2D measurement and spatio-temporal coupling of few-cycle THz pulses, Optics Express* **5**(11) (1999) 243–248.
172. Z. Jiang and X.-C. Zhang, *Terahertz imaging via electrooptic effect, IEEE Transactions on Microwave Theory and Techniques* **47**(12) (1999) 2644–2650.
173. R. K. Lai, J.-R. Hwang, T. B. Norris and J. F. Whitaker, *A photoconductive, miniature terahertz source, Applied Physics Letters* **72**(24) (1998) 3100–3102.
174. T. Löffler, F. Jacob and H. G. Roskos, *THz generation by photo-ionization of electrically biased air, Conference on Lasers and Electro-Optics '00*, vol. 39 of *TOPS*, 356–357, Optical Society of America, San Francisco, CA, U.S.A. (2000).
175. J. Darmo, T. Müller, G. Strasser and K. Unterrainer, *Voltage-controlled intracavity THz generator for self-starting Ti:Sapphire lasers, Conference on Lasers and Electro-Optics '02*, Long Beach C.A, USA (2002), PostDeadline Digest.
176. X.-C. Zhang, Y. Jin and X. F. Ma, *Coherent measurement of THz optical rectification from electro-optic crystals, Applied Physics Letters* **61**(23) (1992) 2764–2766.
177. A. Rice, Y. Jin, X. F. Ma, X.-C. Zhang, D. Bliss, J. Larkin and M. Alexander, *Terahertz optical rectification from ⟨110⟩ zinc-blende crystals, Applied Physics Letters* **64**(11) (1994) 1324–1326.
178. A. Bonvalet and M. Joffre, *Terahertz femtosecond pulses*, C. Rullière ed., *Femtosecond Laser Pulses*, 285–305, Springer-Verlag, Berlin (1998).
179. B. E. A. Saleh and M. C. Teich, *Fundamentals of Photonics*, John Wiley & Sons, Inc., New York (1991).
180. A. Yariv, *Optical Electronics*, 4th ed. Oxford University Press, Oxford (1991).
181. M. Bass, P. A. Franken, J. F. Ward and G. Weinreich, *Optical rectification, Physical Review Letters* **9**(11) (1962) 446–448.
182. T. Yajima and N. Takeuchi, *Spectral properties and tunability of far-infrared difference-frequency radiation produced by picosecond laser pulses, Japanese Journal of Applied Physics* **10**(7) (1971) 907–915.
183. K. H. Yang, P. L. Richards and Y. R. Shen, *Generation of far-infrared radiation by picosecond light pulses in $LiNbO_3$, Applied Physics Letters* **19**(9) (1971) 320–323.
184. J. Morris and Y. R. Shen, *Far-infrared generation by picosecond pulses in electro-optic materials, Optics Communications* **3**(2) (1971) 81–84.
185. D. H. Auston, A. M. Glass and A. A. Ballman, *Optical rectification by impurities in polar crystals, Physical Review Letters* **28**(14) (1972) 897–900.
186. D. Bagasaryan, A. Makaryan and P. Pogosyan, *Cherenkov radiation from a propagating nonlinear polarization wave, JETP Letters* **37** (1983) 595.
187. D. H. Auston, *Subpicosecond electro-optic shock waves, Applied Physics Letters* **43**(8) (1983) 713–715.
188. D. H. Auston, K. P. Cheung, J. A. Valdmanis and D. A. Kleinman, *Cherenkov radiation from femtosecond optical pulses in electro-optic media, Physical Review Letters* **53**(16) (1984) 1555–1558.
189. D. A. Kleinman and D. H. Auston, *Theory of electro-optic shock radiation in nonlinear media, IEEE Journal of Quantum Electronics* **20**(8) (1984) 964–970.
190. J. B. Khurgin, *Optical rectification and terahertz emission in semiconductors excited above the band gap, Journal of the Optical Society of America B: Optical Physics* **11**(12) (1994) 2492–2501.

191. T. J. Carrig, G. Rodriguez, T. S. Clement, A. J. Taylor and K. R. Stewart, *Scaling of terahertz radiation via optical rectification in electro-optic crystals*, *Applied Physics Letters* **66**(2) (1995) 121–123.
192. F. G. Sun, W. Ji and X.-C. Zhang, *Two-photon absorption induced saturation of THz radiation in ZnTe*, *Conference on Lasers and Electro-Optics '00*, vol. 39 of *TOPS*, 479–80, Optical Society of America, San Francisco, CA, U.S.A. (2000).
193. Q. Wu and X.-C. Zhang, *Design and characterization of travelling-wave electrooptic terahertz sensors*, *IEEE Journal of Selected Topics in Quantum Electronics* **2**(3) (1996) 693–700.
194. A. Nahata, D. H. Auston and T. F. Heinz, *Coherent detection of freely propagating terahertz radiation by electo-optic sampling*, *Applied Physics Letters* **68**(2) (1996) 150–152.
195. A. Yariv, *Quantum Electronics*, 3rd ed. Wiley, New York (1989).
196. L. Xu, X.-C. Zhang and D. H. Auston, *Terahertz beam generation by femtosecond optical pulses in electo-optic materials*, *Applied Physics Letters* **61**(15) (1992) 1784–1786.
197. Q. Chen, M. Tani, Z. Jiang and X.-C. Zhang, *Electro-optic transceivers for terahertz-wave applications*, *Journal of the Optical Society of America B: Optical Physics* **18**(6) (2001) 823–831.
198. C. P. Yakymyshyn, K. R. Stewart, E. P. Boden, S. R. Marder, J. W. Perry and W. P. Schaefer, *Second-order non-linear optical properties of 4n-methylstilbazolium tosylate salts*, R. A. Hann and D. Bloor eds., *Organic Materials for Non-linear Optics II*, 108–114, Royal Society of Chemistry, London (1991).
199. X.-C. Zhang, X. F. Ma, Y. Jin, T.-M. Lu, E. P. Boden, P. D. Phelps, K. R. Stewart and C. P. Yakymyshyn, *Terahertz optical rectification from a nonlinear organic crystal*, *Applied Physics Letters* **61**(26) (1992) 3080–3082.
200. A. Bonvalet, M. Joffre, J.-L. Martin and A. Migus, *Generation of ultrabroadband femtosecond pulses in the mid-infrared by optical rectification of 15 fs light pulses at 100 MHz repetition rate*, *Applied Physics Letters* **67**(20) (1995) 2907–2909.
201. P. Y. Han and X.-C. Zhang, *Free-space coherent broadband terahertz time-domain spectroscopy*, *Measurement Science and Technology* **12**(11) (2001) 1747–1756.
202. D. J. Cook and R. M. Hochstrasser, *Intense terahertz pulses by four-wave rectif ication in air*, *Optics Letters* **25**(16) (2000) 1210–1212.
203. D. S. Citrin, *Generation of 10-THz transients from a subpicosecond optical pulse and a 1-THz field in quantum wells*, *Applied Physics Letters* **70**(10) (1997) 1189–1191.
204. A. Nahata, D. H. Auston, C. Wu and J. T. Yardley, *Generation of terahertz radiation from a poled polymer*, *Applied Physics Letters* **67**(10) (1995) 1358–1360.
205. A. M. Sinyukov and L. M. Hayden, *Generation and detection of terahertz radiation with multilayered electro-optic polymer films*, *Optics Letters* **27**(1) (2002) 55–57.
206. J. L. W. Siders, S. A. Trugman, F. H. Garzon, R. J. Houlton and A. J. Taylor, *Terahertz emission from $YBa_2Cu_3O_{7-\delta}$ thin films via bulk electric-quadrupole-magnetic-dipole optical rectification*, *Physical Review B* **61**(20) (2000) 13633–13638.
207. M. S. C. Luo, S. L. Chuang, P. C. M. Planken, I. Brener and M. C. Nuss, *Coherent double-pulse control of quantum beats in a coupled quantum well*, *Physical Review B* **48**(15) (1993) 11043–11050.
208. C. Weiss, G. Torosyan, Y. Avetisyan and R. Beigang, *Generation of tunable narrow-band surface-emitted terahertz radiation in periodically poled lithium niobate*, *Optics Letters* **26**(8) (2001) 563–565.

209. Y. S. Lee, T. Meade, V. Perlin, H. Winful, T. B. Norris and A. Galvanauskas, *Generation of narrow-band terahertz radiation via optical rectification of femtosecond pulses in periodically poled lithium niobate*, *Applied Physics Letters* **76**(18) (2000) 2505–2507.

210. Y. S. Lee, T. Meade, M. DeCamp, T. B. Norris and A. Galvanauskas, *Temperature dependence of narrow-band terahertz generation from periodically poled lithium niobate*, *Applied Physics Letters* **77**(9) (2000) 1244–1246.

211. Y. S. Lee, T. Meade, T. B. Norris and A. Galvanauskas, *Tunable narrow-band terahertz generation from periodically poled lithium niobate*, *Applied Physics Letters* **78**(23) (2001) 3583–3585.

212. M. Li, G. Sucha, P.-Y. Han, A. Galvanaoskas, D. Harter and X.-C. Zhang, *THz generation and detection using 1550-nm pulses from a fiber laser*, *Conference on Lasers and Electro-Optics '00*, vol. 39 of *TOPS*, 559–60, Optical Society of America, San Francisco, CA, U.S.A. (2000).

213. A. S. Weling, B. B. Hu, N. M. Froberg and D. H. Auston, *Generation of tunable narrow-band THz radiation from large aperture photoconducting antennas*, *Applied Physics Letters* **64**(2) (1994) 137–139.

214. M. Joffre, A. Bonvalet, A. Migus and J.-L. Martin, *Femtosecond diffracting fourier-transform infrared interferometer*, *Optics Letters* **21**(13) (1996) 964–966.

215. F. Eickemeyer, R. A. Kaindl, M. Woerner, T. Elsaesser and A. M. Weiner, *Controlled shaping of ultrafast electric field transients in the mid-infrared spectral range*, *Optics Letters* **25**(19) (2000) 1472–1474.

216. J. Y. Sohn, Y. H. Ahn, D. J. Park, E. Oh and D. S. Kim, *Tunable terahertz generation using femtosecond pulse shaping*, *Applied Physics Letters* **81**(1) (2002) 13–15.

217. G. Veitas and R. Danielius, *Generation of narrow-bandwidth tunable picosecond pulses by difference-frequency mixing of stretched pulses*, *Journal of the Optical Society of America B: Optical Physics* **16**(9) (1999) 1561–1565.

218. N. Belabas, J.-P. Likforman, L. Canioni, B. Bousquet and M. Joffre, *Coherent broadband pulse shaping in the mid infrared*, *Optics Letters* **26**(10) (2001) 743–745.

219. V. Ryzhii, I. Khmyrova and M. Shur, *Terahertz photomixing in quantum well structures using resonant excitation of plasma oscillations*, *Journal of Applied Physics* **91**(4) (2002) 1875–1881.

220. X.-C. Zhang, B. B. Hu, J. T. Darrow and D. H. Auston, *Generation of femtosecond electromagnetic pulses from semiconductor surfaces*, *Applied Physics Letters* **56**(11) (1990) 1011–1013.

221. X.-C. Zhang, J. T. Darrow, B. B. Hu, D. H. Auston, M. T. Schmidt, P. Tham and E. S. Yang, *Optically induced electromagnetic radiation from semiconductor surfaces*, *Applied Physics Letters* **56**(22) (1990) 2228–2230.

222. S. Luryi, *Polarization oscillations in coupled quantum wells - a scheme for generation of submillimeter electromagnetic waves*, *IEEE Journal of Quantum Electronics* **27**(1) (1991) 54–60.

223. T. Dekorsky, H. Auer, C. Waschke, H. J. Bakker, H. G. Roskos, H. Kurz, V. Wagner and P. Grosse, *Emission of submillimeter electromagnetic waves by coherent phonons*, *Physical Review Letters* **74**(5) (1995) 738–741.

224. G. A. Garrett, T. F. Albrecht, J. F. Whitaker and R. Merlin, *Coherent THz phonons driven by light pulses and the Sb problem: What is the mechanism?*, *Physical Review Letters* **77**(17) (1996) 3661–3664.

225. R. Merlin, *Generating coherent THz phonons with light pulses*, *Solid State Communications* **102**(2–3) (1997) 207–220.

226. P. Y. Han, G. C. Cho and X.-C. Zhang, *Mid-infrared THz beam sensors: Exploration and application for phonon spectroscopy*, *Ultrafast Phenomena in Semiconductors III*, vol. 3624, 224–33 (1999).

227. R. Kersting, K. Unterrainer, G. Strasser, H. F. Kauffmann and E. Gornik, *Few-cycle THz emission from cold plasma oscillations*, *Physical Review Letters* **79**(16) (1997) 3038–3041.

228. R. Kersting, J. N. Heyman, G. Strasser and K. Unterrainer, *Coherent plasmons in n-doped GaAs*, *Physical Review B* **58**(8) (1998) 4553–4559.

229. W. Pötz, *Infrared light emission from semiconductor double wells*, *Applied Physics Letters* **68**(18) (1996) 2553–2555.

230. R. Kersting, J. N. Heyman, G. Strasser and K. Unterrainer, *Driving intersubband transitions with THz pulses*, T. Elsaesser, J. G. Fujumoto, D. A. Wiersma and W. Zinth eds., *Ultrafast Phenomena XI*, vol. 63 of *Springer Series in Chemical Physics*, 208–210, Springer-Verlag, Berlin (1998).

231. A. Bonvalet, J. Nagle, V. Berger, A. Migus, J.-L. Martin and M. Joffre, *Femtosecond infrared emission resulting from coherent charge oscillations in quantum wells*, *Physical Review Letters* **76**(23) (1996) 4392–4395.

232. R. Harel, I. Brener, L. N. Pfeiffer, K. West, J. M. Vandenberg and S. N. G. Chu, *Coherent terahertz emission from cavity polaritons in semiconductor microcavities*, *Conference on Lasers and Electro-Optics '99*, 461–462, Optical Society of America, Baltimore, MD, U.S.A. (1999).

233. K. Schafer and J. Krause, *Tunable terahertz radiation from Stark wave packets*, *Optics Express* **1**(7) (1997) 210–215.

234. H. G. Roskos, M. C. Nuss, J. Shah, K. Leo, D. A. B. Miller, A. M. Fox, A. Schmitt-Rink and K. Köhler, *Coherent submillimeter-wave emission from charge oscillations in a double-well potential*, *Physical Review Letters* **68**(14) (1992) 2216–2219.

235. C. Waschke, H. G. Roskos, R. Schwedler, K. Leo, H. Kurz and K. Köhler, *Coherent submillimeter-wave emission from Bloch oscillations in a semiconductor superlattice*, *Physical Review Letters* **70**(21) (1993) 3319–3322.

236. C. Chansungsan, L. Tsang and S. L. Chuang, *Coherent terahertz emission from coupled quantum wells with exciton effects*, *Journal of the Optical Society of America B: Optical Physics* **11**(12) (1994) 2508–2518.

237. T. Dekorsky, P. Leisching, K. Köhler and H. Kurz, *Electro-optic detection of Bloch oscillations*, *Physical Review B* **50**(11) (1994) 8106–8109.

238. K. Victor, H. G. Roskos and C. Waschke, *Efficiency of submillimeter-wave generation and amplification by coherent wave-packet oscillations in semiconductor structures*, *Journal of the Optical Society of America B: Optical Physics* **11**(12) (1994) 2470–2479.

239. N. Sarukura, H. Ohtake, S. Izumida, Z. Liu, S. Ono and T. Yamanaka, *Submilliwatt, short-pulse, terahertz radiation from femtosecond-laser irradiated InAs in a magnetic field*, *Conference on Lasers and Electro-Optics '98*, 63, Optical Society of America, San Francisco, CA, U.S.A. (1998).

240. P. Gu, M. Tani, S. Kono, K. Sakai and X.-C. Zhang, *Study of terahertz radiation from InAs and InSb*, *Applied Physics Letters* **91**(9) (2002) 5533–5537.

241. Y. Tominari, T. Kiwa, H. Murakami, M. Tonouchi, H. Wald, P. Seidel and H. Schneidewind, *Resonant terahertz radiation from $Tl_2Ba_2CaCu_2O_{8+\delta}$ thin films by ultrafast optical pulse excitation*, *Applied Physics Letters* **80**(17) (2002) 3147–3149.

242. S. L. Chuang, S. Schmitt-Rink, B. I. Greene, P. N. Saeta and A. F. J. Levi, *Optical rectification at semiconductor surfaces*, *Physical Review Letters* **68**(1) (1992) 102–105.

243. P. N. Saeta, B. I. Greene and S. L. Chuang, *Short terahertz pulses from semiconductor surfaces: The importance of bulk difference-frequency mixing*, *Applied Physics Letters* **63**(25) (1993) 3482–3484.

244. D. You and D. R. D. R. R. Jones, P. H. Bucksbaum, *Coherent generation of far-infrared radiation from InP*, *Journal of the Optical Society of America B: Optical Physics* **11**(3) (1994) 486.

245. P. Y. Han, X. G. Huang and X.-C. Zhang, *Direct characterization of terahertz radiation from the dynamics of the semiconductor surface field*, *Applied Physics Letters* **77**(18) (2000) 2864–2866.

246. X.-C. Zhang, Y. Jin, T. D. Hewitt, T. Sangsiri, L. E. Kingsley and M. Weiner, *Magnetic switching of THz beams*, *Applied Physics Letters* **62**(17) (1993) 2003–2005.

247. X.-C. Zhang, Y. Jin, L. E. Kingsley and M. Weiner, *Influence of electric and magnetic fields on THz radiation*, *Applied Physics Letters* **62**(20) (1993) 2477–2479.

248. H. Ohtake, Z. Liu, S. Izumida, S. Ono and N. Sarukura, *Spectrum control of intense THz-radiation from InAs under magnetic field irradiated with stretched femtosecond laser pulses*, T. Elsaesser, J. G. Fujumoto, D. A. Wiersma and W. Zinth eds., *Ultrafast Phenomena XI*, vol. 63 of *Springer Series in Chemical Physics*, 202–204, Springer-Verlag, Berlin (1998), Proceedings of the 11th International Conference, Garmisch-Partenkirchen, Germany, July 12-17, 1998.

249. S. Ono, T. Tsukamoto, M. Sakai, Z. Liu, H. Ohtake, N. Sarukura, S. Nishizawa, A.Nakanishi and M. Yoshida, *Compact THz-radiation source consisting of a bulk semiconductor, a mode-locked fiber laser, and a 2-T permanent magnet*, *Review of Scientific Instruments* **71**(2) (2000) 554–556.

250. R. McLaughlin, Q. Chen, A. Corchia, C. M. Ciesla, D. D. Arnone, X.-C. Zhang, G. A. C. Jones, E. H. Linfield and M. Pepper, *Enhanced coherent terahertz emission from indium arsenide*, *Journal of Modern Optics* **47**(11) (2000) 1847–1856.

251. S. Ono, T. Tsukamoto, E. Kawahata, T. Yano, H. Ohtake and N. Sarukura, *Terahertz radiation from a shallow incidence-angle InAs emitter in a magnetic field irradiated with femtosecond laser pulses*, *Applied Optics* **40**(9) (2001) 1369–1371.

252. A. Corchia, R. McLaughlin, M. B. Johnston, D. M. Whittaker, D. D. Arnone, E. H. Linfield, A. G. Davies and M. Pepper, *Effects of magnetic field and optical fluence on terahertz emission in gallium arsenide*, *Physical Review B* **64**(20) (2001) 205204/1–5.

253. J. Shan, C. Weiss, R. Wallenstein, R. Beigang and T. F. Heinz, *Origin of magnetic field enhancement in the generation of terahertz radiation from semiconductor surfaces*, *Optics Letters* **26**(11) (2001) 849–851.

254. M. B. Johnston, D. M. Whittaker, A. Corchia, A. G. Davies and E. H. Linfield, *Theory of magnetic-field enhancement of surface-field terahertz emission*, *Journal of Applied Physics* **91**(4) (2002) 2104–2106.

255. N. Sarukura, H. Ohtake, S. Izumida and Z. Liu, *High average-power THz radiated from femtosecond laser-irradiated InAs in a magnetic field and its ellipical polarization characteristics*, *Journal of Applied Physics* **84**(1) (1998) 654–656.

256. S. Izumida, S. Ono, Z. Liu, H. Ohtake and N. Sarukura, *Spectrum control of THz radiation from InAs in a magnetic field by duration and frequency chirp of the excitation pulses*, *Applied Physics Letters* **75**(4) (1999) 451–453.

257. I. Brener, P. C. M. Planken, M. C. Nuss, M. S. C. Luo, S. L. Chuang, L. Pfeiffer, D. E. Leaird and A. M. Weiner, *Coherent control of terahertz emission and car-*

rier populations in semiconductor heterostructures, Journal of the Optical Society of America B: Optical Physics **11**(12) (1994) 2457–2469.

258. D. von der Linde, *Characterization of the noise in continuously operating mode-locked lasers, Applied Physics B: Photophysics and Laser Chemistry* **39**(4) (1986) 201–217.
259. J. M. Chwalek and D. R. Dykaar, *A mixer based electro-optic sampling system for submillivolt signal detection, Review of Scientific Instruments* **61**(4) (1990) 1273–1276.
260. D. H. Auston and P. R. Smith, *Generation and detection of millimeter waves by picosecond photoconductivity, Applied Physics Letters* **43**(7) (1983) 631–633.
261. J. Bromage, I. A. Walmsley and C. R. Stroud Jr., *Direct measurement of a photoconductive receiver's temporal response by dithered-edge sampling, Optics Letters* **24**(23) (1999) 1771–1773.
262. L. Duvillaret, F. Garet, J.-F. Roux and J.-L. Coutaz, *Analytical modeling and optimization of terahertz time-domain spectroscopy experiments, using photoswitches as antennas, IEEE Journal of Selected Topics in Quantum Electronics* **7**(4) (2001) 615–623.
263. S. Kono, M. Tani, P. Gu and K. Sakai, *Detection of up to 20 THz with a low-temperature-grown GaAs photoconductive antenna gated with 15 fs light pulses, Applied Physics Letters* **77**(25) (2000) 4104–4106.
264. S. Kono, M. Tani and K. Sakai, *Ultrabroadband photoconductive detection: Comparison with free-space electro-optic sampling, Applied Physics Letters* **79**(7) (2001) 898–900.
265. M. Tani, K.-S. Lee and X.-C. Zhang, *Detection of terahertz radiation with low-temperature-grown GaAs-based photoconductive antenna using 1.55 μm probe, Applied Physics Letters* **77**(9) (2000) 1396–1398.
266. A. Leitenstorfer, S. Hunsche, J. Shah, M. C. Nuss and W. H. Knox, *Detectors and sources for ultrabroadband electro-optic sampling: Experiment and theory, Applied Physics Letters* **74**(11) (1999) 1516–1518.
267. Z. Jiang and X.-C. Zhang, *Electro-optic measurement of THz field pulses with a chirped optical beam, Applied Physics Letters* **72**(16) (1998) 1945–1947.
268. Q. Wu, F. G. Sun, P. Campbell and X.-C. Zhang, *Dynamic range of an electro-optic field sensor and its imaging applications, Applied Physics Letters* **68**(23) (1996) 3224–3226.
269. D. H. Auston and A. M. Glass, *Optical generation of intense picosecond electrical pulses, Applied Physics Letters* **20**(10) (1972) 398–399.
270. J. A. Valdmanis and G. A. Mourou, *Subpicosecond electrooptic sampling: Principles and applications, IEEE Journal of Quantum Electronics* **22**(1) (1986) 69–78.
271. J. M. Wiesenfeld, *Electro-optic sampling of high-speed devices and integrated circuits, IBM Journal of Research and Development* **34**(2/3) (1990) 141–161.
272. Q. Wu, M. Litz and X.-C. Zhang, *Broadband detection capability of ZnTe electo-optic field detectors, Applied Physics Letters* **68**(21) (1996) 2924–2926.
273. Y. Cai, I. Brener, J. Lopata, J. Wynn, L. Pfeiffer, J. B. Stark, Q. Wu, X.-C. Zhang and J. Federici, *Coherent terahertz radiation detection: Direct comparison between free-space electro-optic sampling and antenna detection, Applied Physics Letters* **73**(4) (1998) 444–446.
274. S.-G. Park, M. R. Melloch and A. M. Weiner, *Comparison of terahertz waveforms measured by electro-optic and photoconductive sampling, Applied Physics Letters* **73**(22) (1998) 3184–3186.

275. P. C. M. Planken, H.-K. Nienhuys, H. J. Bakker and T. Wenckebach, *Measurement and calculation of the orientation dependence of terahertz pulse detection in ZnTe*, *Journal of the Optical Society of America B: Optical Physics* **18**(3) (2001) 313–317.

276. Q. Wu and X.-C. Zhang, *Ultrafast electro-optic field sensor*, *Applied Physics Letters* **68**(12) (1996) 1604–1606.

277. P. Uhd Jepsen, C. Winnewisser, M. Schall, V. Schya, S. R. Keiding and H. Helm, *Detection of THz pulses by phase retardation in lithium tantalate*, *Physical Review E* **53**(4) (1996) R3052–R3054.

278. A. Nahata, A. S. Weling and T. F. Heinz, *A wideband coherent terahertz spectroscopy system using optical rectification and electro-optic sampling*, *Applied Physics Letters* **69**(16) (1996) 2321–2323.

279. Q. Wu and X.-C. Zhang, *Free-space electro-optic sampling of mid-infrared pulses*, *Applied Physics Letters* **71**(10) (1997) 1285–1286.

280. G. C. Cho, H. J. Bakker and H. Kurz, *THz pulse distortion in electro-optic detection by phonon-polariton propagation*, *Conference on Lasers and Electro-Optics '98*, 60–61, Optical Society of America, San Francisco, CA, U.S.A. (1998).

281. P. Y. Han and X.-C. Zhang, *Coherent, broadband midinfrared terahertz beam sensors*, *Applied Physics Letters* **73**(21) (1998) 3049–3051.

282. A. Leitenstorter, *Ultrabroadband THz experiments in femtosecond solid-state physics*, *Quantum Electronics and Laser Science Conference '01*, 163–164, Baltimore, MD, U.S.A. (2001).

283. G. Gallot, Z. Jiangquan, R. W. McGowan, T.-I. Jeon and D. Grischkowsky, *Measurements of the THz absorption and dispersion of ZnTe and their relevance to the electro-optic detection of THz radiation*, *Applied Physics Letters* **74**(23) (1999) 3450–3452.

284. Q. Wu and X.-C. Zhang, *7 terahertz broadband GaP electo-optic sensor*, *Applied Physics Letters* **70**(14) (1997) 1784–1786.

285. M. Vossebrger, M. Brucherseifer, G. C. Cho, H. G. Roskos and H. Kurz, *Propagation effects in electro-optic sampling of terahertz pulses in GaAs*, *Applied Optics* **37**(15) (1998) 3368–3371.

286. H. Cao, T. F. Heinz and A. Nahata, *Electro-optic detection of femtosecond electromagnetic pulses by use of poled polymers*, *Optics Letters* **27**(9) (2002) 775–777.

287. P. Y. Han, M. Tani, F. Pan and X.-C. Zhang, *Use of the organic crystal DAST for terahertz beam applications*, *Optics Letters* **75**(9) (2000) 675–677i.

288. P. Y. Han, M. Tani, F. Pan and X.-C. Zhang, *Characterization and application of DAST at THz frequency*, *Conference on Lasers and Electro-Optics '00*, vol. 39 of *TOPS*, 556–557, Optical Society of America, San Francisco, CA, U.S.A. (2000).

289. M. Walther, K. Jevsky, S. R. Keidig, H. Takahiro and H. Ito, *Far infrared properties of DAST*, *Optics Letters* **25**(12) (2000) 911–913.

290. Q. Wu, T. D. Hewitt and X.-C. Zhang, *Two-dimensional electro-optic imaging of terahertz beams*, *Applied Physics Letters* **69**(8) (1996) 1026–1028.

291. Z. Jiang and X.-C. Zhang, *Single-shot spatiotemporal terahertz field imaging*, *Optics Letters* **23**(14) (1998) 1114–1116.

292. A. S. Weling, M. Bonn, J. Shan, G. A. Reider, A. Nahata and T. F. Heinz, *Simultaneous recording of THz waveforms by multi-channel electro-optic detection*, *Ultrafast Electronics and Optoelectronics*, vol. 28 of *OSA TOPS*, 95–97, Snowmass, Col. U.S.A. (1999).

293. J. Shan, A. S. Weling, E. Knoese, L. Bartels, M. Bonn, A. Nahata, G. A. Reider and T. F. Heinz, *Single-shot measurement of terahertz electromagnetic pulses by use of electro-optic sampling*, *Optics Letters* **25**(6) (2000) 426–428.
294. B. Ferguson, S. Wang, D. Gray, D. Abbott and X.-C. Zhang, *Terahertz imaging of biological tissue using a chirped probe pulse*, N. W. Bergmann ed., *Electronics and Structures for MEMS II*, vol. 4591, 172–184, SPIE, Washington, DC, U.S.A., Adelaide, Australia (2001).
295. Z. Jiang, G. F. Sun and X.-C. Zhang, *Terahertz pulse measurement with an optical streak camera*, *Optics Letters* **24**(17) (1999) 1245–1247.
296. I. Wilke, A. M. MacLeod, W. A. Gillespie, G. Berden, G. M. H. Knippels and A. F. G. van der Meer, *Single-shot electron-beam bunch length measurements*, *Physical Review Letters* **88**(12) (2002) 124801-1–124801-4.
297. J. A. Riordan, F. G. Sun, Z. G. Lu and X.-C. Zhang, *Free-space transient magneto-optic sampling*, *Applied Physics Letters* **71**(11) (1997) 1452–1454.
298. D. M. Mittleman, R. H. Jacobson and M. C. Nuss, *T-ray imaging*, *IEEE Journal of Selected Topics in Quantum Electronics* **2**(3) (1996) 679–692.
299. K. Kawase and N. Hiromoto, *Terahertz wave antireflection coating on Ge and GaAs with fused quartz.*, *Applied Optics* **37**(10) (1998) 1862–1866.
300. D. R. S. Cumming and R. J. Blaikie, *A variable polarisation compensator using artificial dielectrics*, *Optics Communications* **163**(4-6) (1999) 164–168.
301. J. O. White, C. Ludwig and J. Kuhl, *Response of grating pairs to single-cycle electromagnetic pulses*, *Journal of the Optical Society of America B: Optical Physics* **12**(9) (1995) 1687–1694.
302. A. B. Ruffin, J. V. Rudd, S. Feng, H. G. Winful and J. F. Whitaker, *Phase manipulation of free-space THz pulses using transmissive optics*, *Ultrafast Electronics and Optoelectronics*, vol. 28 of *OSA TOPS*, 98–102, Optical Society of America (1999).
303. A. E. Kaplan, *Diffraction-induced transformation of near-cycle and subcycle pulses*, *Journal of the Optical Society of America B: Optical Physics* **15**(3) (1998) 951–956.
304. S. Hunsche, S. Feng, H. G. Winful, A. Leitenstorfer, M. C. Nuss and E. P. Ippen, *Spatiotemporal focusing of single-cycle light pulses*, *Journal of the Optical Society of America A: (Optics & Vision)* **16**(8) (1999) 2025–2028.
305. J. Zhang and D. Grischkowsky, *Whispering-gallery mode terahertz pulses*, *Optics Letters* **27**(8) (2002) 661–662.
306. G. Arjavalingam, Y. Pastol, L. W. Epp and R. Mittra, *Characterization of quasi-optical filters with picosecond transient radiation*, *IEEE Transactions on Antennas and Propagation* **40**(1) (1992) 63–66.
307. J. Bromage, S. Radic, G. P. Agrawal, C. R. Stroud, Jr., P. M. Fauchet and R. Sobolewski, *Spatiotemporal shaping of terahertz pulses*, *Optics Letters* **22**(9) (1997) 627–629.
308. H. Lee, J. Lee and J. Kim, *Picosecond-domain radiation pattern measurement using fiber-coupled photoconductive antenna*, *IEEE Journal of Selected Topics in Quantum Electronics* **7**(4) (2001) 667–673.
309. D. You and P. H. Bucksbaum, *Propagation of half-cycle far infrared pulses*, *Journal of the Optical Society of America B: Optical Physics* **14**(7) (1997) 1651–1655.
310. J. Bromage, S. Radic, G. P. Agrawal, C. R. Stroud, P. M. Fauchet and R. Sobolewski, *Spatiotemporal shaping of half-cycle terahertz pulses by diffraction through conductive apertures of finite thickness*, *Journal of the Optical Society of America B: Optical Physics* **15**(4) (1998) 1399–1405.

311. M. E. MacDonald, A. Alexanian, R. A. York, Z. Popovic and E. N. Grossman, *Spectral transmittance of lossy printed resonant-grid terahertz bandpass filters*, *IEEE Transactions on Microwave Theory and Techniques* **48**(4) (2000) 712–718.

312. S. Sato, S. Hayakawa, T. Matsumoto, H. Matsuo, H. Murakami, K. Sakai, A. E. Lange and P. L. Richards, *Submillimeter wave low pass filters made of glass beads*, *Applied Optics* **28**(20) (1989) 4478–.

313. C. Winnewisser, F. Lewen, J. Weinzierl and H. Helm, *Transmission features of frequency-selective components in the far infrared determined by terahertz time-domain spectroscopy*, *Applied Optics* **38**(18) (1999) 3961–3967.

314. C. Winnewisser, F. Lewen and H. Helm, *Transmission characteristics of dichroic filters measured by THz time-domain spectroscopy*, *Applied Physics A: Materials Science & Processing* **66**(6) (1998) 593–598.

315. C. Winnewisser, F. T. Lewen, M. Schall, M. Walther and H. Helm, *Characterization and application of dichroic filters in the 0.1–3-THz region*, *IEEE Transactions on Microwave Theory and Techniques* **48**(4) (2000) 744–749.

316. S. Wang, T. Yuan, E. D. Walsby, R. J. Blaikie, S. M. Durbin, D. R. S. Cumming, J. Xu and X.-C. Zhang, *Characterization of t-ray binary lenses*, *Optics Letters* **27**(13) (2002) 1183–1185.

317. J. Pearce and D. M. Mittleman, *The propagation of single-cycle THz pulses in random media*, *Optics Letters* **26**(24) (2001) 2002–2004.

318. M. C. Beard and C. A. Schmuttenmaer, *Using the finite-difference time-domain pulse propagation method to simulate time-resolved THz experiments*, *Journal of Chemical Physics* **114**(7) (2001) 2903–2909.

319. B. E. Cole, J. B. Williams, B. T. King, M. S. Sherwin and C. R. Stanley, *Coherent manipulation of semiconductor quantum bits with terahertz radiation*, *Nature* **410**(6824) (2001) 60–63.

320. M. Khazan, R. Meissner and I. Wilke, *Convertible transmission-reflection time-domain terahertz spectrometer*, *Review of Scientific Instruments* **72**(8) (2001) 3427–3430.

321. M. Tani, Z. Jiang and X.-C. Zhang, *Photoconductive terahertz transceiver*, *Electronics Letters* **36**(9) (2000) 804–805.

322. Q. Chen, Z. Jiang, M. Tani and X.-C. Zhang, *Electro-optic terahertz transceiver*, *Electronics Letters* **36**(15) (2000) 1298–1299.

323. Q. Chen and X.-C. Zhang, *Terahertz transceiver*, *Optics and Photonics News* **11**(12) (2000) 46–47.

324. K. P. Cheung and D. H. Auston, *A novel technique for measuring far-infrared absorption and dispersion*, *Infrared Physics* **26**(1) (1986) 23–27.

325. D. R. Grischkowsky, *Optoelectronic characterization of transmission lines and waveguides by terahertz time-domain spectroscopy*, *IEEE Journal of Selected Topics in Quantum Electronics* **6**(6) (2000) 1122–1135.

326. G. Gallot, S. P. Jamison, R. W. McGowan and D. Grischkowsky, *Terahertz waveguides*, *Journal of the Optical Society of America B: Optical Physics* **17**(5) (2000) 851–863.

327. K. Wynne, J. J. Carey, J. Zawadzka and D. A. Jaroszynski, *Tunneling of single-cycle terahertz pulses through waveguides*, *Optics Communications* **176**(4–6) (2000) 429–435.

328. A. Filin, M. Stowe and R. Kersting, *Time-domain differentiation of terahertz pulses*, *Optics Letters* **26**(24) (2001) 2008–2010.

329. M. T. Reiten, D. Grischkowsky and R. A. Cheville, *Optical tunneling of single-cycle terahertz bandwidth pulses*, *Physical Review E* **64**(03) (2001) 036604/1–5.
330. O. Mitrofanov, R. Harel, M. Lee, L. N. Pfeiffer, K. West, J. D. Wynn and J. Federici, *Study of single-cycle pulse propagation inside a terahertz near-field probe*, *Applied Physics Letters* **78**(2) (2001) 252–4.
331. R. Mendis and D. Grischkowsky, *Plastic ribbon THz waveguides*, *Journal of Applied Physics* **88**(7) (2000) 4449–4451.
332. R. Mendis and D. Grischkowsky, *THz interconnect with low-loss and low-group velocity dispersion*, *IEEE Microwave and Wireless Components Letters* **11**(11) (2001) 444–446.
333. S. P. Jamison, R. W. McGowan and D. Grischkowsky, *Single-mode waveguide propagation and reshaping of sub-ps terahertz pulses in sapphire fibers*, *Applied Physics Letters* **76**(15) (2000) 1987–1989.
334. W. Zhang, J. Zhang and D. Grischkowsky, *Quasioptic dielectric tetrahertz cavity: Coupled through optical tunneling*, *Applied Physics Letters* **78**(17) (2001) 2425–2427.
335. M. Nagel, P. Haring Bolívar, M. Brucherseifer, H. Kurz, A. Bosserhoff and R. Büttner, *Integrated THz technology for label-free genetic diagnostics*, *Applied Physics Letters* **80**(1) (2002) 154–156.
336. G. W. Chantry, *Submillimeter Spectroscopy*, Academic Press, New York (1971).
337. J. T. Houghton and S. D. Smith, *Infra-red Physics*, Oxford University Press, Oxford (1966).
338. J. C. Wiltse, *History of millimeter and submillimeter waves*, *IEEE Transactions on Microwave Theory and Techniques* **32**(9) (1984) 1118–1127.
339. M. Born and E. Wolf, *Principles of Optics*, 6th ed. Cambridge University Press (1997).
340. L. Duvillaret, F. Garet and J.-L. Coutaz, *Highly precise determination of optical constants and sample thickness in terahertz time-domain spectroscopy*, *Applied Optics* **38**(2) (1999) 409–415.
341. G. Arjavalingam, Y. Pastol, J.-M. Halbout and G. V. Kopcsay, *Broad-band microwave measurements with transient radiation from optoelectronically pulsed antennas*, *IEEE Transactions on Microwave Theory and Techniques* **38**(5) (1990) 615–621.
342. L. Duvillaret, F. Garet and J. L. Coutaz, *Influence of noise on the characterization of materials by terahertz time-domain spectroscopy*, *Journal of the Optical Society of America B: Optical Physics* **17**(3) (2000) 452–461.
343. T. D. Dorney, R. G. Baraniuk and D. M. Mittleman, *Material parameter estimation with terahertz time-domain spectroscopy*, *Journal of the Optical Society of America A: (Optics & Vision)* **18**(7) (2001) 1562–1571.
344. C. Rønne, L. Thrane, P.-O. Åstrand, A. Wallqvist, K. V. Mikkelsen and S. R. Keiding, *Investigation of the temperature dependence of dielectric relaxation in liquid water by THz reflection spectroscopy and molecular dynamics simulation*, *Journal of Chemical Physics* **107**(14) (1997) 5319–5331.
345. D. Hashimshony, I. Geltner, G. Cohen, Y. Avitzour, A. Zigler and C. Smith, *Characterization of the electrical properties and thickness of thin epitaxial semiconductor layers by THz reflection spectroscopy*, *Journal of Applied Physics* **90**(11) (2001) 5778–5781.
346. L. Ming, J. Fortin, J. Y. Kim, G. Fox, F. Chu, T. Davenport, T.-M. Lu and X.-C. Zhang, *Dielectric constant measurement of thin films using goniometric terahertz time-domain spectroscopy*, *IEEE Journal of Selected Topics in Quantum Electronics* **7**(4) (2001) 624–629.

347. T. Nagashima and M. Hangyo, *Measurement of complex optical constants of a highly doped Si wafer using terahertz ellipsometry*, *Applied Physics Letters* **79**(24) (2001) 3917–3919.

348. S. P. Mickan, A. Menikh, H. Liu, C. A. Mannella, D. Abbott, J. Munch and X.-C. Zhang, *T-ray-based sensing of thin film lipid-protein interactions*, *Physics in Medicine and Biology* **21** (2002).

349. S. P. Mickan, A. Menikh, C. A. Mannella, D. Abbott, J. Munch and X.-C. Zhang, *Bioaffinity detection with terahertz spectroscopy*, D. Nicolau ed., *Proceedings of SPIE - Biomedical Applications of Micro- and Nanoengineering*, vol. 4937, SPIE, Washington, DC, U.S.A., Melbourne, Australia (2002).

350. Z. G. Lu, P. Campbell and X.-C. Zhang, *Free-space electro-optic sampling with a high-repetition-rate regenerative amplified laser*, *Applied Physics Letters* **71**(5) (1997) 593–595.

351. Z. Jiang, M. Li and X.-C. Zhang, *Dielectric constant measurement of thin films by differential time-domain spectroscopy*, *Applied Physics Letters* **76**(22) (2000) 3221–3223.

352. M. Brucherseifer, H. P. M. Pellemans, P. Haring Bolívar and H. Kurz, *THz spectroscopy with ultrahigh sensitivity*, *Conference on Lasers and Electro-Optics '00*, vol. 39 of *TOPS*, 553–554, Optical Society of America, San Francisco, CA, U.S.A. (2000).

353. S. P. Mickan, K.-S. Lee, T.-M. Lu, E. Barnat, J. Munch, D. Abbott and X.-C. Zhang, *Thin film characterization using terahertz differential time-domain spectroscopy and double modulation*, N. W. Bergmann ed., *Electronics and Structures for MEMS II*, vol. 4591, 197–209, SPIE, Washington, DC, U.S.A., Adelaide, Australia (2001).

354. S. P. Mickan, K. S. Lee, T.-M. Lu, J. Munch, D. Abbott and X.-C. Zhang, *Double modulated differential THz-TDS for thin film dielectric characterization*, *Microelectronics Journal* **In Press** (2002).

355. S. P. Mickan, D. Abbott, J. Munch and X. C. Zhang, *Noise reduction in terahertz thin film measurements using a double modulated differential technique*, *Fluctuation and Noise Letters* **2**(1) (2002) 13–29.

356. J. L. Johnson, T. D. Dorney and D. M. Mittleman, *Enhanced depth resolution in terahertz imaging using phase-shift interferometry*, *Applied Physics Letters* **78**(6) (2001) 835–837.

357. S. Krishnamurthy, M. T. Reiten, S. A. Harmon and R. A. Cheville, *Characterization of thin polymer films using terahertz time-domain interferometry*, *Applied Physics Letters* **79**(6) (2001) 875–7.

358. V. Grebenev, E. Knoesel and L. Bartels, *Destructive interference of freely propagating terahertz pulses and its potential for high-resolution spectroscopy and optical computing*, *Applied Physics Letters* **79**(2) (2001) 145–147.

359. M. Nagel, P. Haring Bolívar, M. Brucherseifer, H. Kurz, A. Bosserhoff and R. Büttner, *Integrated planar terahertz resonators for femtomolar sensitivity label-free detection of DNA hybridization*, *Applied Optics* **41**(10) (2002) 2074–2078.

360. P. R. Griffiths, *Chemical infrared Fourier transform spectroscopy*, vol. 43 of *Chemical Analysis*, John Wiley & Sons, Inc., New York (1975).

361. H. Harde and D. G. R. A. Cheville, *Collision-induced tunneling in methyl halides*, *Journal of the Optical Society of America B: Optical Physics* **14**(12) (1997) 3282–3293.

362. H. Harde, J. Zhao, M. Wolff, R. A. Cheville and D. Grischkowsky, *THz time-domain spectroscopy on ammonia*, *Journal of Physical Chemistry A* **105**(25) (2001) 6038–6047.

363. R. H. Jacobsen, D. M. Mittleman and M. C. Nuss, *Chemical recognition of gases and gas mixtures with terahertz waves*, *Optics Letters* **21**(24) (1996) 2011–2013.

364. R. A. Cheville and D. Grischkowsky, *Far-infrared terahertz time-domain spectroscopy of flames*, *Optics Letters* **20**(16) (1995) 1646–1648.

365. R. A. Cheville and D. Grischkowsky, *Observation of pure rotational absorption spectra in the μ_2 band of hot H_2O in flames*, *Optics Letters* **23**(7) (1998) 531–533.

366. D. M. Mittleman, R. H. Jacobsen, R. Neelamani, R. G. Baraniuk and M. C. Nuss, *Gas sensing using terahertz time-domain spectroscopy*, *Applied Physics B: Lasers and Optics* **67**(3) (1998) 379–390.

367. G. Mouret, W. Chen, D. Boucher, R. Bocquet, P. Mounaix and D. Lippens, *Gas filter correlation instrument for air monitoring at submillimeter wavelengths*, *Optics Letters* **24**(5) (1999) 351–353.

368. H. Harde, R. A. Cheville and D. Grischkowsky, *Terahertz studies of collision-broadened rotational lines*, *Journal of Physical Chemistry A* **101**(20) (1997) 3646–3660.

369. H. Harde and D. Grischlowsky, *Coherent transients exicted by subpicosecond pulses of terahertz radiation*, *Journal of the Optical Society of America B: Optical Physics* **8**(8) (1991) 1642–.

370. H. Harde, N. Katzenellenbogen and D. R. Grischkowsky, *Terahertz coherent transients from methyl chloride vapor*, *Journal of the Optical Society of America B: Optical Physics* **11**(6) (1994) 1018–.

371. L. Thrane, R. H. Jacobsen, P. U. Jepsen and S. R. Keiding, *THz reflection spectroscopy of liquid water*, *Chemical Physics Letters* **240** (1995) 330–333.

372. C. Rønne and S. R. Keiding, *THz reflection spectroscopy of $H_2O(l)$ and $D_2O(l)$*, T. Elsaesser, J. G. Fujumoto, D. A. Wiersma and W. Zinth eds., *Ultrafast Phenomena XI*, vol. 63 of *Springer Series in Chemical Physics*, 568–570, Springer-Verlag, Berlin (1998).

373. I. H. Libon, M. Hempel, S. Seitz, N. E. Hecker, J. Feldmann, A. Hayd, G. Zundela, D. Mittleman and M. Koch, *THz spectroscopy of polar liquids*, *Proceedings of SPIE - Terahertz Spectroscopy and Applications*, vol. 3617, 24–29, San Jose, CA, U.S.A. (1999).

374. J. E. Pedersen and S. R. Keiding, *THz time-domain spectroscopy of nonpolar liquids*, *IEEE Journal of Quantum Electronics* **28**(10) (1992) 2518–2522.

375. C. Rønne, K. Jensby, B. J. Loughnane, J. Fourkas, O. F. Nielsen and S. R. Keiding, *Temperature dependence of the dielectric function of $C_6H_6(l)$ and $C_6H_5CH_3(l)$ measured with THz spectroscopy*, *Journal of Chemical Physics* **113**(9) (2000) 3749–3756.

376. J. T. Kindt and C. A. Schmuttenmaer, *Far-infrared dielectric properties of polar liquids probed by femtosecond terahertz pulse spectroscopy*, *Journal of Physical Chemistry* **100**(24) (1996) 10373–10379.

377. M. C. Beard, G. M. Turner, D. S. Venables and C. A. Schmuttenmaer, *Two-dimensional time-resolved THz spectroscopy of solvent response to photoexcitation*, *Trends in Optics and Photonics. Twelfth International Conference on Ultrafast Phenomena*, vol. 43, 592–594, Charleston S.C. USA (2000).

378. D. S. Venables and C. A. Schmuttenmaer, *Time-resolved THz studies of liquid dynamics*, T. Elsaesser, J. G. Fujumoto, D. A. Wiersma and W. Zinth eds., *Ultrafast*

Phenomena XI, vol. 63 of *Springer Series in Chemical Physics*, 565–567, Springer-Verlag, Berlin (1998).

379. D. S. Venables, A. Chiu and C. A. Schmuttenmaer, *Structure and dynamics of non-aqueous mixtures of dipolar liquids. I. Infrared and far-infrared spectroscopy*, *Journal of Chemical Physics* **113**(8) (2000) 3243–3248.
380. D. S. Venables and C. A. Schmuttenmaer, *Spectroscopy and dynamics of mixtures of water with acetone, acetonitrile, and methanol*, *Journal of Chemical Physics* **113**(24) (2000) 11222–11236.
381. D. S. Venables and C. A. Schmuttenmaer, *Structure and dynamics of nonaqueous mixtures of dipolar liquids. II. Molecular dynamics simulations*, *Journal of Chemical Physics* **113**(8) (2000) 3249–3260.
382. M. L. T. Asaki, A. Redondo, T. A. Zawodzinski and A. J. Taylor, *Dielectric relaxation of electrolyte solutions using terahertz transmission spectroscopy*, *Journal of Chemical Physics* **116**(19) (2002) 8469–8482.
383. D. M. Mittleman, J. Cunningham, M. C. Nuss and M. Geva, *Noncontact semiconductor wafer characterization with the terahertz Hall effect*, *Applied Physics Letters* **71**(1) (1997) 16–18.
384. G. C. Cho, P. Y. Han, X.-C. Zhang and H. J. Bakker, *Optical phonon dynamics of GaAs studied with time-resolved terahertz spectroscopy*, *Optics Letters* **25**(21) (2000) 1609–1611.
385. X. F. Ma and X.-C. Zhang, *Determination of ratios between nonlinear-optical coefficients by using subpicosecond optical rectification*, *Journal of the Optical Society of America B: Optical Physics* **10**(7) (1993) 1175–1179.
386. M. Schall, M. Walther, H. Helm and P. U. Jepsen, *Two-phonon processes in II-VI semiconductors investigated with terahertz time-domain spectroscopy*, *Conference on Lasers and Electro-Optics '00*, vol. 39 of *TOPS*, 465–466, Optical Society of America, San Francisco, CA, U.S.A. (2000).
387. C. Zhang, K.-S. Lee, X.-C. Zhang, X. Wei and Y. R. Shen, *Optical constant of ice lh crystal at terahertz frequencies*, *Applied Physics Letters* **79**(4) (2001) 491–493.
388. N. Katzenellenbogen and D. Grischkowsky, *Electrical characterization to 4 THz of N- and P-type GaAs using THz time-domain spectroscopy*, *Applied Physics Letters* **61**(7) (1992) 840–842.
389. Y. Pastol, G. Arjavalingham, J.-M. Halbout and G. V. Kopscay, *Absorption and dispersion of low-loss dielectrics measured with microwave transient radiation*, *Electronics Letters* **25**(8) (1989) 523–524.
390. Y. Pastol, G. Arjavalingam, G. V. Kopcsay and J.-M. Halbout, *Dielectric properties of uniaxial crystals measured with optoelectronically generated microwave transient radiation*, *Applied Physics Letters* **55**(22) (1989) 2277–2279.
391. G. Arjavalingham, Y. Pastol, J.-M. Halbout and G. V. Kopcsay, *Application of picosecond optoelectronics in broadband microwave material measurements*, *Microwave Journal* **32**(11) (1989) 133–140.
392. M. van Exter and D. Grischkowsky, *Carrier dynamics of electrons and holes in moderately doped silicon*, *Physical Review B* **41**(17) (1990) 12140–12149.
393. T.-I. Jeon and D. Grischkowsky, *Characterization of optically dense, doped semiconductors by reflection THz time domain spectroscopy*, *Applied Physics Letters* **72**(23) (1998) 3032–3034.
394. B. I. Greene, J. Federici, D. R. Dykaar, A. F. J. Levi and L. N. Pfeiffer, *Picosecond pump and probe spectroscopy utilizing freely propagating terahertz radiation*, *Optics Letters* **16**(1) (1991) 48–49.

395. M. Schall and P. U. Jepsen, *Photoexcited GaAs surfaces studied by transient terahertz time-domain spectroscopy*, *Optics Letters* **25**(1) (2000) 13–15.

396. R. H. M. Groeneveld and D. Grischkowsky, *Picosecond time-resolved far-infrared experiments on carriers and excitons in GaAs-AlGaAs multiple quantum wells*, *Journal of the Optical Society of America B: Optical Physics* **11**(12) (1994) 2502–2506.

397. M. C. Beard, G. M. Turner and C. A. Schmuttenmaer, *Transient photoconductivity in GaAs as measured by time-resolved terahertz spectroscopy*, *Physical Review B* **62**(23) (2000) 15764–15777.

398. M. C. Beard, G. M. Turner and C. A. Schmuttenmaer, *Subpicosecond carrier dynamics in low-temperature grown GaAs as measured by time-resolved terahertz spectroscopy*, *Journal of Applied Physics* **90**(12) (2001) 5915–5923.

399. P. U. Jepsen, W. Schairer, I. H. Libon, U. Lemmer, N. E. Hecker, M. Birkholz, K. Lips and M. Schall, *Ultrafast carrier trapping in microcrystalline silicon observed in optical pump-terahertz probe measurements*, *Applied Physics Letters* **79**(9) (2001) 1291–1293.

400. R. Huber, F. Tauser, A. Brodschelm, M. Bichler, G. Abstreiter and A. Leitenstorfer, *How many-particle interactions develop after ultrafast excitation of an electron-hole plasma*, *Nature* **414**(6861) (2001) 286–289.

401. D. Grischkowsky and S. R. Keiding, *THz time-domain spectroscopy of high t_c substrates*, *Applied Physics Letters* **57**(10) (1990) 1055–1057.

402. M. Tonouchi, M. Yamashita and M. Hangyo, *Vortex penetration in YBCO thin film strips observed by THz radiation imaging*, *Physica B* **284–288** (2000) 853–854.

403. T. Kiwa and M. Tonouchi, *High frequency properties of YBCO thin films diagnosed by time-domain terahertz spectroscopy*, *Physica C* **362** (2001) 314–318.

404. K.-S. Lee, J. Y. Kim, J. Fortin, Z. Jiang, M. Li, T.-M. Lu and X.-C. Zhang, *Dielectric property measurement of sub-micron thin films by differential time-domain spectroscopy*, T. Elsaesser, S. Mukamel, M. M. Murnane and N. F. Scherer eds., *Ultrafast Phenomena XII*, vol. 66 of *Springer Series in Chemical Physics*, 232–234, Springer-Verlag, Berlin (2000).

405. T. I. Jeon, D. Grischkowsky, A. K. Mukherjee and R. Menon, *Electrical characterization of conducting polypyrrole by THz time-domain spectroscopy*, *Applied Physics Letters* **77**(16) (2000) 2452–2454.

406. T.-I. Jeon, D. Grischkowsky, A. K. Mukherjee and R. Menon, *Electrical and optical characterization of conducting poly-3-methylthiophene film by THz time-domain spectroscopy*, *Applied Physics Letters* **79**(25) (2001) 4142–4144.

407. T.-I. Jeon, K.-J. Kim, C. Kang, S.-J. Oh, J.-H. Son, K. H. An, D. J. Bae and Y. H. Lee, *Terahertz conductivity of anisotropic single walled carbon nanotube films*, *Applied Physics Letters* **80**(18) (2002) 3403–3405.

408. M. Ree, K.-J. Chen, D. P. Kirby, N. Katzenellenbogen and D. Grischkowsky, *Anisotropic properties of high-temperature polyimide thin films: Dielectric and thermal-expansion behaviors*, *Journal of Applied Physics* **72**(5) (1992) 2014–2021.

409. S. Kamba, J. Petzelt, E. Buixaderas, D. Haubrich, P. Vank, P. Kuel, I. N. Jawahar, M. T. Sebastian and P. Mohanan, *High frequency dielectric properties of $A_5B_4O_{15}$ microwave ceramics*, *Journal of Applied Physics* **88**(7) (2001) 3900–3906.

410. I. Geltner, D. Hashimshony and A. Zigler, *Detection and electrical characterization of hidden layers using time-domain analysis of terahertz reflections*, *Journal of Applied Physics* **92**(1) (2002) 203–206.

411. A. G. Markelz, A. Roitberg and E. J. Heilweil, *Pulsed terahertz spectroscopy of DNA, bovine serum albumin and collagen between 0.1 and 2.0 THz*, *Chemical Physics Letters* **320**(1-2) (2000) 42–48.

412. M. Brucherseifer, M. Nagel, P. Haring Bolívar, H. Kurz, A. Bosserhoff and R. Büttner, *Label-free probing of the binding state of DNA by time-domain terahertz sensing*, *Applied Physics Letters* **77**(24) (2000) 4049–4051.

413. S. Hayward and N. Go, *Collective variable description of native protein dynamics*, *Annual Review of Physical Chemistry* **46** (1995) 223–50.

414. A. Roitberg, R. B. Gerber, R. Elber and M. A. Ratner, *Anharmonic wave functions of proteins: Quantum self-consistent field calculations of BPTI*, *Science* **268**(5215) (1995) 1319—1322.

415. M. Walther, B. Fischer, M. Schall, H. Helm and P. U. Jepsen, *Far-infrared vibrational spectra of all-trans, 9-cis and 13-cis retinal measured by THz time-domain spectroscopy*, *Chemical Physics Letters* **332**(3–4) (2000) 389–395.

416. M. Walther, P. Plochocka, B. Fischer, H. Helm and P. U. Jepsen, *Collective vibrational modes in biological molecules investigated by terahertz time-domain spectroscopy*, *Biopolymers* **67**(4–5) (2002) 310–313.

417. J. W. Pitera, M. Falta and W. F. van Gunsteren, *Dielectric properties of proteins from simulation: the effects of solvent, ligands, pH, and temperature*, *Biophysical Journal* **80**(6) (2001) 2546–2555.

418. S. P. Mickan, J. S. Dordick, J. Munch, D. Abbott and X.-C. Zhang, *Pulsed THz protein spectroscopy in organic solvents*, *Conference on Lasers and Electro-Optics '02*, 640, Long Beach, CA, U.S.A. (2002).

419. S. P. Mickan, J. S. Dordick, J. Munch, D. Abbott and X.-C. Zhang, *Terahertz spectroscopy of bound water in nano suspensions*, D. Nicolau ed., *Proceedings of SPIE - Biomedical Applications of Micro- and Nanoengineering*, vol. 4937, SPIE, Washington, DC, U.S.A., Melbourne, Australia (2002).

420. B. B. Hu and M. C. Nuss, *Imaging with terahertz waves*, *Optics Letters* **20**(16) (1995) 1716–1718.

421. S. Hadjiloucas, L. S. Haratzas and J. W. Bowen, *Measurements of leaf water content using terahertz radiation*, *IEEE Transactions on Microwave Theory and Techniques* **47**(2) (1999) 142–149.

422. A. Matei and M. Dressel, *Far infrared spectroscopy of biological material*, G. P. Gallerano and M. R. Scarfi eds., *THz-BRIDGE Workshop*, Mo–3, Capri, Italy (2002).

423. B. Veryret, *Biological effects in the microwave, THz and infrared regions*, G. P. Gallerano and M. R. Scarfi eds., *THz-BRIDGE Workshop*, Mo–11, Capri, Italy (2002).

424. S. W. Smye, J. M. Chamberlain, A. J. Fitzgerald and E. Berry, *The interaction between terahertz radiation and biological tissue*, *Physics in Medicine and Biology* **46**(9) (2001) 101–112.

425. A. J. Fitzgerald, E. Berry, N. N. Zinovev, G. C. Walker, M. A. Smith and J. M. Chamberlain, *An introduction to medical imaging with coherent terahertz frequency radiation*, *Physics in Medicine and Biology* **47**(7) (2002) 67–84.

426. Q. Chen, Z. Jiang, G. Xu and X.-C. Zhang, *Applications of terahertz time-domain measurement on paper currencies*, *Conference on Lasers and Electro-Optics Pacific Rim '99*, vol. 2, 457–458, Optical Society of America (1998).

427. R. A. Cheville and D. Grischkowsky, *Time domain terahertz impulse ranging studies*, *Applied Physics Letters* **67**(14) (1995) 1960–1962.

428. D. M. Mittleman, M. Gupta, R. Neelamani, R. G. Baraniuk, J. V. Rudd and M. Koch, *Recent advances in terahertz imaging, Applied Physics B: Lasers and Optics* **68**(6) (1999) 1085–1094.

429. H. P. M. Pellemans, P. H. Bolívar, M. Brucherseifer, H. Kurz, C. M. Mann, J. W. Bowen and S. Hadjiloucas, *Characterization techniques for passive devices from 150 GHz to 3 THz using THz-transient spectroscopy, Conference on Lasers and Electro-Optics '00*, vol. 39 of *TOPS*, 557–558, Optical Society of America, San Francisco, CA, U.S.A. (2000).

430. R. A. Cheville, R. W. McGowan and D. Grischkowsky, *Late-time target response measured with terahertz impulse ranging, IEEE Transactions on Antennas and Propagation* **45**(10) (1997) 1518–1524.

431. R. A. Cheville, R. W. McGowan and D. Grischkowsky, *Time resolved measurements which isolate the mechanisms responsible for terahertz glory scattering from dielectric spheres, Physical Review Letters* **80**(2) (1988) 269–272.

432. J. O'Hara and D. Grischkowsky, *Quasi-optic terahertz imaging, Optics Letters* **26**(23) (2001) 1918–1920.

433. K. McClatchey, M. T. Reiten and R. A. Cheville, *Time resolved synthetic aperture terahertz impulse imaging, Applied Physics Letters* **79**(27) (2001) 4485–4487.

434. R. W. McGowan, R. A. Cheville and D. Grischkowsky, *Experimental study of the surface waves on a dielectric cylinder via terahertz impulse radar ranging, IEEE Transactions on Microwave Theory and Techniques* **48**(3) (2000) 417–422.

435. M. T. Reiten, D. Grischkowsky and R. A. Cheville, *Properties of surface waves determined via bistatic terahertz impulse ranging, Applied Physics Letters* **78**(8) (2001) 1146–1148.

436. R. R. Jones, D. You and R. H. Bucksbaum, *Ionization of Rydberg wave atoms by subpicosecond half-cycle electromagetic pulses, Physical Review Letters* **70**(9) (1993) 1236–1239.

437. R. R. Jones, *Creating and probing electronic wave packets using half-cycle pulses, Physical Review Letters* **76**(21) (1996) 3927–3930.

438. C. Raman, C. W. S. Conover, C. I. Sukenik and P. H. Bucksbaum, *Ionization of Rydberg wave packets by subpicosecond, half-cycle electromagetic pulses, Physical Review Letters* **76**(14) (1996) 2436–2439.

439. J. L. Krause, K. J. Schafer, M. Ben-Nun and K. R. Wilson, *Creating and detecting shaped Rydberg wave packets, Physical Review Letters* **79**(25) (1997) 4978–4981.

440. D. S. Citrin, *Terahertz sideband generation and coherent control in semiconductor microcavities, Physical Review Letters* **82**(15) (1999) 3172–3175.

441. S. P. Mickan, D. Abbott, J. Munch, X.-C. Zhang and T. van Doorn, *Analysis of system trade-offs for terahertz imaging, Microelectronics Journal* **31**(7) (2000) 503–514.

442. M. T. Reiten, K. McClatchey, D. Grischkowsky and R. A. Cheville, *Incidence-angle selection and spatial reshaping of terahertz pulses in optical tunneling, Optics Letters* **26**(23) (2001) 1900–1902.

443. T. D. Dorney, J. L. Johnson, J. V. Rudd, R. G. Baraniuk, W. W. Symes and D. M. Mittleman, *Terahertz reflection imaging using Kirchhoff migration, Optics Letters* **26**(19) (2001) 1513–1515.

444. A. B. Ruffin, J. Decker, L. Sanchez-Palencia, L. Le Hors, J. F. Whitaker, T. B. Norris and J. V. Rudd, *Time reversal and object reconstruction with single-cycle pulses, Optics Letters* **26**(10) (2001) 681–683.

445. J. L. Johnson, T. D. Dorney and D. M. Mittleman, *Interferometric imaging with terahertz pulses*, *IEEE Journal of Selected Topics in Quantum Electronics* **7**(4) (2001) 592–599.

446. J. O'Hara and D. Grischkowsky, *Synthetic phased-array terahertz imaging*, *Optics Letters* **27**(12) (2002) 1070–1072.

447. K. Uehara, K. Miyashita, K.-I. Natsume, K. Hatakeyama and K. Mizuno, *Lens-coupled imaging arrays for the millimeter and sub-millimeter wave regions*, *IEEE Transactions on Microwave Theory and Techniques* **40**(5) (1992) 806–811.

448. D. Abbott, *Directions in terahertz technology*, *Proc. 22nd IEEE GaAs IC Symposium*, 263–266, Seattle, USA (2000).

449. Z. Jiang and X.-C. Zhang, *Free-space electro-optic sampling of THz radiation with chirped optical beam*, T. Elsaesser, J. G. Fujumoto, D. A. Wiersma and W. Zinth eds., *Ultrafast Phenomena XI*, vol. 63 of *Springer Series in Chemical Physics*, 197–201, Springer-Verlag, Berlin (1998).

450. Z. Jiang and X.-C. Zhang, *Measurement of spatio-temporal terahertz field distribution by using chirped pulse technology*, *IEEE Journal of Quantum Electronics* **36**(10) (2000) 1214–1222.

451. B. Ferguson, S. Wang and X.-C. Zhang, *T-ray computed tomography*, *2001 IEEE/LEOS Annual Meeting Conference Proceedings*, vol. 1, PD1.7–PD1.8, San Diego, CA, U.S.A. (2001).

452. D. M. Mittleman, S. Hunsche, L. Boivin and M. C. Nuss, *T-ray tomography*, *Optics Letters* **22**(12) (1997) 904–906.

453. B. Ferguson, S. Wang, D. Gray, D. Abbott and X.-C. Zhang, *Three dimensional imaging using T-ray computed tomography*, *Conference on Lasers and Electro-Optics '02*, 132, Long Beach, CA, U.S.A. (2002).

454. B. Ferguson, S. Wang, D. Gray, D. Abbott and X.-C. Zhang, *T-ray diffraction tomography*, *OSA TOPS, The Thirteenth International Conference on Ultrafast Phenomena*, vol. 72, 450–451, Washington, DC, U.S.A. (2002).

455. B. Ferguson, S. Wang, D. Gray, D. Abbott and X.-C. Zhang, *T-ray computed tomography*, *Optics Letters* **27**(15) (2002) 1312–1314.

456. Q. Chen and X.-C. Zhang, *Semiconductor dynamic aperture for near-field terahertz wave imaging*, *IEEE Journal of Selected Topics in Quantum Electronics* **7**(4) (2001) 608–614.

457. Q. Chen, Z. Jiang, G. X. Xu and X.-C. Zhang, *Near-field terahertz imaging with a dynamic aperture*, *Optics Letters* **25**(15) (2000) 1122–1124.

458. P. Y. Han, G. C. Cho and X.-C. Zhang, *Time-domain transillumination of biological tissues with terahertz pulses*, *Optics Letters* **25**(4) (2000) 242–244.

459. J. P. Fillard, *Near Field Optics and Nanoscopy*, World Scientific, Singapore (1996).

460. B. T. Rosner and D. W. van der Weide, *High-frequency near-field microscopy*, *Review of Scientific Instruments* **73**(7) (2002) 2505–2525.

461. F. Keilmann, *FIR microscopy*, *Infrared Physics and Technology* **36**(1) (1995) 217–224.

462. S. Hunsche, D. M. Mittleman, M. Koch and M. C. Nuss, *New dimensions in T-ray imaging*, *IEICE Transactions on Electronics* **E81-C**(2) (1998) 269–276.

463. S. Hunsche, M. Koch, I. Brener and M. C. Nuss, *THz near-field imaging*, *Optics Communications* **150**(1–6) (1998) 22–26.

464. I. Brener, S. Hunsche, Y. Cai, M. C. Nuss, J. Wynn, J. Lopata and L. Pfeiffer, *Time resolved near field imaging and diffraction with sub-wavelength far-infrared dipole*

sources, T. Elsaesser, J. G. Fujumoto, D. A. Wiersma and W. Zinth eds., *Ultrafast Phenomena XI*, vol. 63 of *Springer Series in Chemical Physics*, 171–176, Springer-Verlag, Berlin (1998).

465. O. Mitrofanov, M. Lee, J. W. P. Hsu, I. Brener, R. Harel, J. Federici, J. D. Wynn, L. N. Pfeiffer and K. W. West, *Collection mode near-field imaging with 0.5-THz pulses*, *IEEE Journal of Selected Topics in Quantum Electronics* **7**(4) (2001) 600–607.
466. O. Mitrofanov, I. Brener, R. Harel, J. D. Wynn, L. N. Pfeiffer, K. W. West and J. Federici, *Terahertz near-field microscopy based on a collection mode detector*, *Applied Physics Letters* **77**(22) (2000) 3496–8.
467. O. Mitrofanov, I. Brener, M. C. Wanke, R. R. Ruel, J. D. Wynn, A. J. Bruce and J. Federici, *Near-field microscope probe for far infrared time domain measurements*, *Applied Physics Letters* **77**(4) (2000) 591–3.
468. O. Mitrofanov, M. Lee, J. W. P. Hsu, L. N. Pfeiffer, K. W. West, J. D. Wynn and J. F. Federici, *Terahertz pulse propagation through small apertures*, *Applied Physics Letters* **79**(7) (2001) 907–909.
469. N. C. J. van der Valk and P. C. M. Planken, *Electro-optic detection of subwavelength terahertz spot sizes in the near field of a metal tip*, *Applied Physics Letters* **80**(9) (2002) 1558–1560.
470. B. Knoll and F. Keilmann, *Near-field probing of vibrational absorption for chemical microscopy*, *Nature* **399** (1999) 134–137.
471. R. Hillenbrand, T. Taubner and F. Keilmann, *Phonon-enhanced light-matter interaction at the nanometre scale*, *Nature* **418** (2002) 159–162.
472. K. Wynne and D. A. Jaroszynski, *Superluminal terahertz pulses*, *Optics Letters* **24**(1) (1999) 25–27.
473. J. Z. Xu and X.-C. Zhang, *Optical rectification in an area with a diameter comparable to or smaller than the center wavelength of terahertz radiation*, *Optics Letters* **27**(12) (2002) 1067–1069.
474. T. Yuan, S. P. Mickan, J.-Z. Xu, D. Abbott and X.-C. Zhang, *Towards an apertureless electro-optic T-ray microscope*, *Conference on Lasers and Electro-Optics '02*, 637–638, Long Beach, CA, U.S.A. (2002).
475. B. Ferguson and D. Abbott, *Wavelet de-noising of optical terahertz pulse imaging data*, *Fluctuation and Noise Letters* **1**(2) (2001) 65–69.
476. B. Ferguson and D. Abbott, *De-noising techniques for terahertz responses of biological samples*, *Microelectronics Journal* **32**(12) (2001) 943–953.
477. M. Herrmann, M. Tani, K. Sakai and R. Fukasawa, *Terahertz imaging of silicon wafers*, *Journal of Applied Physics* **91**(3) (2002) 1247–1250.
478. R. M. Woodward, B. Cole, V. P. Wallace, D. D. Arnone, R. Pye, E. H. Linfield, M. Pepper and A. G. Davies, *Terahertz pulse imaging of in-vitro basal cell carcinoma samples*, *Conference on Lasers and Electro-Optics '01*, 329–330, Optical Society of America, Baltimore, MD, U.S.A. (2001).
479. Q. Chen and X.-C. Zhang, *Polarization modulation in optoelectronic generation and detection of terahertz beams*, *Applied Physics Letters* **74**(23) (1999) 3435–3437.
480. M. Brucherseifer, P. Haring Bolívar, H. Klingenberg and H. Kurz, *Angle-dependent THz tomography – characterization of thin ceramic oxide films for fuel cell applications*, *Applied Physics B: Lasers and Optics* **72**(3) (2001) 361–366.
481. B. Ferguson and D. Abbott, *Signal processing for T-ray bio-sensor systems*, *Proceedings of SPIE's 2000 Symposium on Smart Materials and MEMS*, vol. 4236, 157–169, Melbourne, Australia (2000).